TIME-FREQUENCY REPRESENTATIONS:

ANALYSIS, SYNTHESIS AND IMPLEMENTATION

A THESIS

submitted by

SOMA SEKHAR DHAVALA

for the award of the degree

of

MASTER OF SCIENCE

DIGITAL SIGNAL PROCESSING LABORATORY
DEPARTMENT OF ELECTRICAL ENGINEERING
INDIAN INSTITUTE OF TECHNOLOGY, MADRAS
CHENNAI-600 036

MARCH 2000

Of course, it is the paradoxes and unusual results that lead to abandonment of ideas, adjustment of our intuition, or the discovery of new ideas

--------- Leon Cohen

THESIS CERTIFICATE

This is to certify that the thesis entitled **TIME-FREQUENCY REPRESENTATIONS: ANALYSIS, SYNTHESIS AND IMPLEMENTATION** submitted by **Soma Sekhar Dhavala** to the Indian Institute of Technology, Madras for the award of the degree of Master of Science by Research, is a bonafide record of research work carried out by him under the joint supervision of Prof. K. M. M. Prabhu and me. The contents of this thesis, in full or in parts, have not been submitted to any other Institute or University for the award of any degree or diploma.

Chennai - 600 036

Date: (S. SRINIVASAN)

Joint Research Guide

TABLE OF CONTENTS

ACKNOWLEDGMENTS

I wish to express my sincere thanks and deep sense of gratitude to my research guides **Prof. K. M. M. Prabhu** and **Prof. S. Srinivasan**, for their invaluable guidance, constant encouragement and keen interest in my work. I am extremely grateful to them for spending their valuable time with me for discussions in spite of their many other commitments and activities. They have been a great source of inspiration to work with and I shall always cherish my association with them with immense pleasure. Their futuristic vision and realistic ideas have created a new enthusiasm and an ever-increasing zeal to work and explore many new things.

I take this opportunity to thank my General Test Committee members **Prof. Ashok Junjhunwala**, **Dr. Vinitha Vasudevan** and **Dr. C. Sivaram Murthy.** They extended their co-operation in helping me with this research work. I am thankful to **Dr. C. Sivaram Murthy** for his general advice at a critical stage of my work.

It gives me immense pleasure to acknowledge **Dr. R. Aravind** who has helped me in many ways. I consider myself too fortunate to attend his courses in Communication Theory and Digital Communication. The Digital IC Design course, a brainchild of **Prof. S. Srinivasan,** in a true sense extracts innovation. The quizzes were really thought provoking. Without DSP and ADSP courses taught by **Prof. K. M. M. Prabhu,** I would not have known many things. I am indebted to him for his valuable lectures. I would like to extend my sincere thanks to **Dr. K. Giridhar** for his discussion on System Identification. I am thankful to **Dr. V. V. Rao** for his critical comments on my work. Special thanks are due to **Dr. Parthasarathy,** Head of the Department of Mathematics, for his timely help in introducing me to **Dr. Nandhini Kannan,** University of Texas, San Antonio, for further discussion on EM algorithm.

It has been a great pleasure and rewarding experience for me to work in the DSP laboratory. My laboratory seniors, **Giri** and **Rajesh,** have set high standards and have shown us a way to follow them. I am thankful to Giri for his discussion on time-frequency analysis. I am particularly thankful to Rajesh for he was the one who

introduced me to incremental EM algorithm when he was working on structured covariance matrix estimation. I spent most my stay in the laboratory discussing with him and they were always rewarding. My heartfelt thanks are to my laboratory mates **Madhu**, **Vijay** and **Dharani.** Madhu's views, his comments and suggestions have helped me to improve my attitude towards work and learnt how to be sincere and honest. Vijay was a live example of a hardworking student and I am fortunate to have a colleague like him. Probably, I was the one who used most of his PC troubleshooting skills to a maximum extent. I have always enjoyed the company of Dharani in a unique way that will be everlasting. I express my special thanks to Shri. L. Thangavelu and Gandhi for their invaluable help and cooperation in the lab along with inexpressible cordiality and affection which they had shown to me.

I would like to express my special thanks to **Nagu, Rakru** and **Babai** for their brotherly attitude and constant encouragement, which made my stay at IIT joyful and memorable. My thanks to my dear Narmadites, **Venku, Subbu, Nag, Mabbu, Bux, Koti, Rami, Jalls, Chinni, Vikky, Din** and many others who have made my IIT life easy by sharing moments of sorrow and times of joy. I wish our friendship will cherish for a long time and I acknowledge with gratitude their encouragement and support.

I am highly indebted to my **Parents** and other family members for their constant encouragement and support in carrying out this research work. Finally, I thank one and all who have helped me either directly or indirectly on all my activities at IIT, Madras.

Soma Sekhar Dhavala

ABSTRACT

We have carried out the analysis of various signals using chirp transform employing chirps as an expansion set. The orthogonality, linear dependency of the expansion set, and some simple properties, like the magnitude response, have been investigated. A divide and conquer approach has been used to iteratively estimate the components in a multicomponent scenario. Wigner-based estimation of the spectrum and short-time Fourier transform with optimized windows has been proposed. Since, we have been using chirp signals as the expansion; we have considered its use in system identification.

With enough motivation given to tile the time-frequency plane in an arbitrary fashion, we have considered chirplets to represent the signal. A unified approach to signal analysis/synthesis based on these chirplets has been proposed. The spectrogram of the signal to be analyzed/synthesized has been modeled as a mixture of bivariate normal pdfs. The parameters of the chirplets are estimated using the incremental variant of the EM algorithm. K-Means clustering algorithm has been used prior to mixture modeling to classify the realizations generated from the band-rejection algorithm that acts as initial estimate to the EM algorithm. By comparing a bivariate normal pdf and spectrogram of a Gaussian amplitude modulated chirp signal, a set of mapping rules have been derived that will directly synthesize the signal corresponding to the component of the mixture density. The rules have been analyzed with an insight into chirplet decomposition and how different t-f tilings can be obtained.

While addressing the implementation aspects of the time-frequency representations using time-recursive approach, we have reviewed the architectures of the short-time Fourier

transform (STFT). We have proposed a trivial, yet novel, pre-processor to avoid buffering time in computing the discrete Fourier transform of non-sequential data using the time-recursive approach. The architectures of the STFT have been extended to generalized time-frequency distributions (GTFDs) having real-valued kernels. The algorithm exploits the symmetry and real-valuedness of the GTFDs to reduce the computational complexity. Later, the concept has been extended to running windowed GTFDs that takes into account the overlapping between adjacent window shifts.

LIST OF TABLES

LIST OF FIGURES

NOTATIONS IN BRIEF

The following are some national conventions used in this thesis:

$\int dt$	:	All integrals without limits imply integration from $-\infty$ to ∞, i.e., $\int_{-\infty}^{\infty} dt$ unless otherwise specified
$\partial(n)$	:	It refers to a sequence that is zero always except at $n = 1$ at where it is one
$\frac{\partial}{\partial x}$	:	Partial differentiation operator with respect to x
x^*	:	Complex conjugate of x
x^T	:	Transpose of matrix x
x^{-1}	:	Inverse of matrix x
$\lvert x \rvert$	:	Determinant of matrix x
$E[.]$	:	Expectation operator
$Re(.)$	:	Real part of the argument
$Im(.)$	:	Imaginary part of the argument
$ln(x)$	:	Natural logarithm of x
$f_{X;\Theta}(x;\theta)$	:	The notation expresses the dependency of the pdf of X on value of unknown parameter θ
$\binom{n}{p}$	:	Binomial coefficient $\frac{n!}{p!\,(n-p)!}$

CHAPTER 1

INTRODUCTION

1.1. INTRODUCTION

Given a time series, one can readily see how the energy is distributed over time. By performing Fourier transform to obtain the spectrum, one can see how the energy is distributed in frequency. However, as most signals encountered in practical situations are nonstationary, a joint representation of the signal in time and frequency is required. Time-frequency distributions (TFDs) characterize a signal in time and frequency simultaneously and provide more revealing picture of the signal's characteristics. However, these time-frequency representations perform prominently for certain classes of signals, because of their resolution tradeoffs and cross terms. Therefore, TFDs that track the instantaneous frequency and truly represent the signal have been extensively investigated. Extending the analysis domain beyond time and frequency gives a redundant representation of the signal. Possible dimensions of interest can be shear in frequency, shear in time, scale and rotation. Such multi-dimensional analysis may results in a compact representation, but is computationally inefficient. Hence, adaptive signal decompositions employing finite size bases are gaining importance. Recently, computationally tractable estimation procedures for obtaining the signal's projection onto a non-finite size dictionary have been proposed. This generalization of the existing representations leads to an efficient way of representing large classes of signals in subspaces spanned by operators like, shear in frequency, rotation, scale, etc. .

Specifying the signal's characteristics to be synthesized in joint time-frequency plane circumvents the problems associated with the conventional time-domain or frequency-domain approaches leading to a more efficient way of synthesizing time-varying signals. Short-time Fourier transform and Wigner-based synthesis have been paid much attention in the TFDs in time-variant filtering, since TFD-based signal synthesis removes the constraints of stationarity. The properties of the continuous-time TFDs are well understood. However, the discretization of these distributions is not straightforward unlike the Fourier transform. Many definitions are given to sample these distributions with each one of them having their own advantages and disadvantages. Eventhough, an attempt has been made to define discrete TFDs that closely follow their continuous counterparts, the computational viewpoint is still the Fourier transform interpretation of the generalized autocorrelation function. As WVD is the most widely used TFD, many algorithms have been proposed to compute it. Recently, time-recursive approach has been used to compute the short-time Fourier transform because of its localized communication and regularity. But the implementation of TFDs using the time-recursive approach has not yet been considered. We positively try to answer the many challenging issues concerning with the analysis of nonstationary signals, synthesis of a time-variant signals and implementation issues of GTFDs. Thus, our objective lies in:

1. Devising an algorithm to analyze a non-stationary signal called chirp transform with chirp rate and shift in time as parameters and analyze different signals in the transform-domain with applications in system identification and spectral estimation, and provide motivation to tile the time-frequency (t-f) plane.

2. Modeling the t-f plane, given a spectrogram, as a mixture of normal pdfs, estimate the number chirplets, their orientation and location, and analyze the mapping rules which synthesize the signal from the mixture components. We present the view point of chirplet decomposition, which can be interpreted as an adaptive signal representation method.

3. Extending the architecture of short-time Fourier transform (STFT) to generalized TFDs (GTFDs). We propose an algorithm to compute Wigner-Ville distribution (WVD) and GTFDs having real symmetric kernels and devise a scheme to compute running-windowed GTFDs (RWGTFDs) using the time-recursive approach.

1.2. CONTENTS OF THE THESIS

The remaining chapters of the thesis are organized as follows:

1. Chapter 2 reviews the existing methodology to depict the signal in time and frequency; and the construction of adaptive signal representations. Various time-frequency, time-scale and signal decomposition algorithms are reviewed and it forms the necessary background to understand the remaining chapters.

2. Chapter 3 deals with the synthesis of signals from time-frequency distributions. A review of Wigner-based and spectrogram-based signal synthesis algorithms is carried out. The descritization issues of TFDs and the implementation aspects of WVD, spectrogram and GTFDs are considered in this chapter.

3. Chapter 4 presents the analysis of nonstationary signals using chirp transform employing chirps as the expansion set. Various properties of the chirp transform and its applications in spectral estimation and system identification are dealt with.

4. Chapter 5 presents a unified approach to signal analysis/synthesis based on chirplets. The estimation of chirplets and their parameters by modeling the t-f plane as a mixture of normal densities computed using incremental variant of EM algorithm is considered. A view point of chirplet decomposition is presented that can be considered as an adaptive signal representation.

5. Chapter 6 envisages the usage of time-recursive approach in computing GTFDs. A pre-processor for avoiding buffering time in computing discrete Fourier transform using time-recursive approach has been addressed in this chapter. An algorithm for computing WVD has also been proposed in this chapter. It also deals with the algorithm for computing the running-windowed GTFDs having real-valued symmetric kernels.

6. Chapter 7 gives the conclusions drawn from this work and recommends the lines for future work.

CHAPTER 2

TIME-FREQUENCY ANALYSIS METHODS

2.1. INTRODUCTION

The distribution of signal energy in the time or frequency-domain is very straightforward. The distribution of energy in time is defined as the squared magnitude of the signal, $|x(t)|^2$, and the energy distribution in frequency is defined as the magnitude of the Fourier transform, $|X(\omega)|^2$. The Fourier transform, being a unitary operator, provides a different but equivalent representation of the signal. However, neither the signal nor its Fourier transform indicates how the energy is distributed simultaneously in time and frequency. For example, consider time-frequency distributions of two synthetic signals shown in Fig. 2.1. The two signals appear identical only if the time or the frequency energy distribution is considered. However, the two signals are clearly not identical from its time-frequency distribution. Hence, to distinguish such signals and to provide a more revealing picture of the signal's characteristics, a joint time-frequency representation is necessary. Time-frequency distributions (TFDs) are two-dimensional functions that indicate the joint time-frequency energy content of a signal. They have been utilized in a wide range of signals, including speech, music and other acoustic signals, biological signals, radar and sonar signals, and geographical signals. Most TFDs of interest are members of Cohen's class. However, the current representations are adaptive and offer more advantageous properties like Affine class, L-Wigner distribution, etc. In this chapter we review TFDs of Cohen's class, the Affine class and some adaptive signal representations and form a sufficient background to understand Chapters three and four.

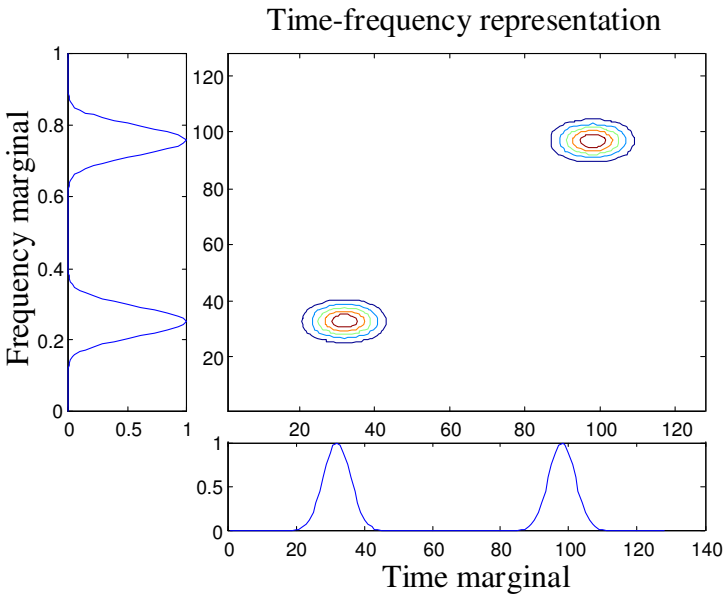

Fig. 2.1. (a) Frequency marginal, time-frequency representation and time marginal of a low frequency signal followed by a high frequency signal

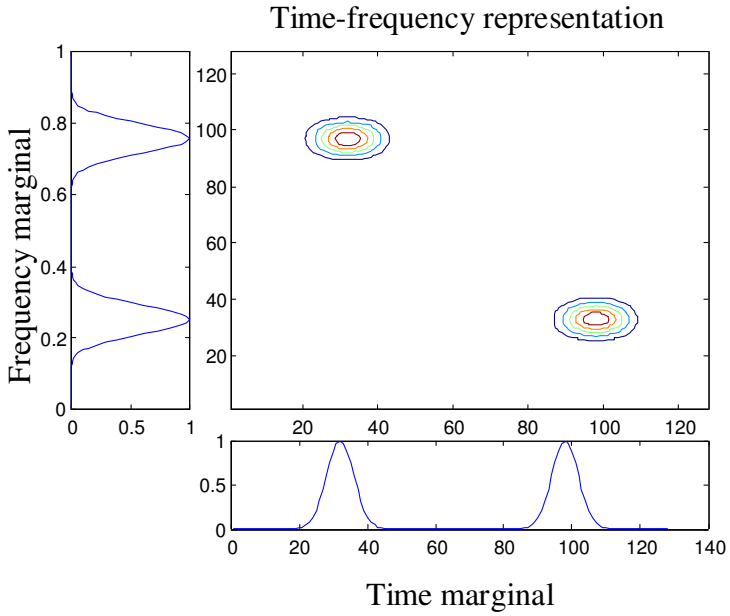

Fig. 2.1. (b) Frequency marginal, time-frequency representation and time marginal of a high frequency signal followed by a low frequency signal

2.1.1. Brief Historical Perspective

The origin of time-frequency analysis goes back to 1940s when Gabor's instrumental work on signal representation based on elementary Gaussian elements for a proper description of the signal in combined time and frequency domains took place. Later, the work done by Wigner in the field of quantum mechanics had been applied to signal processing by Ville. Page had developed the concept of instantaneous power spectrum as the rate of change of energy spectrum in the range $-\infty$ to T. Levin used the same definition for the segment T and ∞, and defined a new function as the average of both the types of instantaneous power spectra (Cohen, 1989). TFDs for the nonstationary process were considered by (Flandrin *et al*, 1985). In 1968, a fundamental result was published by Rihackzak that was stemmed from physical observations, now known as the Rihaczek distribution (Rihaczek, 1968). The existing results were given a mathematical treatment and an insight had been provided into their properties by Claasen and Mecklenbrauker in their series of papers (Claasen *et al*, 1980a) and in particular, the Wigner-Ville distribution (WVD) was investigated. Cohen had generalized the concept of time-frequency analysis by unifying the definition of TFDs having different properties. Adaptive signal representations have been given a lot of attention to overcome some of the difficulties associated with TFDs. These representations were mainly investigated by Jones and Baranuik (Jones *et al*, 1993b), Choi and Williams (Choi *et al*, 1989) and Jones and Parks (Jones *et al*, 1992a). The recent focus is towards extending the analysis domain beyond time and frequency to obtain more redundant representations (Mann, 1995). We will discuss some of these methods in the subsequent Chapters.

2.1.2. Objectives of TFDs

Before we present what the TFDs should reflect, it would be appropriate to define the instantaneous frequency (IF) and the group delay, as:

$$f_s(t) = \frac{1}{2\pi}\frac{d}{dt}\arg[s(t)] \text{ and } t_s(f) = \frac{1}{2\pi}\frac{d}{df}\arg[S(f)], \text{ respectively.} \quad (2.1)$$

The IF which represents the energy concentration in the frequency domain as a function of time describes the signal's true characteristics. However, the concept of IF is meaningless for multicomponent and nonanalytic signals, where IF is an ambiguous representation. Hence the TFDs are expected to represent the true energy along the path of the instantaneous frequency even when the constraints are lifted. Thus the TFDs are required to attain the following goals:

- Discriminate multicomponents signal from monocomponent signals.
- Facilitate the separation of multicomponents signal from monocomponent signals.
- Track the IF as accurately as possible.
- Existence of an inversion method to uniquely reconstruct the signal.

2.2. GENERAL CLASSES OF TFDs

The TFDs can be classified according to their properties. Two types of time-frequency distributions are those that are linear or quadratic functions of the signal. Examples of linear time-frequency distributions are short-time Fourier transform (STFT) and wavelet transform (WT). Examples of quadratic time-frequency distributions are the spectrogram,

scalogram, WVD, etc. A general classification is shown in Fig. 2.2 (O'Neill, 1997). They are also classified according to their behavior when an operator is applied to a signal.

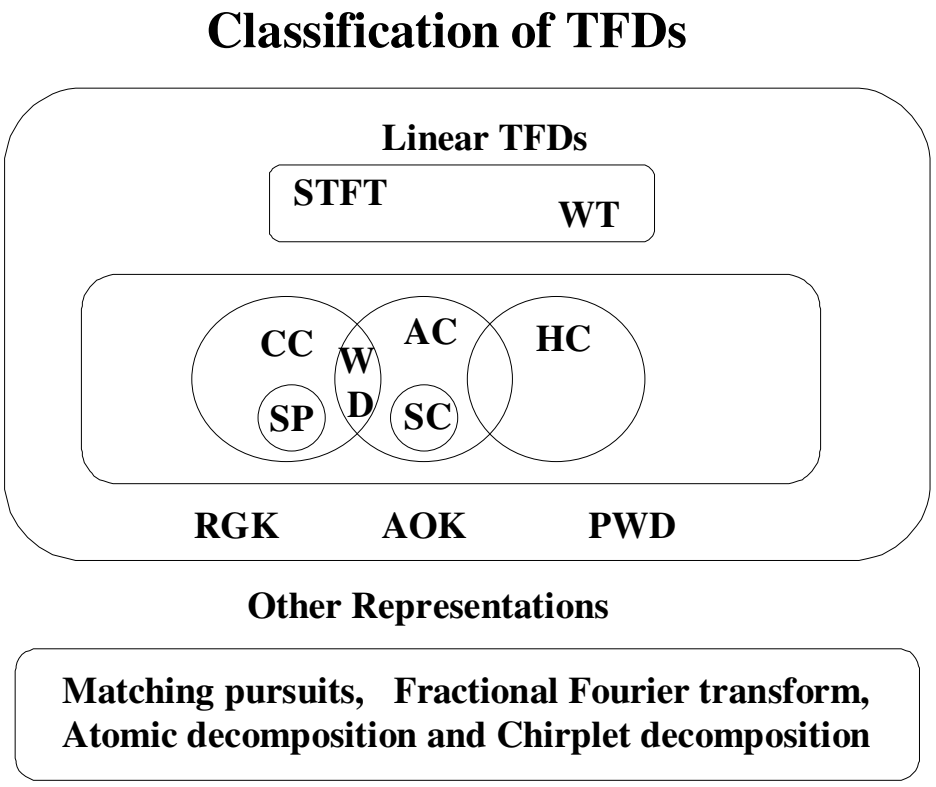

STFT: Sort time Fourier transform, WT: Wavelet transform, CC: Cohen's class, AF: Affine class, HC: Hyperbolic class, WD: Wigner distribution, SP: Spectrogram, SC: Scalogram, RGK: Radially Gaussian kernel, AOK: Adaptive optimal kernel, PWD: Polynomial Wigner distribution

Fig. 2.2. Classification of time-frequency representations

Three prominent examples of operators are the time-shift operator, the frequency shift operator and the scale operator. We review some general classes of quadratic distributions, Affine class and shift-covariant class. Finally, we present the adaptive signal representations that give flexibility in analyzing the signal by depicting them in domains other than time and frequency.

2.2.1. Cohen's Class

To distribute the energy of the signal over time and frequency, several authors have proposed different methods with each of them having unique properties. A unified approach proposed by Cohen can be expressed as:

$$C(t,\omega) = \frac{1}{2\pi}\iiint s(u+\frac{\tau}{2})\, s^{*}(u-\frac{\tau}{2})\, \phi(\theta,\tau)\, e^{-j\omega\tau}\, e^{j\theta(u-t)}\, du\, d\tau\, d\theta, \qquad (2.2)$$

where $\phi(\theta,\tau)$ is an arbitrary function called the kernel by Classsen and Meclenbrauker (Claasen *et al*, 1980a). The kernel can be a function of time and frequency. In general it is preferred to be of low pass in nature because it acts as a filtering means in the ambiguity function (AF) domain. Kernel determines the properties of the TFDs build upon them. Stated otherwise, the desired properties get reflected as constraints on the kernel. We have mentioned some desired properties of the kernel at a later stage. The kernels can be time and frequency dependent but they are not considered to be of Cohen's class (Cohen, 1995). Some adaptive representations vary the kernel in time and/or frequency dependent fashion to match the signal's characteristics. We will now briefly review some of the TFDs belonging to the Cohen's class.

2.2.2. Wigner-Ville Distribution

The Wigner[†] distribution is the prototype of distribution that is qualitatively different from spectrogram (magnitude squared of the STFT). The WVD has been successfully used in analyzing nonstationary signals, i.e., signals whose frequency behavior varies with time. The WVD of a signal $s(t)$ is given by

[†] Wigner and Wgner-Ville terms are interchangeably used

$$W(t,\omega) = \frac{1}{2\pi}\int s(t+\frac{\tau}{2})\, s^{*}(t-\frac{\tau}{2})\, e^{-j\omega\tau}\, d\tau . \tag{2.3}$$

This equation can be obtained by setting the kernel equal to one in Eqn. (2.2). Most of the properties of WVD can be obtained with this interpretation. Perhaps the most remarkable property of the WVD is that for a Gaussian windowed linear chirp signal, defined as:

$$s(t) = e^{-\alpha t^2} e^{j(a_0 + a_1 t + a_2 t^2)} \tag{2.4}$$

WVD concentrates the energy of the signal along the instantaneous frequency of the signal, given by:

$$W_s(t,\omega) = e^{-(\omega - a_1 - 2a_2 t)^2}\, e^{-2\alpha t^2} . \tag{2.5}$$

The distribution and the instantaneous frequency are shown in Fig. 2.3. The WVD of the sum of two signals is not the sum of individual WVDs. Instead, it will be the sum of their WVDs plus another component that is the cross WVD of the two signals:

$$W_{x+y}(t,\omega) = W_x + W_y + 2Re\{W_{x,y}(t,\omega)\}, \tag{2.6}$$

where the cross Wigner distribution of the two signals is defined as:

$$W_{x,y}(t,\omega) = \int x(t+\frac{\tau}{2})\, y^{*}(t-\frac{\tau}{2})\, e^{-j\omega t}\, d\tau . \tag{2.7}$$

The cross Wigner distribution of the two signals is commonly called a cross term. All quadratic time-frequency distributions, including spectrogram, will contain cross terms.

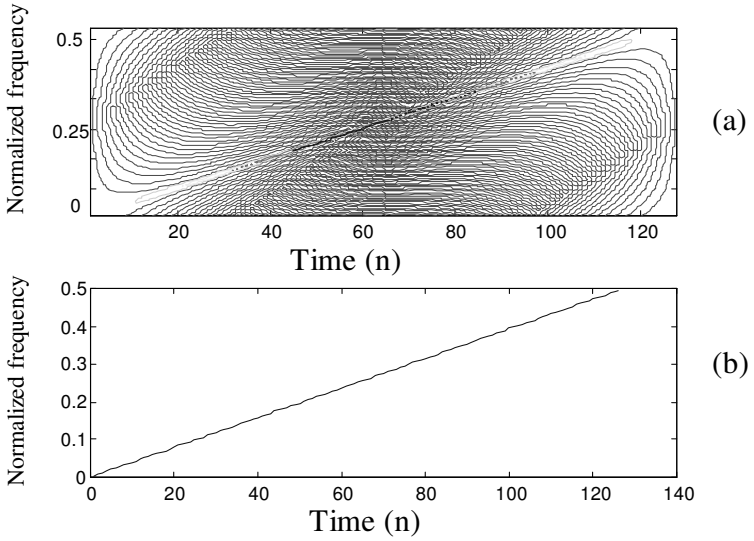

Fig. 2.3. (a) Wigner distribution and (b) Instantaneous frequency of a linear FM signal

Cross terms can also occur within a single component signal, e.g., non-linear frequency modulated signals. An example of cross terms within a signal is shown in Fig. 2.4. An auto term is defined, rather vaguely, as parts of the Wigner distribution that corresponds to the true spectrum of the signal.

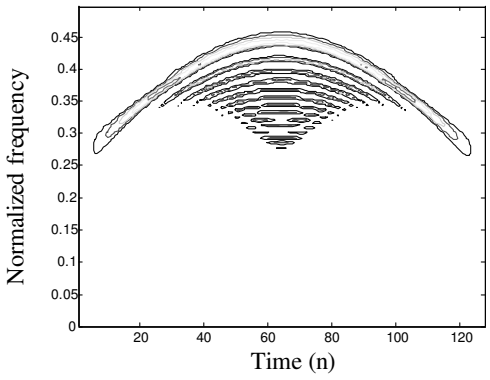

Fig. 2.4. Illustration of cross terms in a monocomponent signal

The cross terms do not actually represent the signal's energy and are hence undesirable. The structure of cross terms has been investigated and well understood by many researchers (Bikadash *et al*, 1993). Suppose the two auto terms are separated in time by Δt and in frequency by Δf, as shown in Fig. 2.5, there will be a cross term centered

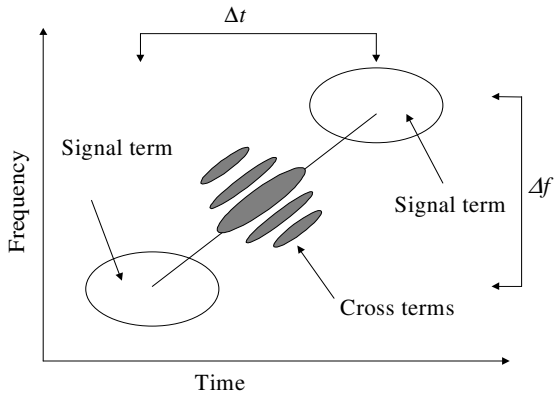

Fig. 2.5. The interference geometry in the time-frequency plane

between the two auto terms in the time-frequency plane and it oscillates in the time direction with a rate Δf and in the frequency direction with a Δt rate. Later, we will see how we can employ kernel as a filtering means to suppress these cross terms at the expense of the degradation in auto term resolution. Inspite of these spurious cross terms, the Wigner distribution has been often employed because of its capability to resolve multicomponent signals that are time-frequency disjoint. Of all the quadratic representations, Wigner distribution alone attains simultaneous resolution in time and frequency. Besides, it satisfies most of the properties that a TFD has to satisfy. Some distributions belonging to Cohen's class are tabulated in Table 2.1. A more detailed discussion can be found in (Hlawatsch *et al*,1992a).

Table 2.1: Different time-frequency distributions belonging to the Cohen's class

S. No.	Time-Frequency Distribution	$\phi(\theta,\tau)$	$C_s(t,f)$
1	Page distribution	$e^{-j\pi\theta\tau}$	$2\,\mathrm{Re}\left\{ s^*(t)\, e^{j2\pi ft} \int_{-\infty}^{t} s(t') e^{-j2\pi ft'} dt' \right\}$
2	Levin distribution	$e^{-j\pi\theta\tau}$	$2\,\mathrm{Re}\left\{ s^*(t)\, e^{j2\pi ft} \int_{t}^{\infty} s(t') e^{-j2\pi ft'} dt' \right\}$
3	Wigner distribution	1	$\int_{\tau} s\left(t+\tau/2\right) s^*\left(t-\tau/2\right) e^{-j2\pi f\tau} d\tau$
4	Choi-Williams Distribution	$exp(-\tau^2\theta^2/\sigma)$	$\iint \phi(\theta,\tau) A_s(\theta,\tau) e^{j2\pi(tv-f\tau)} d\tau\, d\theta$ here $A_s(\theta,\tau)$ is the Ambiguity function.
5	Spectrogram	$\int h^*(v-\frac{\tau}{2}) h(v+\frac{\tau}{2})$ $exp(-j\theta v)\, dv$ where h is the window function	$\left\| \int e^{-j2\pi f} s(\tau) h(\tau - t) d\tau \right\|^2$
6	Rihaczek Distribution	$e^{-j\pi\tau\theta}$	$\int_{\tau} x(t+\tau)\, x^*(t)\, e^{-j2\pi f\tau}$
7	Generalized Exponential Distribution	$exp\left(-\left(\frac{\tau}{\tau_0}\right)^{2M} \left(\frac{\theta}{\theta_0}\right)^{2N} \right)$	$\iint \phi(\theta,\tau) A_s(\theta,\tau) e^{j2\pi(t\theta-f\tau)} d\tau\, d\theta$ here $A_s(\theta,\tau)$ is the Ambiguity function.
8	Butterworth Distribution	$\frac{1}{1+\left(\frac{\tau}{\tau_0}\right)^{2M} \left(\frac{\theta}{\theta_0}\right)^{2N}}$	$\iint \phi(\theta,\tau) A_s(\theta,\tau) e^{j2\pi(t\theta-f\tau)} d\tau\, d\theta$ here $A_s(\theta,\tau)$ is the Ambiguity function.

2.2.3. Choi-Williams Distribution

The inherently associated cross terms in all bilinear distributions are of major concern in spectral estimation and in multicomponent signal separation. By looking at the kernel as filtering function in the ambiguity function (AF) domain, there have been many kernels which reduce these cross terms. However, kernels constrained to construct distributions of desired properties are of utmost importance. In the AF domain, the locus of the auto terms falls around the origin while those of cross terms lies away from origin. Choi and Williams have identified this property of the AF and have chosen a kernel that has larger weights in the vicinity of the auto terms and smaller weights farther away from the origin in the AF domain, given as: $\phi(\theta,\tau) = e^{-\frac{\theta^2\tau^2}{\sigma}}$

The CWD can be expressed as (Choi *et al*, 1989):

$$CWD(t, f) = \int e^{-j2\pi f\tau} \int \frac{1}{\sqrt{4\pi\tau^2/\sigma}} s(u+\frac{\tau}{2}) s^*(u-\frac{\tau}{2}) e^{-\frac{(u-t)^2}{4\tau^2/\sigma}} du\, d\tau \qquad (2.8)$$

The capability of CWD in suppressing the cross terms without much degradation in auto term can be controlled by a proper choice of the kernel spread (i.e., σ). A resolution comparison of several distributions and a detailed discussion of CWD can be found in (Jones *et al*, 1992a).

2.2.4. Spectrogram

The classical definition of spectrogram can be considered as the squared magnitude of the short-time Fourier transform (Nawab *et al*, 1988). However, spectrogram can be

considered as a member of Cohen's class with the kernel being the ambiguity function of the analysis window, and it is given by:

$$S(t,\omega;h) = \left| \int s(\tau)h(t-\tau)e^{-j\omega\tau}d\tau \right|^2. \tag{2.9}$$

The properties of the spectrogram obviously change with a change in the window function. The interesting property of the spectrogram is that, unlike other bilinear TFDs, it is always nonnegative. Apparently it seems that the spectrogram does not suffer from cross terms, but strictly speaking the cross terms in this representation exactly fall in the auto term region and interfere with them. Hence, spectrogram can be considered as a smoothened version of the WVD to suppress cross terms and as a natural consequence the auto term resolution reduces. A comparison of CWD, WVD and spectrogram for a synthetic signal in their cross term suppression and auto term resolution is shown in Fig. 2.6.

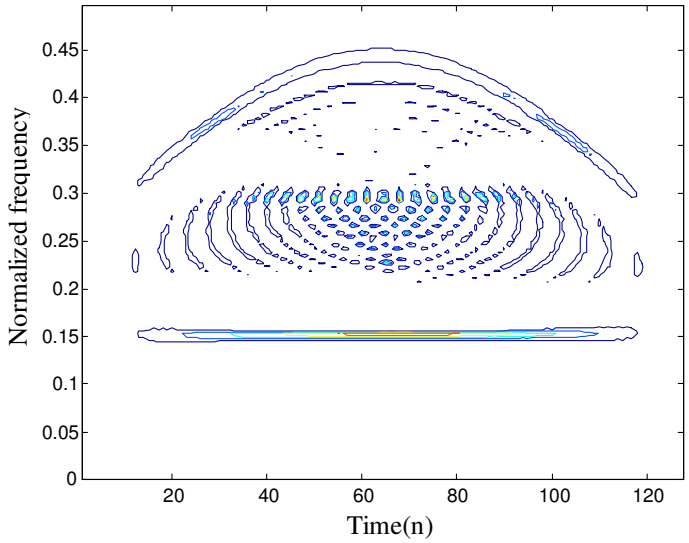

(a)

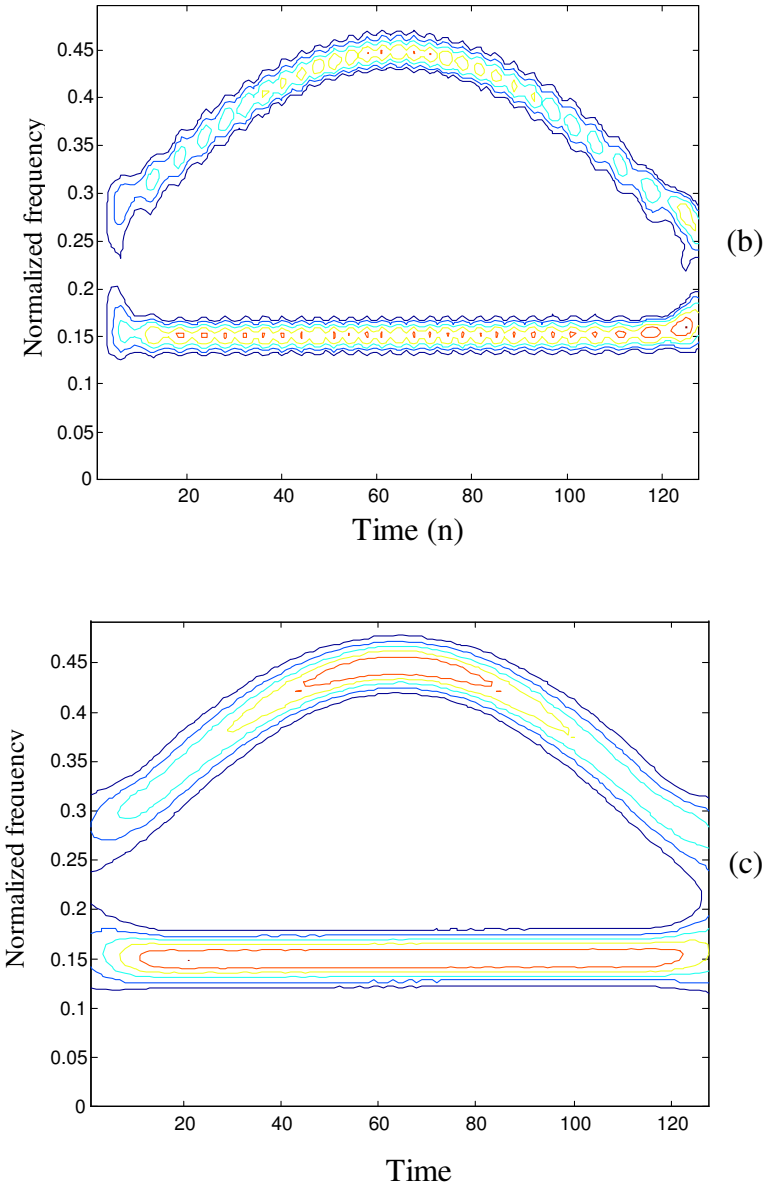

Fig. 2.6. Resolution and cross terms comparison of (a) Wigner distribution, (b) Choi-Williams distribution and (c) Spectrogram of multicomponent signal

2.2.5. Properties of TFDs in Cohen's Class

As indicated earlier, the properties of the distributions constructed in the Cohen's class reflect as constraints on the kernel. We look at the kernel's behavior to get the desired property. We briefly mention some properties now. Many other properties like finite time

support, strong time support, inversion and realizability have been discussed with proofs in (Giridhar, 1998).

a) Marginals: Instantaneous Energy and Energy Density Spectrum

Integrating the distribution along one axis gives the energy density in the other domain. For the time marginal to give instantaneous energy the kernel must be constrained as:

$\phi(\theta,0) = 1$ and for the frequency marginal to give the energy density spectrum $\phi(0,\tau) = 1$.

b) Total Energy

If the marginals are given, then the total energy will be the energy of the signal. Evaluating the integral in the expression for distribution with respect to time and frequency shows that for the total energy to be preserved, the kernel should satisfy: $\phi(0,0) = 1$.

c) Uncertainty Principle

Any joint distribution that satisfies the marginals will yield the uncertainty principle. Thus the condition for the uncertainty principle is that both marginals must be correctly given.

d) Reality

Since time-frequency distributions are usually considered to be energy distributions, they should be real and positive. For the distribution to be real, the kernel has to satisfy the constraint:

$$\phi(\theta,\tau) \;=\; \phi^{*}(-\theta,-\tau).$$

e) Positivity

The constraint on the kernel is difficult to evaluate and the characteristic function approach is used to check for positivity. In general, we are interested in distributions satisfying marginals. Wigner had shown that distributions which simultaneously satisfy marginals and positivity cannot exist. Loughlin-Pitton-Atlas have devised a scheme to construct positive distributions. Eventhough one is interested in distribution with marginals, it would be more appealing for an energy function to be positive-valued. Unfortunately such is not the case.

f) Time and Frequency Shifts

If we translate a signal shifted in time by t_0, we expect the distribution to be translated in time by the same amount. This can happen only if the kernel is time independent. Similarly, if the kernel is frequency independent the distribution would be shift invariant in frequency.

That is, $\phi(\theta,\tau\ ;\ t,\omega) \;=\; \phi(\theta,\tau).$

g) Scale Invariance

If a signal is linearly scaled, then the spectrum is inversely scaled. Hence, when a signal $s(t)$ is scale d by a factor of a, the requirement on the distribution is that:

$$C_{sc}(t,\omega) \;=\; C(at,\ \omega/a) \qquad \text{for } s_{sc}(t) \;=\; \sqrt{\text{a}}\ s(at). \tag{2.10}$$

The above equation holds well for $\phi(\theta,\tau)=\phi(\theta\tau)$. The kernel of this type is also known as product kernel.

2.2.6. Limitations

The unified approach has been presented to construct new distributions with desired properties by varying the properties of the kernel. However, the kernel is not varied in time and frequency dependent fashion and hence the distribution is independent of the signal characteristics and does not reflect the true characteristics because of the inherently associated cross terms in bilinear distributions, and signal dependent kernels have to be investigated.

2.3. AFFINE CLASS

The Cohen's class includes all the quadratic distributions that are invariant to shifts in time and frequency. We can define an operator (e.g., shift in time , shift in frequency, shear in frequency, etc.) and construct distributions that are covariant to shifts on these operators. When we choose scale and time shifts as the operators, we obtain the Affine class (O'Neil, 1997). Time-frequency distributions in the Affine class can be computed through smoothening of the Wigner distribution, as WVD is covariant to both shift in frequency and scale. For example, the Affine class can be written as:

$$A(t,\omega) \;=\; \iint W(t',\omega')\;\phi(\omega(t'-t),\omega'/\omega)\;dt'\;d\omega'. \qquad (2.11)$$

The relationship between the Affine class and the wavelet transform is similar to the relationship between Cohen's class and the short-time Fourier transform. The scalogram is defined as the squared magnitude of the wavelet transform. We can construct

innumerous distributions that fundamentally differ from Cohen's class, but can be constructed using the same general structure by defining a new set of operators on which the class would be covariant. Recently, Papandreo *et al*, have defined another class of quadratic class called "hyperbolic class". This class consists of all quadratic time-frequency distributions that are covariant to hyperbolic shifts in time (Papandreo *et al*, 1993). The hyperbolic time shift operator is defined as:

$$(H_h)(t) \quad = \quad e^{-jh \log t}\, x(t). \tag{2.12}$$

More information on the existence and construction of arbitrary operators can be found in (Baraniuk *et al*, 1996). Higher order distributions were proposed to match very specific signals that have nonlinear frequency modulation or polynomial instantaneous frequency, e.g., Wigner-bispectrum, polynomial Wigner distribution and L-Wigner distribution (Stankovic, 1994).

2.4. ADAPTIVE TFDs

The TFDs in the Cohen's class can be obtained by convolving the Wigner distribution with the kernel function. As mentioned earlier, the purpose of this kernel is to filter out cross terms and maintain the resolution of the auto terms. Since the structure of the auto terms in the Wigner distribution changes with signals, the kernels that work well for one signal may not work well for other signals. A fixed kernel results in good performance for only certain configurations of ambiguity function auto terms and cross terms. Since the locations of the auto components and cross components depend on the signals to be analyzed, we expect to obtain good performance for a broad class of signals by using only the signal dependent kernel. Jones *et al* have proposed methods for creating signal

adaptive kernels (Jones *et al*, 1993a). The optimal kernel design is formulated in the ambiguity plane because of its property to distinguish the auto components and cross components, and can be formulated as:

$$\max_{\phi} \int_{-\infty}^{\infty}\int_{-\infty}^{\infty} \left|A(\theta,\tau)\,\phi(\theta,\tau)\right|^2 d\theta\ d\tau\,,$$

which is subject to the constraints: $\phi(0,0) = 1$ and $\phi(\theta,\tau)$ is radially non-increasing. TFD of a bat signal using the adaptive optimal kernel design is shown in Fig. 2.7. A fast algorithm to compute the above representation is proposed in (Jones *et al*, 1994b). Further, constraining the kernel to be a radially Gaussian kernel is proposed in (Jones *et al*, 1993c). Jeong *et al* have investigated the kernel design for reduced interference (Jeong *et al*, 1992a). Jones *et al* have considered the problem of finding a best estimate using short-time Fourier transform (STFT) by choosing a concentration measure and then adapting the window parameter in each time and frequency bin using this measure (Jones *et al*, 1992b). They claim that it outperforms all representations in terms of concentration, but it is computationally very extensive.

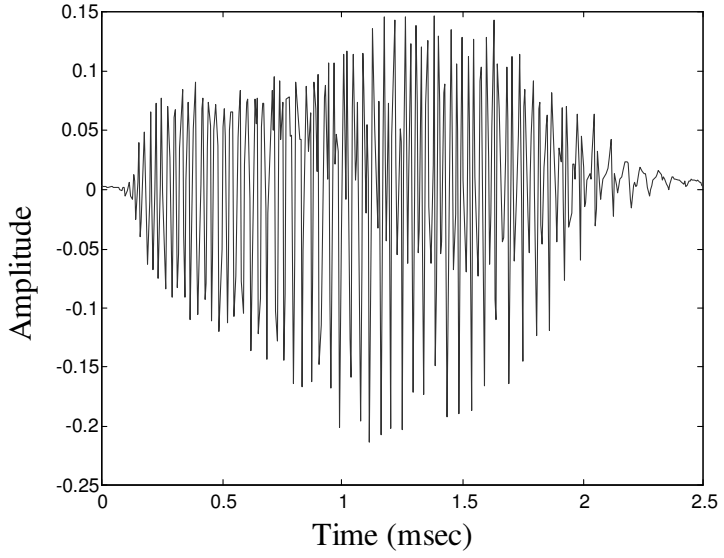

(a)

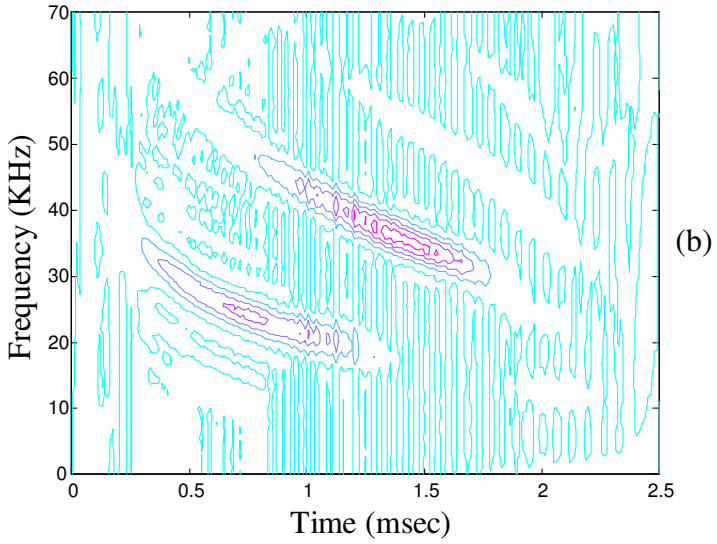

(b)

Fig. 2.7. (a) A bat signal and (b) Adaptive optimal kernel time-frequency representation of the signal

2.5. OTHER REPRESENTATIONS

Flexible decompositions are particularly important for representing signal components whose localizations in time and frequency vary. Hence, a multidimensional parameter space is considered to reveal the signal's inner structure more effectively. Extending the analysis domain beyond time and frequency is gaining momentum. However, the existing methods have their limitations from the computational point of view (Baraniuk *et al*, 1996b). We now review some decomposition algorithms.

2.5.1. Matching Pursuits

The matching pursuits algorithm decomposes any signal into a linear expansion of waveforms that are selected from a redundant dictionary of functions (Mallat *et al*, 1993). These waveforms are chosen in order to match the signal's structures best. These are

general procedures to compute adaptive signal representations. Decompositions of signals over the family of functions that are well localized in time and frequency have found many applications in signal processing. Such functions are called time-frequency atoms. A general family of time-frequency atoms can be generated by scaling, translating and modulating the window signal. In general, we can represent a signal expanded in terms of these atoms, as:

$$f(t) = \sum_{n=-\infty}^{\infty} a_n \, g_{\gamma n}(t). \tag{2.13}$$

This algorithm finds its expansion set by successive approximations of f with orthogonal projections on elements of the dictionary. The vector f can be decomposed into:

$$f = \left\langle f, g_{\gamma 0} \right\rangle g_{\gamma 0} + Rf, \tag{2.14}$$

where Rf is the residue vector after approximating f in the direction of $g_{\gamma 0}$. The above equation is computed iteratively until the residue vector approaches a threshold assuring that the signal can be reconstructed from the expansion set with a tolerable error. Adaptive time-frequency representations can be constructed using these expansion coefficients. Some of its applications in spectral estimation, denoising, multicomponent separation, etc., can be found in (Mallat *et al*, 1993).

2.5.2. Atomic Decomposition

Atomic decomposition expands any signal in terms of four parameter time-frequency atoms that are localized in the time-frequency plane. The Gaussian function is chosen as the basic atom because of its minimum area property in the time-frequency plane. The

four-parameter atom is obtained by successive applications of scaling, rotation, time and frequency-shift operators to the Gaussian elements, giving:

$$g_\beta(t) \triangleq \left(\Gamma_\alpha\, g_s\right)(t-u)\, e^{j\upsilon t}$$

$$\triangleq g_{s,\alpha}(t-u)\, e^{j\upsilon t}\,, \tag{2.15}$$

where $\beta \triangleq (s,\alpha,u,\upsilon) \in \Omega$ is the index of the atom. The scaled and rotated atom is found as:

$$g_{s,\alpha} = \frac{\sqrt{s}\, e^{c}}{\pi^{1/4}\left(\sin^2\alpha + s^4\cos^2\alpha\right)^{1/4}}\; exp\left(-\frac{s^2 - j(s^4-1)\cos\alpha\ \sin\alpha}{2(\sin^2\alpha\ +\cos^2\alpha)}t^2\right), \tag{2.16}$$

where $c = \frac{\pi}{4} - \frac{arc\ tan(s^2\ \ cot\alpha)}{2}$.

The decomposition is done via the matching pursuits in which the dictionary is constituted by the four-parameter space. A similar kind of approach in representing the signal as a sum of chirped Gaussians can be found in (Bultan, 1999). Adjustment of rectangular shell shapes adapted to the local structure will permit a clearer representation of the signal. The oblique cells are obtained by chirping the Gaussian. Its applications in finding the drift rate and separation of multicomponents are also presented.

2.5.3. Fractional Fourier Transform

The fractional Fourier transform (FRFT) rotates the time-frequency plane with a specified angle. This can cause the analysis grid to shear in time-frequency plane and can represent signals of dispersive nature. It is defined for any function *f(t)*, as:

$$f_{-\alpha}(t) \triangleq (\Gamma_{-\alpha} f)(t)$$

$$\triangleq \sqrt{\frac{1-j\cot\alpha}{2\pi}}\; e^{j\frac{\cot\alpha}{2}t^2} \int f(\tau) e^{j\frac{\cot\alpha}{2}\tau^2} e^{-j\csc\alpha\, t\tau}\; d\tau \tag{2.17}$$

where Γ is the rotation operator corresponding to the counter-clockwise rotation of α radians. The FRFT is equal to the Fourier transform at $\pi/2$. The discretization of FRFT is considered in (Bultan *et al*, 1998). An example depicting the rotation of the time-frequency plane at an angle of $\pi/2$ is shown in Fig. 2.8.

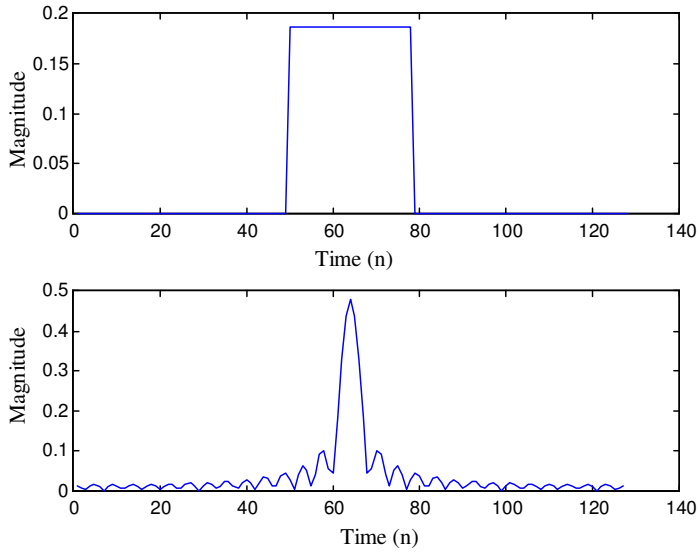

Fig. 2.8. (a) A rectangular pulse and (b) It's Fractional Fourier transform at $\alpha=\pi/2$

2.5.4. Short-Time Fourier Transform

The STFT analysis and synthesis are fundamental for describing any quasi-stationary signals such as speech. As mentioned in our earlier discussion, the Fourier transform does not explicitly show the time localization of the frequency components. So the time

localization can be obtained by suitably pre-windowing the signal *s(t)* (Nawab *et al*, 1988). The STFT can be defined as :

$$S_x(u,\zeta) = \left\langle x, g_{u,\zeta} \right\rangle = \int x(t)\, g(t-u)\, e^{-j\zeta u}\, dt\,. \tag{2.18}$$

It uses an atom which is the product of a sinusoidal wave with a symmetric finite energy window function *g*. These atoms are obtained by time translations and frequency modulations of the original window function:

$$g_{u,\zeta}(t) = g(t-u)\, e^{j\zeta t}\,. \tag{2.19}$$

The atom is time centered at τ and frequency centered at ζ. Multiplication by a relatively short window effectively suppresses the signal outside the neighborhood around the "analysis time" *u*. The effect of varying the length of the window is shown in Fig. 2.9.

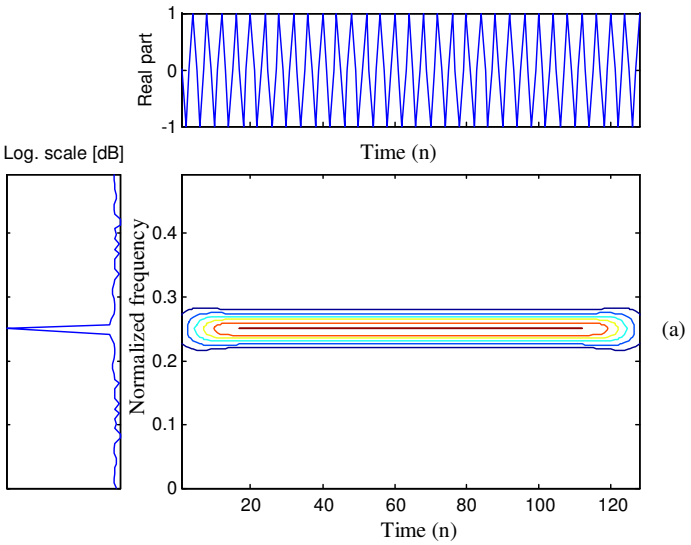

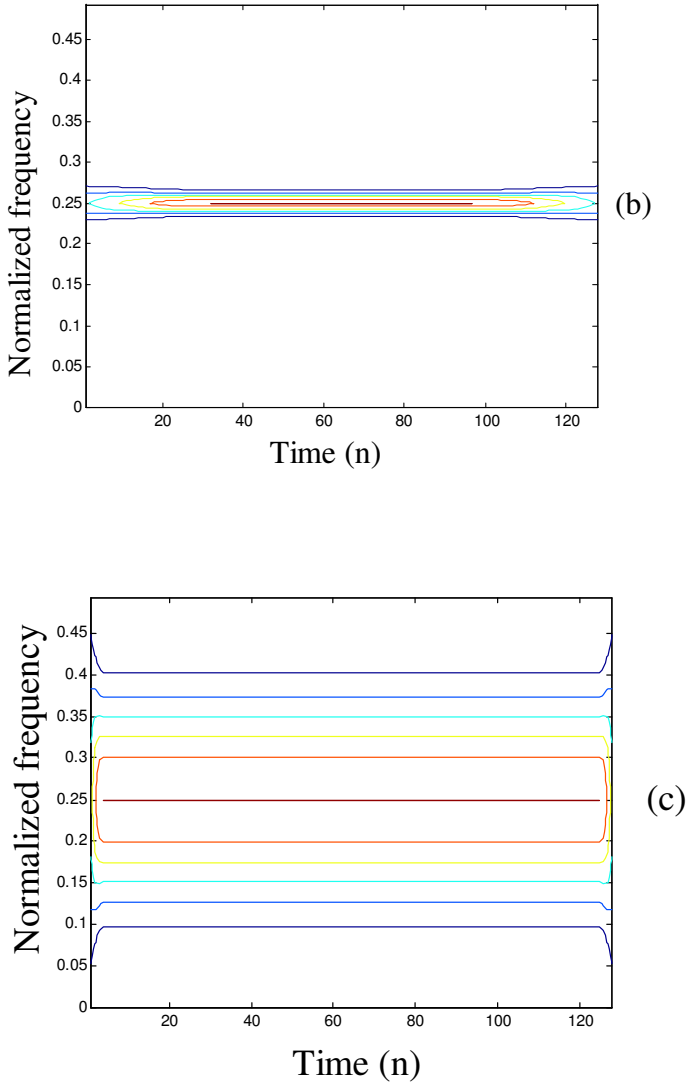

Fig. 2.9. (a) Energy spectral density, real part and STFT of a 128 point truncated sinusoid, (b) STFT with 64 point Hamming window and (c) STFT with 7 point Hamming window

The localization and energy concentration of STFT depends only on the window and does not vary unless the window is changed, i.e., the time and frequency spread are

constant throughout. This can be considered as a bank of filters having constant bandwidth as exemplified in Fig. 2.10.

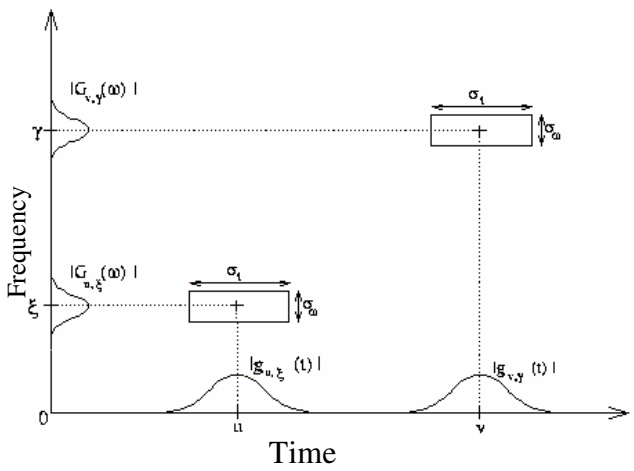

Fig. 2.10. Time-frequency tilings in STFT analysis

2.5.5. Wavelet Transform

The wavelet transform (WT) provides an alternative to the classical STFT or Gabor transform for the analysis of nonstationary signals. It also provides a unified framework for a number of techniques such as multiresolution analysis, subband coding, and wavelet series expansions that have been developed for various signal processing applications. In contrast to the STFT, the WT uses short windows at high frequencies and long windows at low frequencies. The continuous wavelet transform can be defined as:

$$WT_x(u,s) = \left\langle \mathrm{x}, \psi_{u,s} \right\rangle = \int_{-\infty}^{\infty} \mathrm{x(t)} \frac{1}{\sqrt{\mathrm{s}}} \psi^* \left(\frac{t-u}{s} \right) dt \,, \tag{2.20}$$

where the mother wavelet ψ is a zero-averaging function centered a round zero with finite energy. The *db4* mother wavelet and the scaling function are shown in Fig. 2.11. The atoms are obtained by translations and dilations of the mother wavelet as:

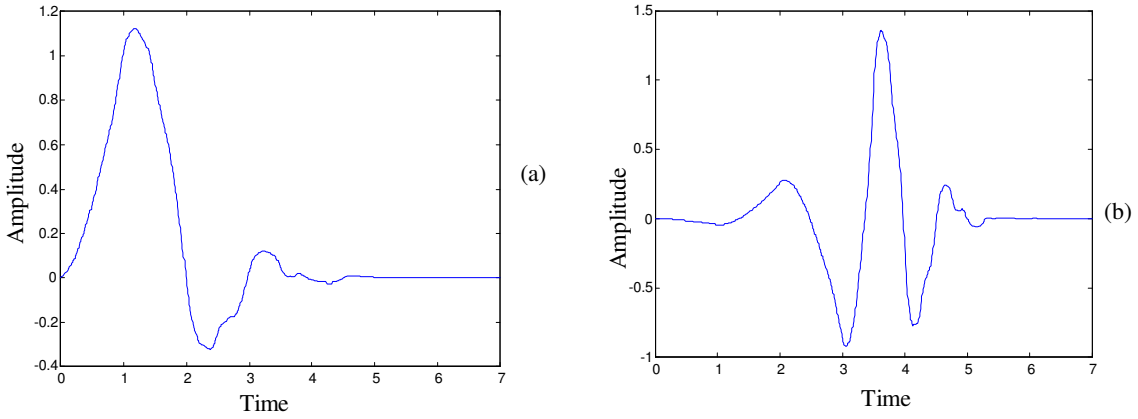

Fig. 2.11. (a) The *db4* scaling function and (b) The *db4* mother wavelet

$\psi_{u,s}(t) = \frac{1}{\sqrt{s}} \psi\left(\frac{t-u}{s}\right)$ that is centered around *u*. If the frequency centering of ψ is η, then the frequency centering of the dilated function is η / s. The time spread of the above function is proportional to *s* and the frequency spread is inversely proportional to *s*. It is as though the filters have a constant Q, bandwidth being proportional to the frequency. The time-frequency support of the WT is shown in Fig. 2.12. The WT applied to a narrow rectangular pulse demonstrates the time localization properties shown in Fig. 2.13. It can be observed from the figure that at lower scales or in high frequency regions, the WT is localized in time. However, at higher scales the frequency resoution is better. Wavelet analysis is capable of revealing aspects of data that other signal analysis techniques miss, for example aspects like trends, breakdown points, discontinuities in

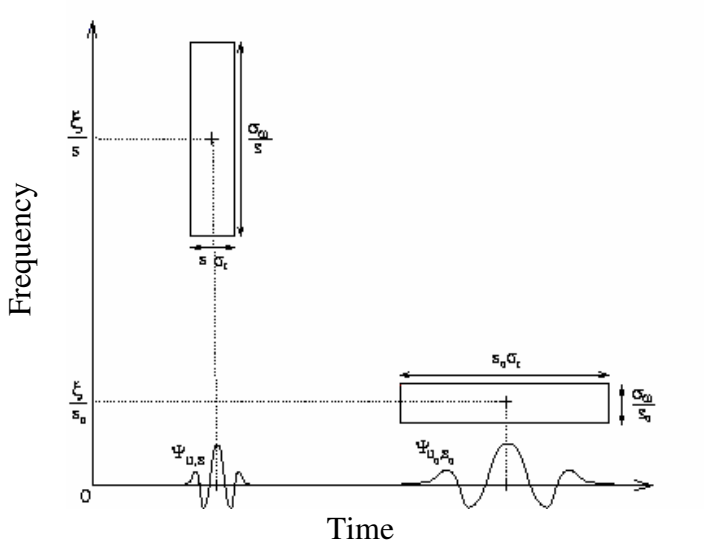

Fig. 2.12. Time-frequency tilings in the wavelet analysis

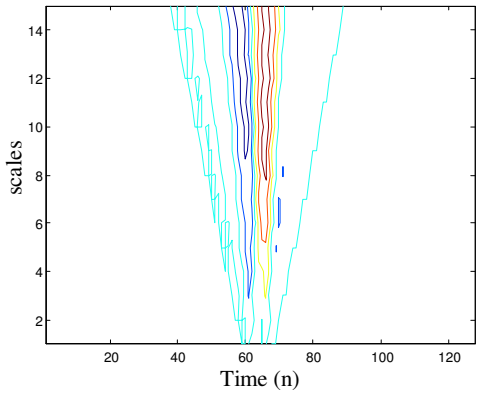

Fig. 2.13. Wavelet tranform of a narrow rectangular pulse using *db4* wavelet

higher derivatives and self-similarity. Further, because it affords a different view of data than those presented by traditional techniques, wavelet analysis can often compress or de-noise a signal without appreciable degradation. A good review on wavelet transform, its applications, the filter bank interpretation and fast computations can be found in (Rao *et al*, 1998).

CHAPTER 3

REVIEW OF SIGNAL SYNTHESIS ALGORITHMS AND IMPLEMENTATION ASPECTS OF TFDs

3.1. INTRODUCTION

In this chapter we review various signal synthesis algorithms based on short-time Fourier transform (STFT), Wigner-Ville distribution (WVD) and linear signal space. Later, we consider the discretization issues of the time-frequency distributions. The aliasing problems in bilinear representations, the definitions of generalized time-frequency distribution (TFDs) and the computational aspects of WVD and other TFDs are also considered.

3.2. SIGNAL SYNTHESIS ALGORITHMS

Signal synthesis is concerned with the estimation of a signal whose time-frequency characteristics are in the desired fashion. The advantage of specifying the behavior of the signal to be synthesized in time-frequency plane is that its characteristics can be time-variant or nonstationary, which is not available either in the time or frequency-domain representation. This additional information motivates us to process the signal in the joint time-frequency domain. The classical method of signal synthesis is the STFT approach, since the description of a signal jointly in time and frequency can be better understood by Fourier transforming the short segments of the signal. However, TFDs that offer better resolution than STFT can give flexibility in designing the time-variant filters because of

some interesting properties like marginals, instantaneous energy, etc. Review of some of these approaches will follow.

3.2.1. STFT-Based Synthesis

The concepts of STFT analysis and synthesis have been widely used in analyzing and modeling of quasi-stationary signals, such as speech. The viewpoint can either be thought of as a filter-bank model or by a block-by-block analysis. In the filter bank model, the input signal is filtered by a bank of band-pass filters, which span the frequency range of interest (Crochiere, 1980). In the synthesis procedure, a signal can be reconstructed from its STFT spectra by summing the outputs of the band-pass filters. This method of analysis and synthesis is referred to as the filter-bank summation method (FBS). The FBS method is motivated by the following relation between a sequence and its STFT:

$$\hat{x}(n) = \left[\frac{1}{N\, w(0)}\right] \sum_{k=0}^{N-1} X(n,k)\, e^{j\frac{2\pi n k}{N}} \quad , \tag{3.1}$$

where, without loss of generality, we assume that *w(0)* is non-zero. The FBS method is shown in Fig. 3.1. Perfect reconstruction is possible by constraining the analysis window as:

$$w(n) N \sum_{r=-\infty}^{\infty} \delta(n - rN) = N w(0) \delta(n) . \tag{3.2}$$

This will be clearly satisfied for any causal analysis window whose length is less than the number of analysis filters *N*. The above equation is often referred to as the FBS constraint because this requirement of the analysis window ensures the exact signal recovery.

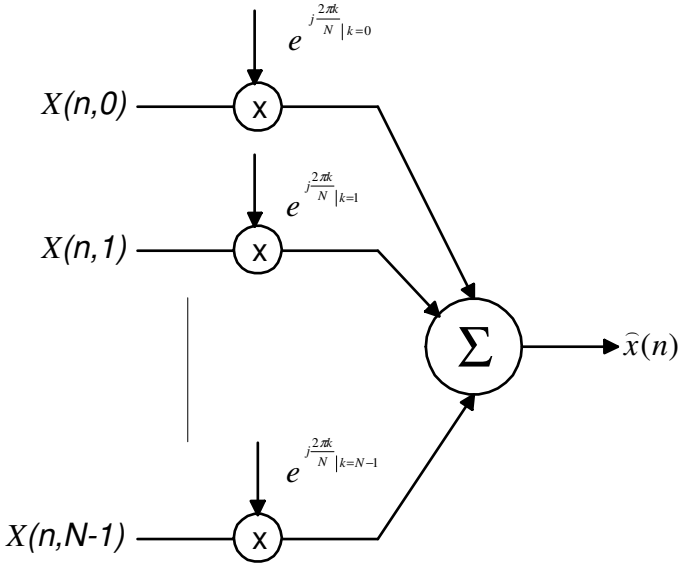

Fig. 3.1. Filter bank summation method of synthesis

Another classical approach, the overlap-and-add method (OLA), synthesizes signals from its STFT spectra by inverse transforming the STFT spectra to recover the short-time segments of the signal in time (Allen *et al*, 1977). These overlapped signal segments are then appropriately summed to reproduce the time signal. Just as the FBS method has been motivated from the filtering viewpoint of that STFT, the OLA method is motivated from the Fourier transform view point of the STFT and can be understood by the following relation:

$$\hat{x}(n) = \left[\frac{1}{W(0)}\right] \sum_{p=-\infty}^{\infty} \frac{1}{N} \left[\sum_{k=0}^{N-1} X(p,k) e^{j\frac{2\pi kn}{N}}\right], \tag{3.3}$$

where $W(0) = \sum_{n=-\infty}^{\infty} w(n)$.

In the OLA method, we take the inverse discrete Fourier transform (IDFT) for each fixed time in the STFT. However, instead of dividing out the analysis window from each of the resulting short-time series sections, we perform an overlap-and-add operation between the short-time sections. This method works provided the analysis window is designed such that the sections overlap-and-add operation effectively eliminates the analysis window from the synthesized sequence. A unique representation of the signal by the magnitude of its STFT under restrictions on the signal and the analysis window of the STFT is considered in (Nawab *et al*, 1983). When a signal's STFT is modified in a time variant or invariant fashion, the resulting spectra may not be a valid STFT. In such cases, the signal is approximated to the modified STFT in a least-squares sense. The necessary and sufficient conditions on the analysis filter under which perfect reconstruction of the input signal is possible have been considered in (Dembo *et al*, 1988). They have also dealt with the synthesis of an optimal signal (optimality criteria being the minimum mean-squared error) from the modified spectra.

3.2.2. WVD-Based Synthesis

WVD has received considerable attention in the recent years as an analysis tool for nonstationary or time-varying signals. Besides this, it satisfies most of the properties of the Cohen's class, which makes it very attractive for time-frequency analysis. Hence, WVD is considered to be a better representation in the time-frequency plane and often the signals are modified in the WVD domain. The signal synthesis problem from this modified or specified WVD was first formulated and studied by Boudrex-Bartels and Parks using the least-squares procedure (Boudreaux *et al*, 1986). It involves an

approximation of the modified distribution, which makes use of the even or odd-indexed samples only. They included applications in time-varying filtering and signal separation. Another application mentioned has been an algorithm that can be used to reduce the group delay of digital filters and the design of analysis windows for the STFT. The outer-product approximation (OPA) is based on the fact that WVD representation is intimately tied to the outer-product operation (Yu *et al*, 1987). The OPA synthesizes the signal in segments in order to remove any length restriction. The synthesis procedure involves an approximation of a 2-D function as a product of two 1-D functions. However, the adequate combination of the synthesized signals seems to be a problem. The OPA interpretation is important when the testing of a time-frequency function as a valid WVD has to be investigated. The "overlapping method" (OM) of signal synthesis has a recursive structure and has no constraint on the length of the signal unlike the OPA method. Another suboptimal approach similar to OM has been considered in (Krattenthaler *et al*, 1991). The basis function approximation (BFA) approach involves expressing a time-frequency function as a bilinear combination of basis and cross-WD. A least-squares approximation (LSA) leads to an eigenvalue-eigenvector decomposition of a symmetric matrix. It has been observed that there are two significant eigen values that correspond to the even and the odd -indexed sequences. If the modified or specified WVD is a valid representation, then the above methods can be used for the exact signal recovery. If the modified or specified WVD is not a valid representation, then the LSA and the BFA involve least-squares estimation.

3.2.3. Bilinear Signal Synthesis

Any bilinear signal representation (BSR) is given by

$$T_{x,y}(\sigma,\varepsilon) = \iint u_T(\sigma,\varepsilon;t_1,t_2)\, q_{x,y}(t_1,t_2)\, dt_1\, dt_2 , \tag{3.4}$$

where $q_{x,y}(t_1,t_2) = x(t_1)\, y^*(t_2)$ is the outer product of the individual signals $x(t)$and $y(t)$, and $u_T(\sigma,\varepsilon;t_1,t_2)$ is a kernel function specifying the BSR. $T_{x,y}(\sigma,\varepsilon)$ is the cross BSR of the two individual signals $x(t)$ and $y(t)$; the corresponding auto BSR is then defined as $T_{x,x}(\sigma,\varepsilon)$. The generalized synthesis problem can be stated as follows (Hlawatsch, 1992b):

Let T be a given modified / specified BSR and $\hat{T}$ be the model function. The objective is to find a signal $s(t)$ such that the model function $\hat{T}$ approximates the specified/ modified BSR. The model function, in general, will not be the exact BSR unless the specified BSR is a valid representation and in which case it is natural to look for the model function $\hat{T}$ in the sense that it minimizes the synthesis error $\varepsilon_x = \underset{x}{arg\,min} \left\| \hat{T} - T_x \right\|$, where

$$\varepsilon_x^2 = \left\| \hat{T} - T_x \right\|^2 \triangleq \int_{\sigma}\int_{\varepsilon} \left| \hat{T}(\sigma,\varepsilon) - T(\sigma,\varepsilon) \right|^2 d\sigma\, d\varepsilon . \tag{3.5}$$

The WVD-based synthesis is a special case of the above stated problem, where BSR is replaced by WVD. A constrained synthesis problem in the framework of BSR has been considered in (Hlawatsch, 1993), which encompasses the WVD and the ambiguity function as special cases. Two methods based on the orthogonal projection operators and the orthogonal bases to characterize the signal space have been developed. It has been

shown that constraining the signal space prior to synthesis gives a greater flexibility in designing a time-variant filter with desirable properties.

The design of a linear, time-invariant filter with a specific pass region was considered in (Hlawatsch, 1994). By defining a time-frequency subspace, a unified approach to the time-frequency (TF) signal expansion and TF filtering has been proposed. It was further shown that the optimal TF space is the eigen space of the TF region. Time-frequency projection filters derived by projecting the TF region onto the TF subspace and by a linear combination of the signals in the subspace can be used to synthesize the signal. The computational aspects have been also given .

3.3. IMPLEMENTATION OF TFDs

In this Section, we consider the implementation aspects of the time-frequency representations. As any TFD in the Affine class or the Cohen's class can be expressed as smoothening of WVD, the transition from continuous to discrete cases will be explained based on WVD. We review the interpretation of the Cohen's class as smoothening of the WVD that justifies this approach. However, the definition of the discrete case is not evident and a lot of investigation is going on to define the continuous counterparts that will preserve most of the properties as well as simple from the implementation point of view. The generalization of the discrete Cohen's class can then be dealt with in a similar fashion as is done for the WVD case.

3.3.1. Aliasing in the TF Plane

We define the following terms to understand and interpret the problem of aliasing:

a) Ambiguity function (AF):

$$A_x(\theta,\tau) = \int x(t+\frac{\tau}{2})\, x^*(t-\frac{\tau}{2})\, e^{-j\theta t}\, dt. \tag{3.6}$$

b) Temporal autocorrelation function (TACF):

$$R_x(t,\tau) = x(t+\frac{\tau}{2})\, x^*(t-\frac{\tau}{2}). \tag{3.7}$$

c) Spectral autocorrelation function (SACF):

$$R_x(\theta,\omega) = X(\omega+\frac{\theta}{2})\; X^*(\omega-\frac{\theta}{2}). \tag{3.8}$$

Discretization of the continuous time WVD requires sampling the TACF. However, by recalling Eqn. (3.7), the existence of noninteger samples makes the sampling process ambiguous and has pulled much of the controversy (Bergmann, 1991). Claasen and Mecklenbrauker have proposed a scheme to compute the discrete time WVD. The definition of WVD for a sampled signal is (Claasen, 1980a):

$$W_x(n,\omega) = 2 \sum_{k=-\infty}^{\infty} x(n+k)\, x^*(n-k)\, e^{-j2\omega k}. \tag{3.9}$$

It can be easily seen from the above equation that the resulting spectrum is periodic in ω with period π. On the other hand, the spectrum $X(\omega)$ of the signal $x(n)$ is periodic in ω with 2π. If the analog signal is sampled at the Nyquist rate, then it appears that the contributions in the range $\pi/2 < |\omega| < \pi$ of the signal's spectrum is folded in the range $|\omega| < \pi/2$ in the WVD spectrum. Therefore, distortion can be avoided only by

oversampling the signal atleast by a factor of two (Claasen *et al*, 1980b). The aliasing is caused by the fact that only the even or odd samples are used in computing the distribution. Information is thereby lost, unless the odd or even samples fully describe the signal or the signal is oversampled. The utilization of the information provided by the Nyquist sampled signal has motivated further research in this direction.

3.3.2. Sampling the TACF

Various techniques exist for sampling the TACF that finally lead to discretization of the underlying distribution. To compute samples of the TACF, one must work with the samples of the underlying continuous signal. From this signal, there are two common ways of computing it. The first method is called the "half outer-product" sampling scheme. The "Half outer-product" sampling requires only even or odd-indexed samples to compute the TACF (O'Neill, 1997). It is defined for: $R_x^h(n, m) \forall\ n\ Z$ *and even m.* The "full outer product" scheme is defined for: $R_x^f(n,m) \forall\ n \pm \frac{m}{2} \in Z$ *and* $m \in Z$. As is evident from the definition, this occurs for $n \in Z$ *and m even* and also for $n \in Z + \frac{1}{2}$ *and m odd*. Hence, it uses all the available samples and results in a nonaliased SACF. The continuous case of TACF, "half outer-product" sampling, "full outer-product "and "double outer-product" sampling schemes for TACF and the spectral repetition in SACF domain are all depicted in Fig. 3.2. All the definitions for generalizing the discrete versions of the Cohen's class in one way or the other use these sampling schemes. The generalized TFDs (GTFDs) can now be computed in the same way as is done for the WVD case. This approach was followed to compute the discrete versions

which was first investigated by Boashash and Black (Boashash *et al*, 1987). He used the "half outer product" sampling scheme on an over sampled signal.

(a) Continuous case

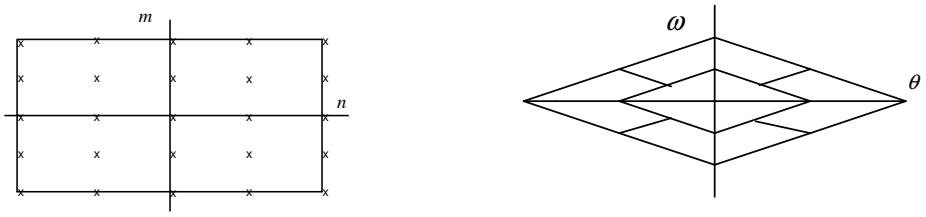

(b) Half outer product sampling

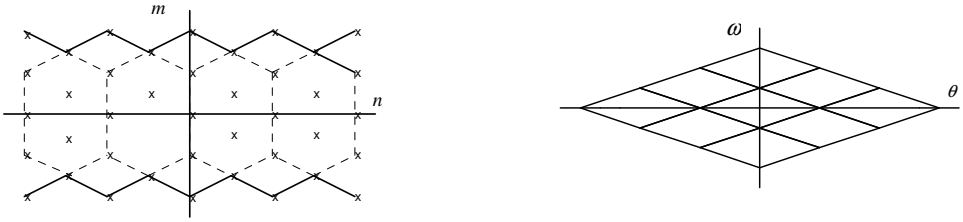

(c) Full outer product sampling

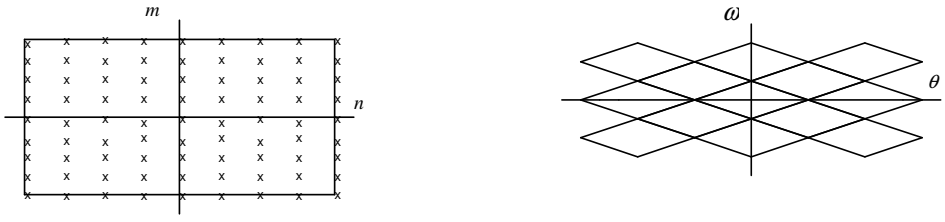

(d) Double outer product sampling

Fig. 3.2 Different sampling schemes for the TACF and the resulting repetitions in the SACF. On the left are the pictorial representations of the continuous, half, full and double outer product sampling schemes, and on the right are the resulting SACFs

The GTFDs can be represented by:

$$C_x(n,\omega) = 2\int_0^{2\pi} e^{-\theta t}\, e^{j\theta u} \sum_{u=-\infty}^{\infty} \sum_{\tau=-\infty}^{\infty} x(u+\tau)\, x^*(u-\tau)\, \phi(\theta,2\tau)\, e^{-j2\omega k}\, d\theta . \quad (3.10)$$

It is shown in (Morris *et al*, 1996) that even the TACF computed from the oversampled signal causes the GTFD to have a mirror spectra distanced by π; this requires pre-processing of the signal for identifying the "true" time-varying spectrum of the given sequence. This has motivated Jeong *et al* to consider a more appropriate definition that resembles the continuous Cohen's class called the alias-free GTFDs (AF-GTFDs) using the "full outer-product" sampling (Jeong *et al*, 1992b). However, the properties of either GTFDs or AF-GTFDs are different from the Cohen's class. A detailed analysis of the properties of the AF-GTFDs can be found in (O'Neil, 1997).

3.4. COMPUTATIONAL ASPECTS

In this Section, we consider the computation of different distributions in the Cohen's class. The different interpretations of the GTFDs, e.g., smoothening of the WVD, two-dimensional Fourier transform of the generalized autocorrelation function (GACF), Fourier transform of the two-dimensional convolution of kernel, TACF, etc., lead to different approaches. Very little effort has been made to specific distributions, except the

Choi-Williams distribution (CWD) and the WVD. Hence, we concentrate on computing the WVD, the CWD and the different approaches to computing the GTFDs.

3.4.1. Computation of WVD

Because of the optimal time-frequency concentration in the joint plane for analytic and quadratic signals, WVD has been considered to be the most reliable estimate of the "true spectrum". Since the sampling of WVD in the discrete case leads to a generalized definition of the GTFDs, it is natural to expect that the implementation issues can, in general, be carried to GTFDs as well, particularly the data flow. Boashash has first addressed the problem of computing the WVD with the fast Fourier transform (FFT) technique that we now consider (Boashash *et al*, 1987).

The sampled WVD can be expressed as:

$$W_x(n,\omega) = 2T \sum_{k=-\infty}^{\infty} x(n+k)\, x^*(n-k)\, w(n+k)\, w^*(n-k) e^{-j2\omega k}, \tag{3.11}$$

where w is a window function of length $2L+1$ that satisfies $w(n) = 0 \; for \; |n| > L$.

From the above equation, it is evident that

$$W_x(n,\omega) = W_x(n,\omega+\pi). \tag{3.12}$$

Hence, the WVD will be periodic in π. If the signal were real, this would imply that to avoid aliasing, sampling rate constraint should be

$$f_s \geq 4B,$$

where B is the bandwidth of the signal.

In this case, we must transform the real signal into analytic signal *z(n)* corresponding to *x(n),* and is defined in the time domain as:

$$z(n) = x(n) + jH[x(n)] \tag{3.13}$$

where *H[.]* represents the Hilbert transform. Further discussion on computing the analytic signal can be found in (Reilly *et al*, 1994). If the signal is replaced by its analytic part, the periodicity is unchanged, however, the absence of negative frequencies does not cause aliasing which would occur if the signal were sampled at the Nyquist rate. Hence, the sampling rate constraint becomes the well-known Nyquist rate as:

$$f_s \geq 2B.$$

To apply the FFT technique the frequency variable must be sampled. In his work, Boashash has ignored the scaling of twiddle factor by a factor of two. Claasen and Mecklenbrauker have noted that since the spectra is periodic in π, rather than sampling the frequency axis in the range $[0 - 2\pi]$, sampling the spectra in the interval $[0 - \pi]$ is sufficient which results in the kernel equivalent to the FFT kernel and can be computed without any modifications or post-processing (Claasen *et al*, 180a). It can be shown that:

$$W_x(n, \frac{m\pi}{N}) = 2T \sum_{k=-\infty}^{\infty} x(n+k)\, x^*(n-k)\, w(n+k)\, w^*(n-k) e^{-j\frac{2mk}{N}}. \tag{3.14}$$

Standard Fourier transform techniques require the time sequence to be indexed from *0* to *N-1*. Some pre-processing is required to re-arrange the data so that the above equation can be used for applying the FFT techniques. An efficient way of computing the above equation by cosine part and sine part of the DFT was considered in (Pei *et al*, 1992). We follow this sampling scheme in Chapter 6, when we deal with the implementation issues of GTFDs.

3.4.2. Computation of CWD

The distribution of interest in the Cohen's class other than WVD is the Choi-Williams distribution. Because of its variable trade-offs in auto term resolution to cross term suppression, CWD has been widely used in many applications, the example being in moving target detection in radar signal processing (Giridhar, 1998). Since the kernel is known specifically, instead of computing Eqn. (3.14) using a brute force technique, integrating the expression with respect to θ reduces to a double summation. This can be expressed mathematically using the kernel $\phi(\theta,\tau) = e^{-\frac{\theta^2\tau^2}{\sigma}}$ as:

$$CW_x(n,\omega) = 2\sum_{\tau=-\infty}^{\infty} e^{-j2\omega\tau} \sum_{u-\infty}^{\infty} \frac{1}{\sqrt{4\pi\tau^2/\sigma}}\, e^{-\frac{(u-n)^2\sigma}{4\tau^2}}\, x(u+\tau)x^*(u-\tau). \qquad (3.15)$$

The method presented in (Barry, 1992) uses matrix calculation to compute the above equation. Instead of computing Eqn. (3.15) directly over all indices, pre-processing of the data to make it a summation over non-zero sampling points greatly reduces the number of computations. He have observed that any time frequency representation can be calculated by performing a weighed element mapping over the outer product matrix and then Fourier

transforming the resulting function of τ. The weighed matrix elements are determined by the kernel function. However, it requires the regular butterfly structure which in turn requires global communication and the order of complexity is directly proportional to the signal length, i.e., number of multipliers in the pre-processing stage earlier to the FFT stage directly depends on the signal length. We will follow the data alignment in terms of matrix in our subsequent discussion on implementing GTFDs using the time-recursive approach outlined in Chapter 6.

3.4.3. Generalized Autocorrelation Function Approach

There exist various schemes for computing the generalized TFDs. This is followed from the interpretation of the Cohen's class in various ways. For example, the Cohen's class can be expressed in terms of AF as:

$$C_x(t,\omega;\phi) = \iint A_x(\theta,\tau)\,\phi(\theta,\tau)\,e^{-j\tau\omega}\,e^{j\theta t}\;d\tau\;d\theta, \tag{3.16}$$

and in terms of WVD as:

$$C_x(t,\omega;\phi) = \iint W_x(t',\omega')\,\psi(t-t',\omega-\omega')\;d\tau'\;d\omega', \tag{3.17}$$

where $\psi(t,\omega) = \iint \phi(\theta,\tau)\,e^{-j\tau\omega}\,e^{j\theta t}\;d\tau\;d\theta$.

The most attractive method of computation stems from the Fourier transform viewpoint of the GTFDs. If we define the generalized ACF as:

$$R_x(t,\tau) = \int_{-\pi}^{\pi}\int x(u+\frac{\tau}{2})\,x^*(u-\frac{\tau}{2})\,\phi(\theta,\tau)\,e^{j\theta u}\,e^{-j\theta t}du\;d\theta\;, \tag{3.18}$$

then it is evident that any time-frequency distribution can be represented as a Fourier transform of the generalized ACF, given by:

$$C_x(t,\omega) = \int_{-\infty}^{\infty} R_x(t,\tau)\, e^{-j\omega\tau}\, d\tau . \qquad (3.18)$$

However, when the kernel is real and symmetric or conjugate symmetric, then the generalized ACF would be real-valued. Morris and Quan have exploited this fact to compute the real-valued TFDs, especially WVD, CWD and spectrogram (Quian *et al*, 1990). The direct evaluation of the FFT over the generalized ACF does not take into account the redundancy in calculations. Hence, they computed the discrete Fourier transform (DFT) using the discrete sine transform (DST) and the discrete cosine transform (DCT) modules to obtain the resulting spectrum. The CWD can be computed using this approach, while the GACF can be obtained by the method discussed in the previous Section.

3.4.4. Spectrogram Decomposition

A new interpretation of the GTFDs as a weighed sum of spectrograms was provided by (Cunningham *et al*, 1994a). Spectrogram decomposition and weighed reversal correlator decomposition (WRCD) were investigated in the context of linear signal synthesis algorithms They extended the concept to represent arbitrary TFD as a weighed combination of spectrograms with orthonormal windows. Based on this fact the spectral representation of the linear operator $\breve{\psi}$, associated with each real-valued TFD, they have represented arbitrary TFD as a weighed combination of the spectrograms. The TFDs were

analyzed and the resolution comparisons of different TFDs were made based on the above approximations. Since the spectrogram is a nonnegative distribution, while representing a negative distribution, the weights of the corresponding spectrograms will be negative. In such a case, the interpretation of the linear operator becomes hard to understand. WRCD has been derived to represent high-resolution TFDs that are in general negative. A fast algorithm that mainly works on the above principle that any arbitrary TFDs can be expressed as a weighed combination of spectrograms was proposed in (Cunnigham *et al*, 1994b). It is claimed that the parallel stages of the spectrogram implementation blocks lead to faster implementation.

CHAPTER 4

CHIRP TRANSFORM

4.1. INTRODUCTION

Analysis of multicomponent signals is a potential task in non-parametric modeling. STFT with optimized windows, kernel design for reduced interference, etc., are some of the approaches concerned with improving resolution and suppressing cross terms. The recent focus of signal processing is on extending the analysis domain to shear, scale, translation, etc., which has led to the evolution of chirplet transform containing all the above spaces with possible extension to even more dimensions (Mann *et al*, 1995). The principle involved in wavelets 'scaling', together with chirping and shifting the wavelet, causes the analyzing grid in t-f plane sheared, scaled and shifted. Hence, it can be considered as a generalization of STFT and wavelet analysis; and therefore can give a good estimate of the true spectrum for a large vocabulary. However, many a time, the signal need not be analyzed in all subspaces, but a few may well represent the signal's inner structure, as nonlinear frequency modulation can be approximated by piecewise linear FM, the case pertinent to the problem in spectral estimation of nonstationary signals. We restrict the analysis to a two-dimensional space comprising of chirping and shifting only, called the chirp transform. The tilings can be made arbitrary by allowing the nonlinearity of the frequency modulation to vary. However, from the computational and data storage point of view, this is cumbersome, uneconomical and unyielding (Baraniuk *et al*, 1996b). Different time-frequency tilings matched to the signal's characteristics give a better representation of the signal. In this Chapter, to understand the concept of arbitrary t-f

tilings and their usefulness not only as adaptive signal representation schemes but also as signal processing tools, we consider chirps as an expansion set, where the chirp is a linear frequency modulated signal. The chirps with chirp rate and translation in time being the parameters are used to carry out the analysis in the transform domain. We present an analysis methodology in the transform domain for various signals after we discuss the orthogonality of the expansion set. Based on the interpretation and properties of the transform, we discuss its application in spectral estimation and system identification. In the spectral estimation problem, we present two methods based on WVD and STFT with optimized windows. Recently, nonstationary signals have been used in system identification, because of the wideband spectrum and time localization (Shalvi *et al*, 1996). This can be considered as denoising plus conventional system identification problem. We can make use of the localization of the chirp transform to a specific type of signal whose inner structure best matches with the expansion set in denoising experiments.

4.2. CHIRP TRANSFORM

The origin of chirp transform is not new, as it can be found dating back to 1820's (Lawrence, 1965) in optics known as Fresnal transformation, given by

$$S(a) = \int s(t)\, e^{-j(t+a)^2}\, dt \tag{4.1}$$

the basis of which can be found in chirplet transform with amplitude modulated chirp subjected to dilations. The analysis equation of the chirp transform is given by introducing another parameter, β, the chirp rate, as:

$$S(\beta,a) = \int s(t)\, e^{-j\beta(t+a)^2/2}\, dt\,, \tag{4.2}$$

where '*a*' is a time shift of the basis function that gets reflected as a frequency shift in the frequency domain and $S(\beta,a)$ is the subspace of chirplet transform. It can be expressed as the inner product of *s(t)* and the expansion set (the reason for calling expansion set instead of basis will be explained shortly) as:

$$S(\beta,a) = \langle s(t)\,, e^{j\beta(t+a)^2/2} \rangle. \tag{4.3}$$

The synthesis equation is given by

$$\hat{s}(t) = \int\int S(\beta,a)\, e^{j\beta(t+a)^2/2}\; d\beta\; da\,. \tag{4.4}$$

The integral given in Eqn. (4.2) is in the form of Liebnitz's integral and can be solved by assuming slowly varying envelope for s*(t)* (Papoulis, 1984). However, the magnitude of the expansion coefficients can be obtained by using Moyal's law without imposing constraints. This helps us in studying the behavior of the transform analytically for various signals. Moyal's law can also be used to study the overlapping (in other words, time-frequency overlap for nonstationary signals and orthogonality in stationary cases) of two signals in the time-frequency plane, which is defined as:

$$\left| \int s_1(t)\, s_2^*(t)\, dt \right|^2 = \iint W_1(t,f)\, W_2(t,f)\, dt\, df\,, \tag{4.5}$$

where W_1 and W_2 correspond to the WVD of the s_1 and s_2, respectively. Before we present the applications and analysis of various signals, we take a brief look at the properties of

the expansion set. In the following derivation, we prove that the signal can be reconstructed from the synthesis equation.

Let $\hat{s}$ be the signal reconstructed from the inverse transformation. Then

$$\hat{s}(t) = \int\int S(\beta,a)\, e^{j\beta(t+a)^2/2}\, da\, d\beta,$$

$$= \int\int\int s(\tau)\, e^{-j\beta(\tau+a)^2/2} e^{j\beta(t+a)^2/2}\, d\tau\, da\, d\beta. \qquad (4.6)$$

After simplifying the above equation we get,

$$= \int\int\int s(\tau)\, e^{-j\beta(\tau^2-t^2)/2} e^{-j\beta a(\tau-t)}\, d\tau\, da\, d\beta \qquad . \qquad (4.7)$$

Integrating the above equation with respect to a gives us

$$= \int\int s(\tau)\, e^{-j\beta(\tau^2-t^2)/2}\, \partial(\beta(\tau-t))\, d\tau\, d\beta. \qquad (4.8)$$

We consider the above integral in the following cases:

1. $(\tau-t)\neq 0$ *and* $\beta\neq 0$: The integral is clearly equal to zero since $\partial(\beta(\tau - t)) = 0$ in the region of interest.
2. $(\tau-t)=0$ *and* $\forall\beta$: The integral becomes *s(t)*.
3. $\forall(\tau-t)$ *and* $\beta=0$: When $\beta=0$, the integral becomes $\int s(\tau)\, d\tau$.
4. $(\tau-t)=0$ *and* $\beta=0$: It also results in the same value as it is with the previous case, i.e., $\int s(\tau)\, d\tau$.

The final value of the integral would be the sum of the above different cases. It is to be noted that we have computed the expression twice at $(\tau - t) = 0$ *and* $\beta = 0$, firstly in $(\tau - t) = 0$ *and* $\forall \beta$, and next explicitly at $\forall(\tau - t)$ *and* $\beta = 0$. Hence, the final value of the integral would be:

$$\hat{s}(t) \;=\; 0 + s(t) + \int s(\tau)\, d\tau - \int s(\tau)\, d\tau \;=\; s(t). \tag{4.9}$$

Further investigation is required on the existence and uniqueness of the inverse transformation and more mathematical treatment is necessary, even though we have made an attempt to discuss its uniqueness in the following pages. Now we try to prove that the expansion set is not orthogonal because they are not linearly dependent.

In general, we shall say that two functions *x(t)* and *y(t)* are orthogonal if their inner product is zero:

$$\langle x, y \rangle = 0. \tag{4.10}$$

To investigate the orthogonality, we consider two atoms, s_1 and s_2 from the expansion set with different parameters (β_1, a_1) and (β_2, a_2), respectively.

Then,

$$\langle s_1, s_2 \rangle = \int e^{j\beta_1 (t+a_1)^2/2}\; e^{-j\beta_2 (t+a_2)^2/2}\; dt. \tag{4.11}$$

Since our objective is to find out the inner product magnitude, without loss of generality, we use Moyal's law to evaluate the absolute squared of the inner product of the two

atoms. By noting that the WVD of any atom, which is of the form described above, is given by:

$$WVD_{s(t)}(t,\omega) = \partial(\omega - \beta t - \beta a) \tag{4.12}$$

and recalling Eqn. (4.5), we obtain

$$\left|\langle s_1, s_2 \rangle\right|^2 = \int\int \partial(\omega - \beta_1 t - \beta_1 a_1)\ \partial(\omega + \beta_2 t + \beta_2 a_2)\ dt\, d\omega. \tag{4.13}$$

As mentioned earlier, the atoms which result in zero inner product are said to be orthogonal. This interpretation looks simpler when the atoms are stationary. In the present case, since the spectrum is varying in a time-dependent fashion we need to look into the joint t-f plane. We infer from Eqn. (4.13) that it goes conditionally to zero and the instances when the integral becomes non-zero are:

$$t(\beta_1 - \beta_2) + (\beta_1 a_1 - \beta_2 a_2) = 0. \tag{4.14}$$

The above equation implies that the instant at which the instantaneous spectra are crossing (since the instantaneous spectra can overlap at only one instant given by the above condition), the inner product is non-zero. Hence, we say that when two atoms are time-frequency disjoint they are orthogonal, i.e., their instantaneous spectra do not cross (or overlap)[†]. The case when $\beta_1 = \beta_2$ in the above equation is of particular importance, since the expansion set is orthogonal in this subspace. For most of the analysis purpose, we exploit the fact that when the transform domain containing the chirp rate that

[†] When the concept of instantaneous frequency fails as is the case for multicomponent signals or nonanalytic signals, we shall look into the WVD.

corresponds to the signal under analysis gives the coefficient of maximum amplitude and we can identify components in the transform domain by looking either for local maxima or global maxima. In general, the expansion set is not orthogonal since the atoms are not always linearly dependent. When two functions are linearly dependent, then they cannot be orthogonal. To check whether the atoms are linearly independent or not we may compute the wronskain of the expansion set, where the wronskain of N functions (vectors) is defined as (Leon, 1994):

$$W = \begin{vmatrix} f_1 & f_2 & .... & f_N \\ f_1' & f_2' & .... & f_N' \\ \vdots & & & \vdots \\ f_1^{N-1} & f_2^{N-1} & ..... & f_N^{N-1} \end{vmatrix}, \tag{4.15}$$

where f^{n} corresponds to the n^{th} derivative of the function f. Substituting the atoms in place of f to compute the wronskain (for the sake of analysis we consider only two atoms, s_1 and s_2), we get

$$W = 2j\, e^{j\beta_1 (t+a_1)^2/2}\, e^{j\beta_2 (t+a_2)^2/2} \left(t(\beta_1 - \beta_2) + (\beta_1 a_1 - \beta_2 a_2) \right). \tag{4.16}$$

The result is same as that of Eqn. (4.14) and hence the expansion set is linearly dependent. Fortunately, they are orthogonal in the subspace containing all atoms with $\beta_i = \beta_j \; \forall \, i = j$.

4.3. CHOICE OF PARAMETERS

No discretization procedure exists for the above transformation. Hence, a close analysis on the t-f plane is required on how to choose β. We represent β and $a \in \Re$ in such a way

that they do not range from - ∞ to +∞ but belong to $\Re$ which suffices to approximate the signal reasonably. Now we will have a closer look at the phase term of the expansion set:

$$j\varphi(t) = j\beta(t+a)^2/2 = j\beta t^2/2 + j\beta ta + j\beta a^2/2. \quad (4.17)$$

The first term on the right hand side of the above equation causes chirping, the middle term causes a frequency shift (i.e., modulation in time domain) and the last term is just a phase constant. The instantaneous frequency of the expansion set is given as:

$\varphi'(t) = \beta t + \beta a$, which is in the form of $y = mx + c$. Based on this rule, different locations covered by varying β and a are depicted in Fig. 4.1. The angle corresponding to the slope of the above expression is represented as '*chirp rate in radians*' for easy visualization of the chirp rate parameter in the t-f plane. In our simulations and analysis, we have varied β from –4 to 4 ; and *a* from -127 to 127 where the signal length is 128 samples. At $\beta = 0$, the transform coefficients represent the DC term in the Fourier transform. It is for this reason that, at $\beta = 0$ the parameter '*a*' does not cause any frequency shift since the middle term on the right hand side of Eqn. (4.17) is zero. Hence, for slowly varying signals, i.e., $\beta \approx 0$, shifting in time does not alter the spectrum.. To accommodate such slowly varying signals and model sinusoids, a/β has to be used, and this ensures the desired frequency shift. A slowly varying signal (approximately a sinusoid) generated using $\beta = 0.001 \; and \; a = 2000$ and $\beta = 0.001 \; and \; a = 4000$ are shown in Fig. 4.2. We can observe from the figure that the periodicity is almost doubled in the latter case. In a similar manner, we can sweep the entire frequency plane by choosing the appropriate values for *a*. Close analysis is required on the t-f plane to select the expansion set and to select the dictionary appropriately.

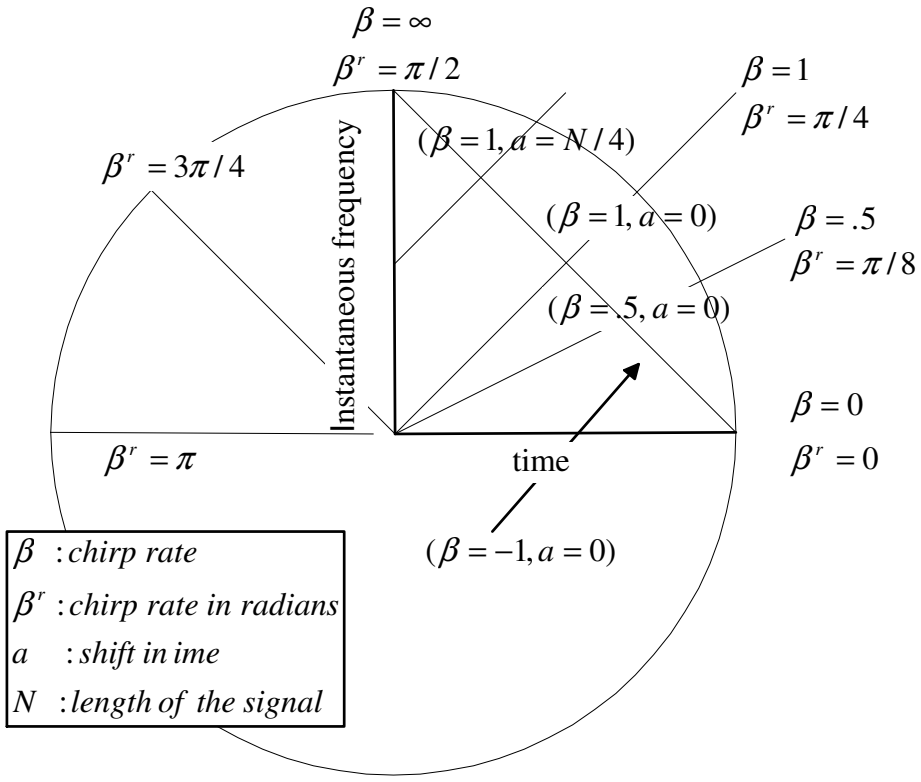

Fig. 4.1. Time-frequency locations and the energy concentration of the atoms in the expansion set and equivalent representation as a rotation parameter

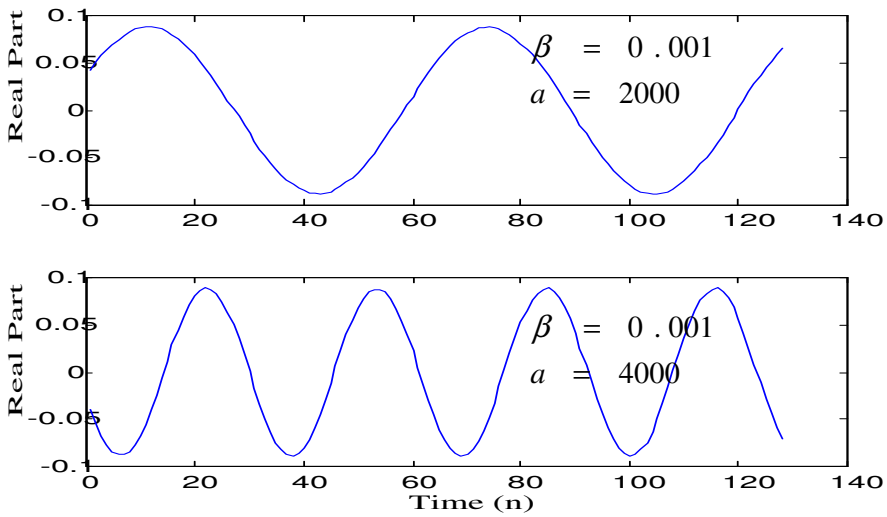

Fig. 4.2. Modeling of slowly varying signals

4.4. ANALYSIS IN THE TRANSFORM DOMAIN

We are interested in the transform coefficients where the expansion set would be orthogonal. To analytically solve the integrals and observe the synthesis criteria, we have chosen Gaussians as they have closed form expressions and easy to solve.

Let the signal be

$$s(t) = \left(\frac{\alpha}{\pi}\right)^{\frac{1}{4}} e^{-\frac{\alpha t^2}{2}} e^{j\beta_1 t^2/2}, \tag{4.18}$$

then, $S(\beta_1, a) = \int s(t) e^{-j\beta_1 (t+a)^2/2} dt$ (4.19)

can be given by

$$S(\beta_1, a) = \left(\frac{\alpha}{\pi}\right)^{\frac{1}{4}} \int e^{-\alpha t^2/2} e^{-j\beta_1 at} e^{-j\beta_1 a^2/2} dt .$$

Rewriting the above equation, we get

$$S(\beta_1, a) = \left(\frac{\alpha}{\pi}\right)^{\frac{1}{4}} e^{-j\beta_1 a^2/2} \int e^{-\frac{\alpha}{2}(t + j\frac{\beta_1 at}{\alpha})^2} e^{-j\frac{\beta_1^2 a^2}{2\alpha}} dt$$

$$= \left(\frac{4\pi}{\alpha}\right)^{\frac{1}{4}} e^{-j\beta_1 a^2/2} e^{-\frac{\beta_1^2 a^2}{2\alpha}} . \tag{4.20}$$

When we analyze the above signal using the chirp transform at a chirp rate equal to the signal, we obtain the following information:

The magnitude is controlled by the window parameter (i.e., amplitude modulation) in such a way that its spread is inversely proportional to the spread of the window. As $\alpha \to 0$, the magnitude response becomes an impulse, since the signal and expansion set are orthogonal. The phase response is insensitive to the amplitude variation, except that

the phase is varying with the same chirp rate as does the signal and the magnitude response is controlled by the envelope of the signal. The magnitude response of the chirp signal for different windows is shown in Fig. 4.3. Now we move the window position time centered at $t_{0,}$ i.e.,

$$s(t) = \left(\frac{\alpha}{\pi}\right)^{\frac{1}{4}} e^{-\frac{\alpha(t-t_0)^2}{2}} e^{j\beta_1 t^2/2}$$

and the chirp transform of the signal at β_1 can be computed as is done in Eqn. (4.20) to get

$$S(\beta_1, a) = \left(\frac{4\pi}{\alpha}\right)^{\frac{1}{4}} e^{-\frac{\beta_1^2 a^2}{2\alpha}} e^{-j\beta_1(a+t_0)^2/2} e^{-j\beta t_1^2 a^2}. \tag{4.21}$$

The above result says that shifting the window (not the phase term of the signal) causes the phase response to shift by the same amount and the magnitude response is the same as the earlier one but the direction is opposite. We now shift the time centering of the phase term of the signal by t_0, keeping the window time centered at the origin. Then,

$$s(t) = \left(\frac{\alpha}{\pi}\right)^{\frac{1}{4}} e^{-\frac{\alpha t^2}{2}} e^{j\beta(t-t_0)^2/2}$$

$$S(\beta_1, a) = \left(\frac{4\pi}{\alpha}\right)^{\frac{1}{4}} e^{-\frac{\beta_{12}^2(a-t_0)^2}{2\alpha}} e^{-j\beta_1(a+t_0)^2/2} e^{-j\beta_1 t_0^2}. \tag{4.22}$$

The anticipated results are shift in magnitude response as well as in phase response without the change in numerical values. We observe shift in, both magnitude response and phase response, because of the time centerings of the window and phase term of the signal are not the same.

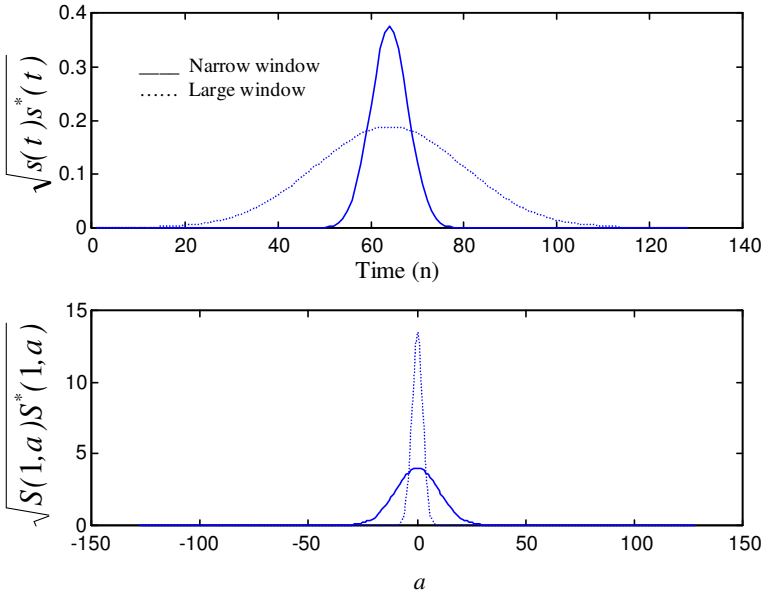

Fig. 4.3. (a) Envelope of the signal with different windows and (b) Magnitude response variation of the chirp transform at $\beta = 1$

We make the following conclusions after the observations:

- A shift in phase term of the signal is responsible for the shift in the magnitude response but not in the phase response of the transform.
- The location of the window determines the location of the phase response, which has the same instantaneous law as the signal does (i.e., $\beta(.)^2$) and it does not alter the magnitude response.

The results are similar to the properties of Fourier transform, since we are analyzing in the orthogonal subspace. We strengthen this viewpoint by observing the magnitude response for various signals of theoretical importance. An impulse, a rectangular gated sinusoid and a Guassian windowed chirp signals have been analyzed using the chirp transform. To study the interdependency of the coefficients, we concentrate at the chirp

rates corresponding to the test signals. In Fig. 4.4(a), the chirp transform of an impulse at $\beta = 0.01, 1 \; and \; 20$, respectively, is shown. For a rectangular windowed sinusoid, the chirp transform at the same chirp rate has a magnitude response similar to the Fourier transform of a rectangular pulse as shown in Fig. 4.4(b). It is to be observed that the transform has maximum amplitude in the region corresponding to $\beta = 0.01$ where the signal is orthogonal. Similarly, a Gaussian enveloped linear FM component analyzed using the chirp transform has a magnitude response again a Gaussian along the orhtogonal axis i.e., $\beta = 1$, depicted in Fig. 4.4(c). This Fourier transform interpretation of the individual components in the subspace of the chirp transform corresponding to their chirp rates helps us in identifying the individual components in a multicomponent scenario.

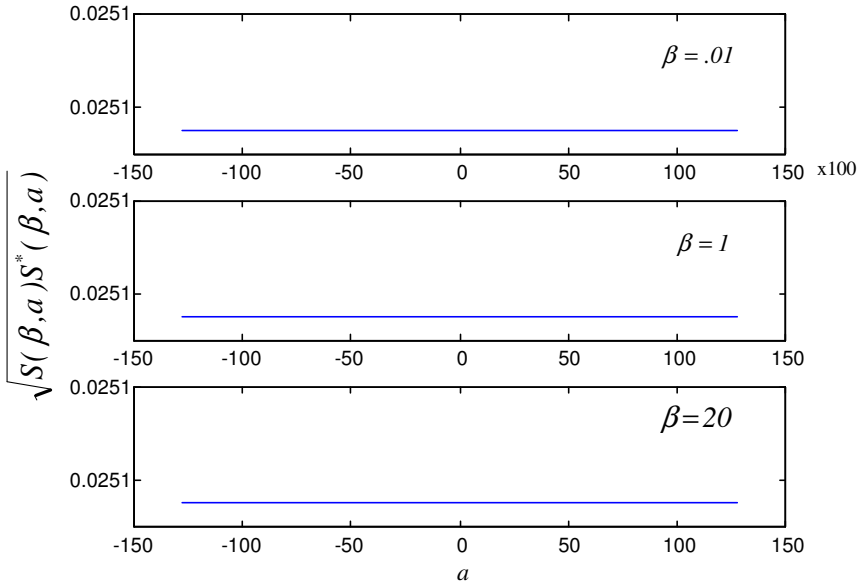

Fig. 4.4. (a) Chirp transform of an impulse

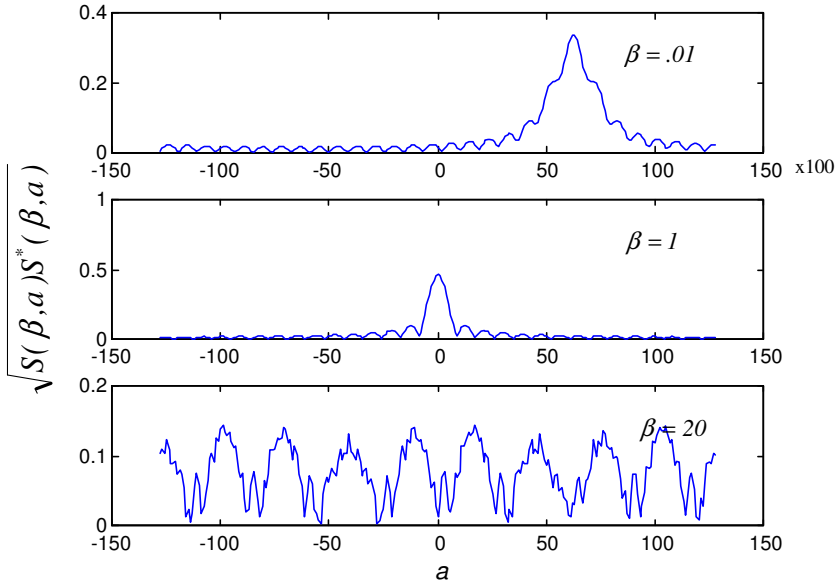

Fig. 4.4. (b) Chirp transform of a rectangular gated chirp

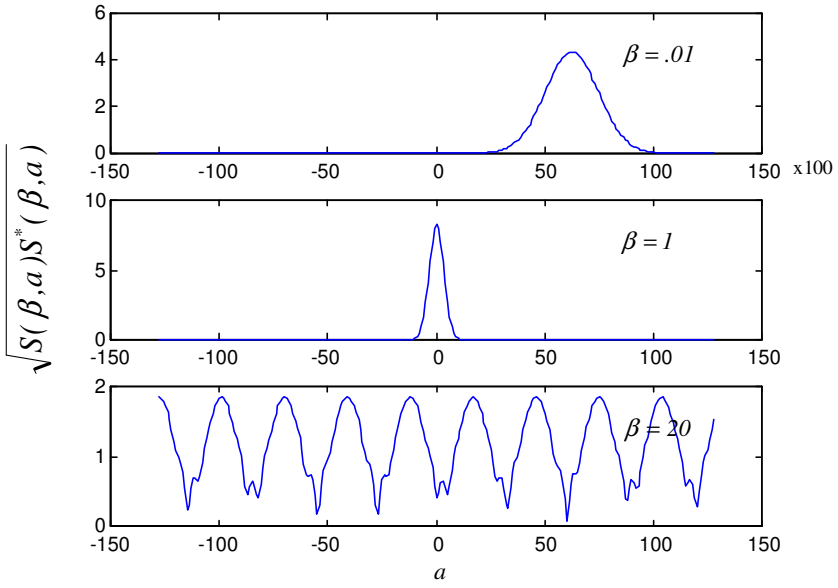

Fig. 4.4. (c) Chirp transform of a Gaussain windowed chirp

The signal can be reconstructed from any one of these axes since the synthesis is not unique. This redundency in signal representation can be used to isolate components and precisely represent them. For example, let a dictionary *A* contain the words *go, and* and *bring,* and let another dictionary *B* be redundant, containing the words *go, and, bring* and *fetc*h. If we use *A* to form a sentence using *go and bring*, we require three words. Where as if use B, the same idea can be conveyed with either three words or one word *fetch*. Hence, we can convey the meaning more precisely with dictionary *B,* whereas it is possible only in one way with dictionary *A*.

4.5. APPLICATIONS

Signal analysis in the transform domain is of importance, since it paves the way for application of various spectral estimation techniques and the interpretation of the signal in the transform domain leads to different applications. Spectral estimation based on WVD and optimized STFT are considered and system identification that demonstrates the chirp transform as a denoising tool will also be considered.

4.5.1. Spectral Estimation

Spectral estimation is concerned with estimating the true spectrum of the desired component of the signal in a multicomponent scenario or under noisy conditions. The objective of any TFR to concentrate the energy along the instantaneous frequency cannot be attained unless some processing of the signal is done. In order to estimate the true spectrum of a signal, we can utilize the information in the chirp transform to isolate individual components and then apply any TFD to the separated component. Since the transformation is redundant, it is extremely difficult to separate the individual components at the same time. We need to look for either a local maxima or a global

maxima to detect that component of the signal which generates it. Then, the component is estimated by the synthesis procedure and subtracted from the signal. Now the effect of the isolated component is eliminated and the transform gives a less complex representation. This divide and conquer approach, similar to the idea behind matching pursuits, can be continued until all the components are identified or the residue left out does not give rise to a local maxima, which implies that the residue does not match with the expansion set and cannot be represented precisely. To demonstrate this idea, we take up analyzing the test given in (Jones *et al*, 1994a) that consists of two impulses, two rectangular gated sinusoids of different frequencies and a Gaussian signal. We add two more components: two parallel Gausssian windowed chirps with one component intersecting in time and frequency with that of the gated sinusoid of higher frequency. The test signal used and its WVD are shown in Fig. 4.5.

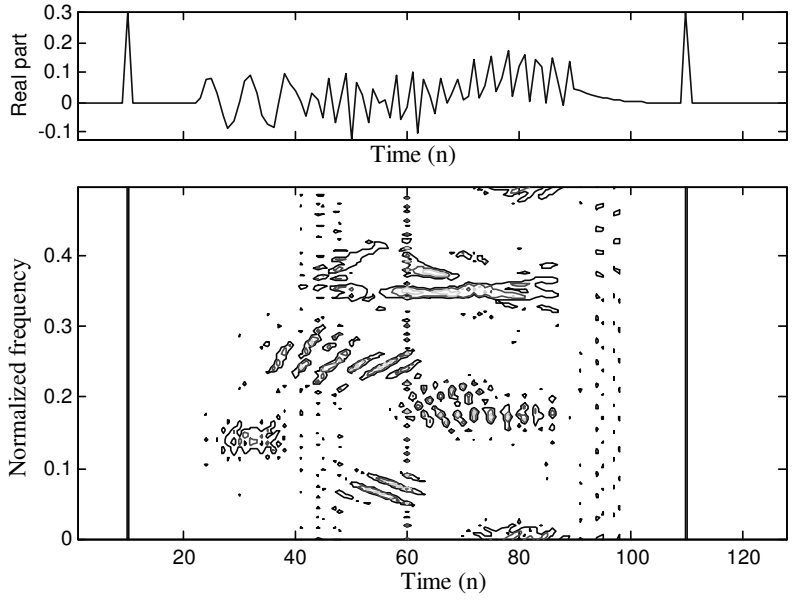

Fig. 4.5. A test signal consisting of two impulses, two rectangular windowed sinusoids, two Gaussian windowed chirps and a Gaussian signal and the WVD of the test signal

Apparently it is visible that signal has many components and separation into individual components is difficult using conventional techniques. The magnitude of the chirp transform of the test signal at two local maxima ($\beta = 0.01, 1$) and at $\beta = 20$ is shown in Fig. 4.6.

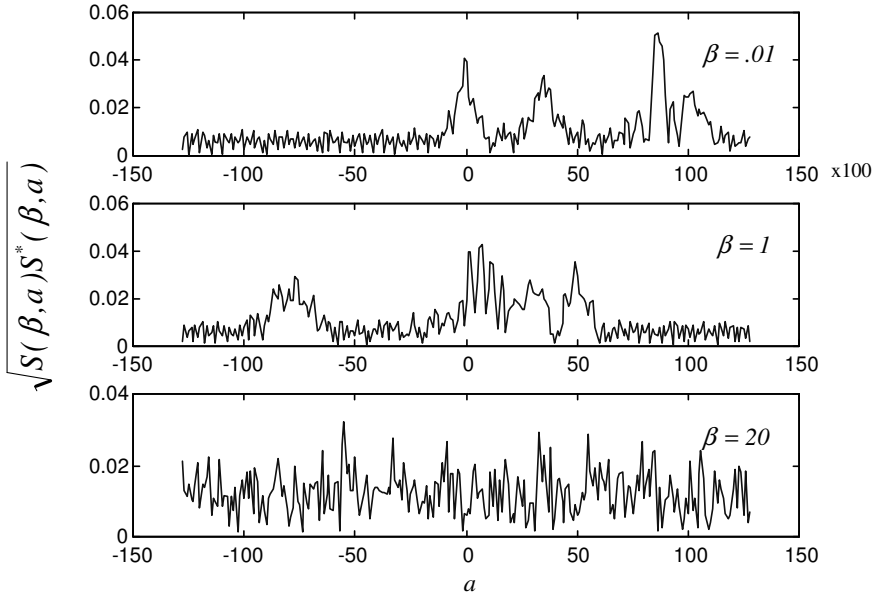

Fig. 4.6. Chirp transform of the test signal

The components are clearly visualized in the transform domain and can be identified by windowing. We can estimate the component we are interested in by using these modified coefficients along the axis corresponding to the component and by substituting in the synthesis equation. The Gaussian signal (orthogonal along $\beta = 0.01$) estimated by windowing the transform coefficients at $\beta = 0.01$ is shown in Fig. 4.7, together with the test signal. The magnitude of the transform, after the estimated signal has been removed, is depicted in Fig. 4.8.

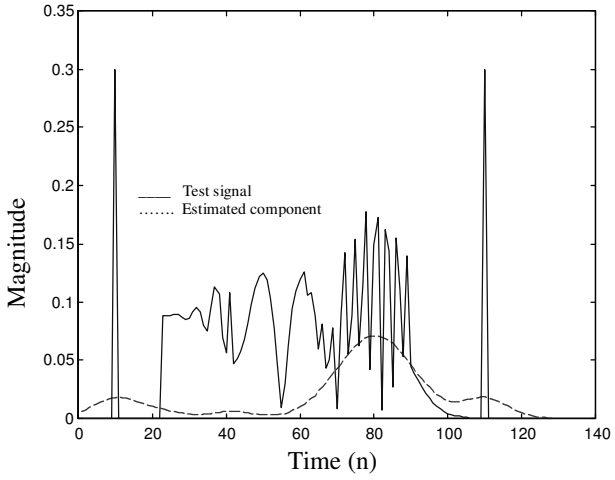

Fig. 4.7. Magnitude of the test signal and the estimated component

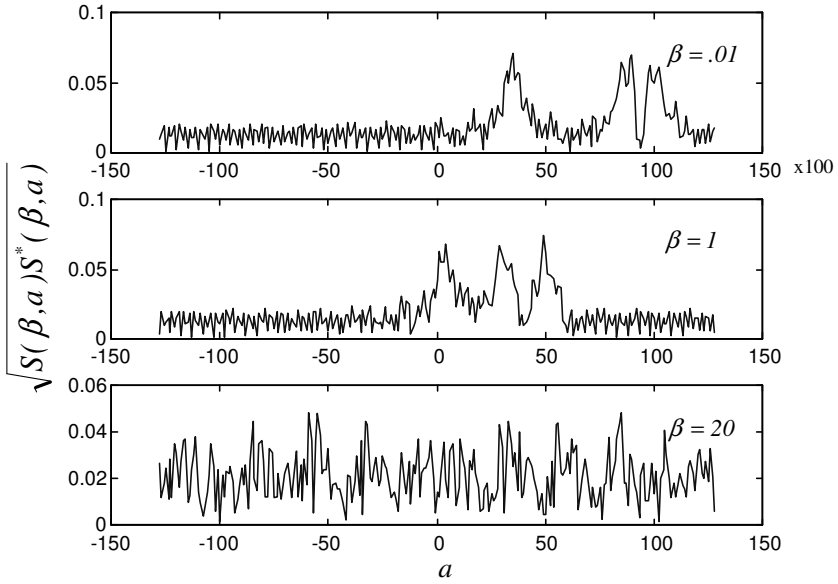

Fig. 4.8. Chirp transform after the estimated component is removed

It can be clearly observed from the above figure that the eliminated component simplifies the analysis procedure. The processed signal is again transformed and the same procedure is repeated until all the components are identified. After four iterations, the magnitude of the transform along the same axis is depicted in Fig. 4.9.

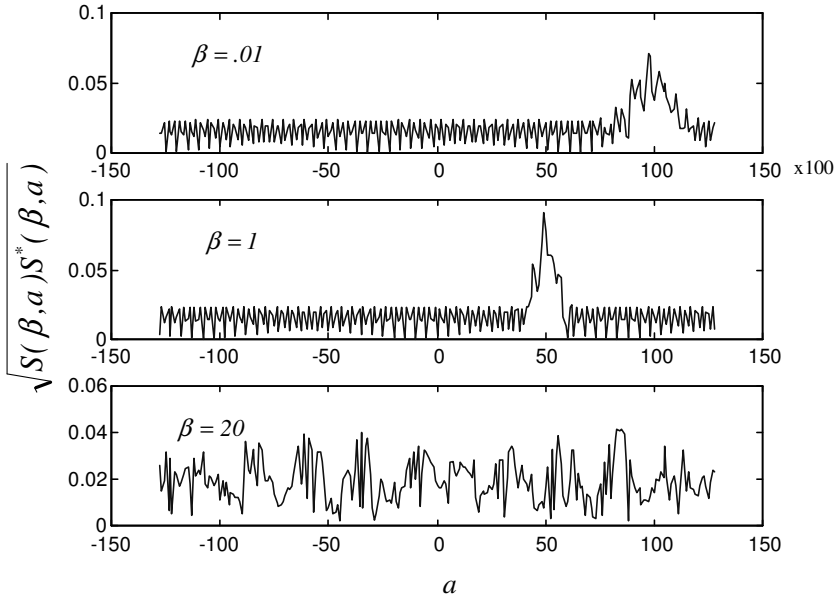

Fig. 4.9 Chirp transform after four iterations

Since it neither gives a local nor a global maxima, we stop the iterative analysis followed by synthesis and approximate the signal as a linear combination of the estimated components and the residue. The WVD of the residue that essentially consists of two impulses after five iterations (which means that five components are identified) is shown in Fig. 4.10. Applying the WVD to each isolated component gives the spectrum of the signal with maximum auto term resolution and almost no cross terms, as the WVD attains maximum resolution in the time and the frequency domains simultaneously among all bilinear distributions. Applying WVD to a signal having *N* components, we get

$$WVD(s_\beta) = \sum_{i=1}^{N} WVD(s_i, s_i) + \sum_{i=1}^{N} \sum_{j=1 i \neq i}^{N} WVD(s_i, s_j). \tag{4.23}$$

The auto terms exactly represent the true spectrum (cross terms can be completely neglected because the components are identified) and the resulting simple scheme could be a non-invertable representation given by

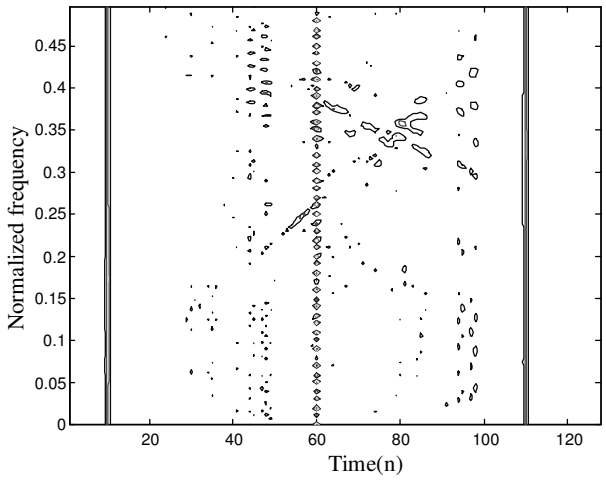

Fig. 4.10. WVD of the residue

$$WVD(s_\beta) = \sum_{i=1}^{N} WVD(s_i) \ . \tag{4.24}$$

However, such a procedure may be misleading while analyzing nonlinear FM signals which result in cross terms even in the absence of other components. To alleviate this problem, we may use short time Fourier transform with optimized window parameter. It directly follows from Eqn. (4.24) that

$$STFT(s_\beta) = \sum_{i=1}^{N} STFT(s_i) \tag{4.25}$$

To find the optimal window parameter, we use the concentration measure (Jones *et al*, 1994a)

$$M(t,a) = \frac{\iint \left| STFT_a(\tau,\omega)\, w(\tau - t) \right|^4 d\tau\, d\omega}{\left(\iint \left| STFT_a(\tau,\omega)\, w(\tau - t) \right|^2 d\tau\, d\omega \right)^2}, \tag{4.26}$$

that essentially searches for the window parameter which results in concentrated representation in the frequency direction, where $STFT_a(\tau,\omega)$ is the $STFT$ of the signal; the analysis window with the parameter γ is given by:

$h(t) = (\frac{\gamma}{\pi})^{\frac{1}{4}} e^{-\frac{\gamma t^2}{2}}$ and $w(t)$ is a symmetric window function to measure the concentration in a specified region (it is not the analysis window used in STFT). This window parameter is searched over all time instants. In our problem, we have considered the parameter as the amplitude modulation law, which is indirectly the window length (noting that the tails of a Gaussian pulse can be neglected outside the interval spanning a length of thrice the standard deviation). We wish to compute the integral in Eqn. (4.26) for the expansion set. Instead of computing the above equation directly, we can further simplify the concentration measure by observing the following characteristics of the expansion set:

The expansion set at a particular β has the same time dependent frequency spread and it does not vary with time. To illustrate this point, let us consider a signal of the form

$$s(t) = \left(\frac{\alpha}{\pi}\right)^{\frac{1}{4}} e^{-\frac{\alpha t^2}{2}+j\frac{\beta t^2}{2}}.$$

Then the spread in frequency at a given time is given by:

$$\sigma^2_{\omega/t} = \frac{1}{2}(\alpha+a)+\frac{1}{2}\frac{\beta^2}{\alpha+a}. \qquad (4.27)$$

Since it does not vary with over time and is also invariant in frequency shift in the signal spectrum, we can confine our search for the window parameter to a single time instant t_0. Thus, the modified concentration measure can be given as:

$$M(a) = \frac{\int \left| STFT_a(t_0, \omega) \right|^4 d\omega}{\left(\int \left| STFT_a(t_0, \omega) \right|^2 d\omega \right)^2}. \tag{4.28}$$

The parameter that maximizes this measure for various values of chirp rates have been found experimentally and are shown in Fig. 4.11.

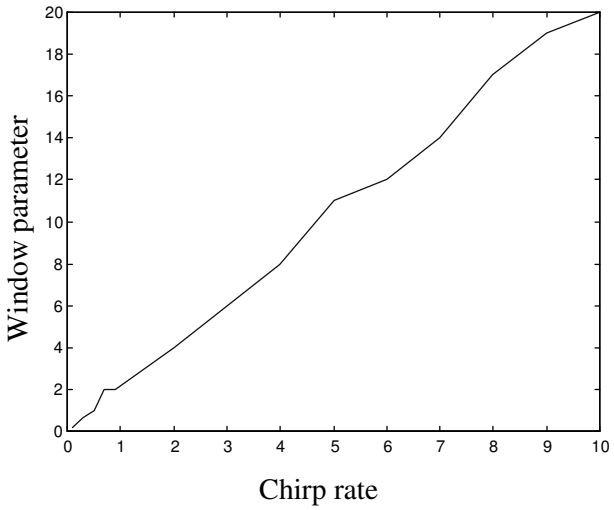

Fig. 4.11 Window parameter estimated from Eqn. (4.28)

It can be observed from the figure that the window parameter is almost varying linearly with the chirp rate. It can be analytically justified as follows:

For slowly varying signals, i.e., $\beta \approx 0$, the signal is almost stationary and the window can be of infinite length, i.e., $a \approx 0$. For highly nonstationary signals, like an impulse, where $\beta \approx \infty$, the window should be very small to localize the signal in time, i.e., $a \approx \infty$. Now, we will mathematically validate the result by recalling that the optimal window parameter can be obtained by minimizing the time dependent frequency spread. For purely frequency modulated signals, the optimal window parameter is given by (Cohen, 1995):

Optimal window length $\approx \frac{1}{2\left|\varphi''(t)\right|}$, where $\varphi(t)$ is the phase of the signal. The above method of computing the optimal window also results in the same value that the parameter *a* is linearly varying with β. STFT of a multicomponent signal and chirp transform of the signal are shown in Fig. 4.12.

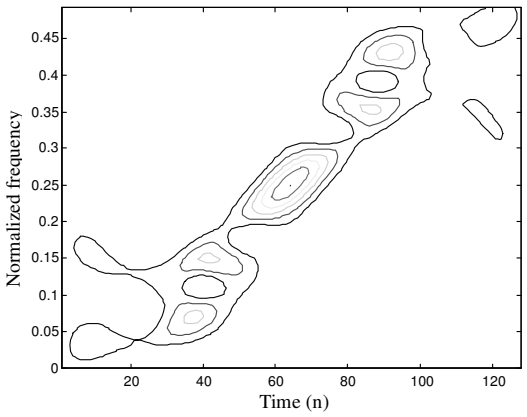

Fig. 4.12. (a) STFT of a multicomponent signal consisting of a sinusoidal FM and a linear FM components

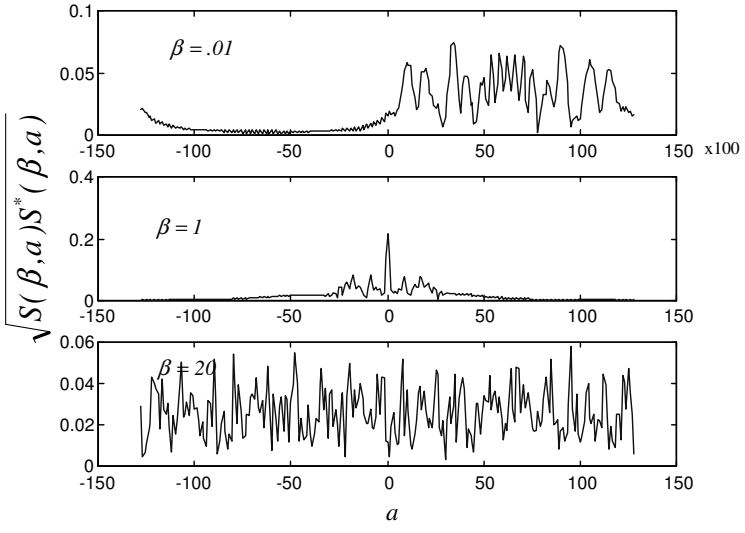

Fig. 4.12 (b) Chirp transform of the multicomponent signal

Using the iterative estimation of the component, we can isolate the linear FM component that generates the local maxima, as is clearly visible from the above figure. We can apply WVD to the estimated component but applying WVD to the residue may result in cross terms. Hence we use the optimized STFT to the residue. The WVD of the estimated component and optimized STFT of the residue are shown in Fig. 4.13.

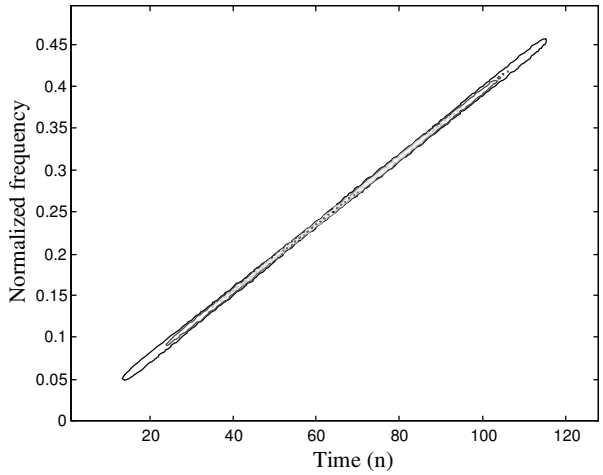

Fig. 4.13. (a) WVD of the estimated component

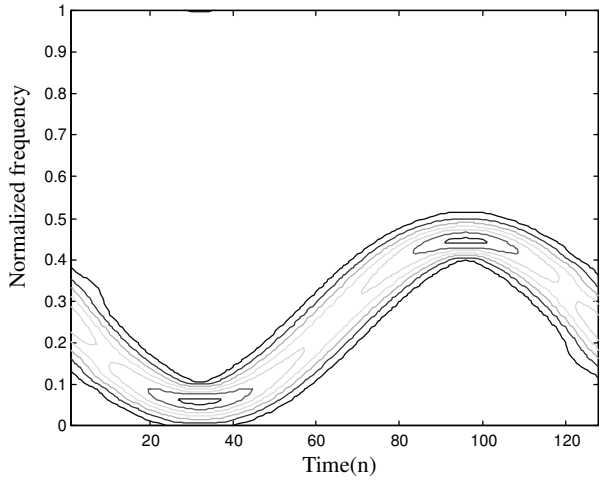

Fig. 4.13. (b) Optimized STFT of the residue

4.5.2. System Identification

System identification is a classical problem in signal processing which has many applications in many fields, including channel estimation in wireless communications. In general, the problem can be stated as follows:

$y(n) = \sum_k x(k)\, h(n-k) + v(n)$, where

$x(n)$: Transmitted signal.

$h(n)$: Impulse response of an LTI channel.

$v(n)$: Zero-mean additive Gaussian noise.

$y(n)$: Received signal with noise.

$\breve{y}(n)$: Received signal without noise (true signal).

The problem is to identify the linear time-invariant (LTI) system transfer function $H(\omega)$ of $h(n)$, given the input and output signals. The conventional method of solving this problem is the cross spectral method, which is equivalent to the least squared method in stationary cases, and can be formulated as

$H(\omega) = \frac{S_{xy}(\omega)}{S_{xx}(\omega)}$, where $S_{xx}(\omega)$ is the auto spectrum of $x(n)$ and $S_{xy}(\omega)$ is the cross spectrum of $x(n)$ and $y(n)$. If the additive noise is a zero-mean Gaussian process and statistically independent of the signal $x(n)$, then the estimate is asymptotically unbiased and its error variance approaches the Cramer-Rao lower bound. However, noise removal is not possible if the known transmitted signal were the pseudo random signal, which is correlated with the noise. Xia (Xia, 1997) has considered chirp signals instead of pseudo random signals for their wideband characteristics and localization in the joint time-

frequency plane making the uncorrelated additive Gaussian noise removal possible and observed an improvement of 15dB over conventional system identification techniques. In the present context, we try to use chirp transform as a denoising tool, which is schematically shown in Fig. 4.14

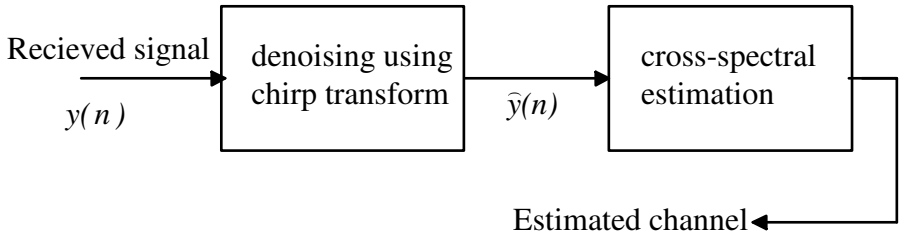

Fig. 4.14. System identification using chirp transform as a denoising tool

Mask design: If we attempt to remove the noise in the joint time-frequency plane, it has to be done by observing the pattern of the received signal and noise. As noise occupies the whole spectrum and any received signal spectrum is dominated by the known transmitted signal, we can design a mask to eliminate the noise components. In the chirp transform domain, we concentrate in the region corresponding to the transmitted signal for the following reason (Xia, 1997):

Assume the chirp signal $x(n) = exp(j\beta n^r)$ for some constants $r \geq 2$ and $\beta \neq 0$,

then

$$\begin{aligned} \breve{y}(n) &= \sum_k h(k)\, x(n-k) \\ &= \sum_k h(k)\, exp(j\beta (n-k)^r) \\ &= exp(j\beta n^r) \sum_k h(k)\, exp\left(j\beta \sum_{l=0}^{r-1} \binom{r\text{-}1\text{-}l}{l} n^l k^{r-l}\right) \end{aligned} \tag{4.29}$$

which is dominated by the original chirp *x(n)* for finite tap LTI systems *h(k)*. As a special case, when r =2, $\breve{y}(n) = x(n)G(2\beta n)$, where $G(\omega)$ is the Fourier transform of the signal $h(n)x(n)$. When the channel *h(n)* has only a finite tap, the function $G(\omega)$ is usually smooth. Since the transmitted signal was known to both the transmitter and the receiver, by the above property, its pattern in the transform domain may help in designing the mask for filtering noise. The mask cannot be designed based on the characteristics of the input signal, because the expansion set is strongly correlated with the input signal and the resulting mask that concentrates the transform in the vicinity of the input signal is very much localized. The spectral characteristics of the input signal can only be used to determine the location of the mask. Hence, thresholding (or masking in the transform domain) is done in a conservative manner. Our experiments have revealed that to model (or estimate) any channel that is an LTI system, soft thresholding the coefficients can be done by choosing a Gaussian window of length 50 which is appropriate. True channel characteristics and the estimated channel using cross-spectral estimation are shown in Fig. 4.15. The chirp transform of the received signal at $\beta = 1$ at *0*dB *SNR* and the masked transform are shown in Fig. 4.16. Then, the received signal is synthesized from this modified transform to obtain the denoised signal. The synthesized signal from the modified chirp transform is now used to estimate the channel by cross-spectral estimation. The estimated channel after denoising and the received signal after denoising together with received signal under no noise conditions, are shown in Fig. 4.17. To obtain the mean *SNR* curves, we have repeated the experiment over 100 iterations by varying the channel and the noise. The mean SNR curves for different original *SNR*, and the *SNR* after denoising, are shown in Fig. 4.18.

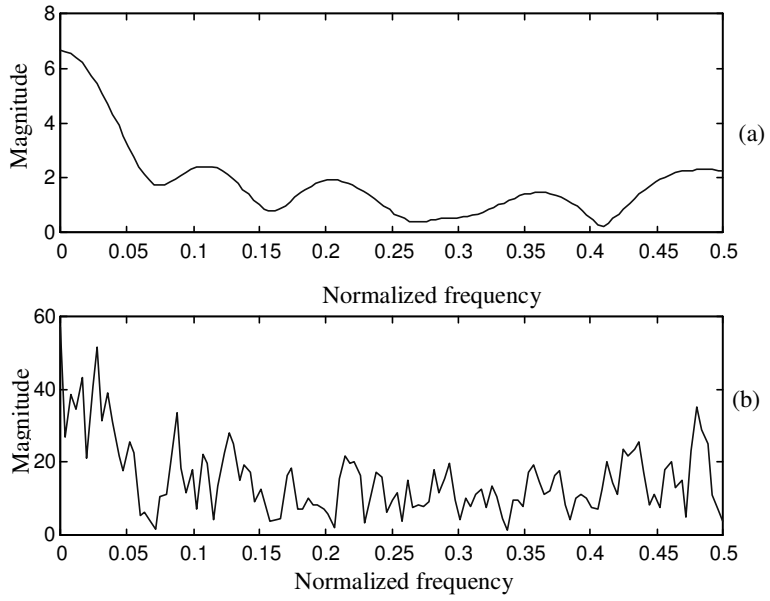

Fig. 4.15. (a) True channel characteristics and (b) The estimated channel using cross-spectral estimation method

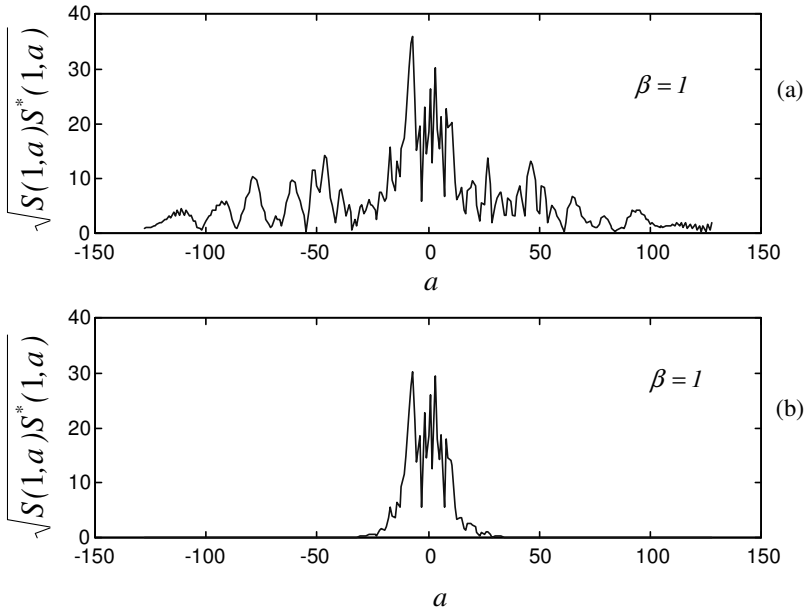

Fig. 4.16. (a) Chirp transform of the received signal at $\beta = 1$ and (b) The masked transform

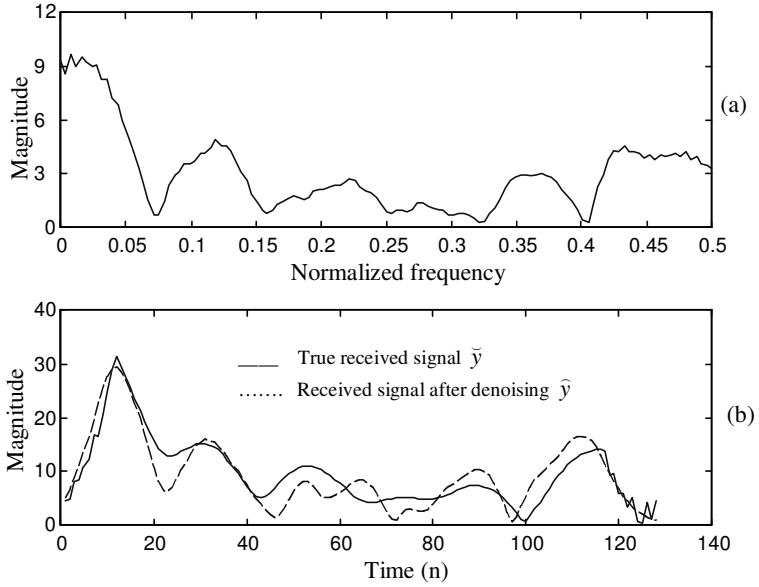

Fig. 4.17. (a) Estimated channel after denoising done using chirp transform and (b) True received signal $\hat{y}$ and the received signal after denoising $\breve{y}$

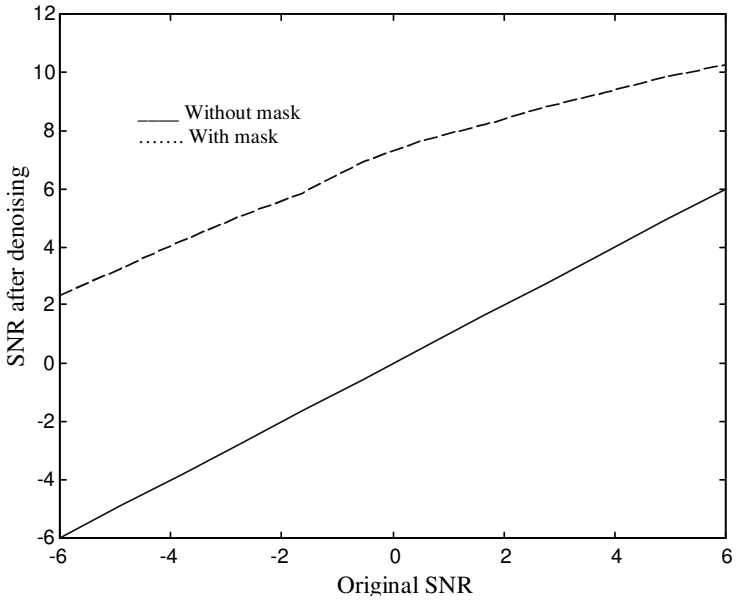

Fig. 4.18. Mean SNR curves with mask (denoising) and without mask (conventional cross-spectral estimation using chirp signal)

The *SNR*s in different cases can be computed as:

$$SNR_{Afer\ denoisnig} = 10\log_{10}\frac{\sum_{n}\left|\breve{y}(n)\right|^2}{\sum_{n}\left|\breve{y}(n)-\hat{y}(n)\right|^2} \text{ and}$$

$$SNR_{Original} = 10\log_{10}\frac{\sum_{n}\left|\breve{y}(n)\right|^2}{\sum_{n}\left|\breve{y}(n)-y(n)\right|^2}. \quad (4.30)$$

It can be observed from Fig. 4.18 that there is a declinement in the *SNR* improvement with increasing original *SNR*. This has been accounted for the fact that soft thresholding allows the noise components that sit in the region corresponding to the transmitted input signal and that the noise suppression capability of the chirp transform lies in rejecting all components which lie *outside* the region of the input signal. In the method proposed by Xia, *iterative time-variant filtering* that progressively improves the *SNR* has been used. However, in the chirp transform domain such a repeated analysis followed by synthesis aiming at reducing the noise did not result in a significant improvement. The reason being:

The noise components that interfere with the signal components cannot be masked in the chirp transform domain and it can be done if and only if the true mask (the mask that exactly separates the noise components from the signal) is known.

As a logical extension of the above algorithm, the role of the signal is now replaced by interference and we may use chirp transform as an exciser for chirp-like interference in spread spectrum communication. Akansu and Bultan (Bultan *et al*, 1998) have shown that when the interference is strongly correlated with the basic atoms, chirps in the present

case, interference excision is possible and demonstrated that it outperforms the Fourier-based excision techniques.

4.6. CONCLUSIONS

In this Chapter, we have developed chirp transform with chirps as the expansion set. The orthogonality of the expansion set, reconstruction of the signal using synthesis equation and discretization issues are considered. Some simple properties like shifting in time, frequency and variation of the envelope are discussed. Different signals, e.g., impulse, sinusoid and chirps are analyzed in the transform domain to enable us to investigate nonstationary signals. With the help of a multicomponent test signal, iterative analysis-synthesis based estimation technique that has the origin in adaptive signal decomposition is investigated. To estimate the frequency content of the residue, optimized window parameters for STFT are obtained using a much simplified concentration measure. Later, the problem of system identification has been addressed, where we demonstrate chirp transform as a denoising tool and observe significant improvement over conventional system identification.

CHAPTER 5

CHIRPLET DECOMPOSITION

5.1. INTRODUCTION

Of the many possible solutions that exist for analyzing signals in different domains by going beyond time and frequency, the promising ones are those which adapt the tilings in the time-frequency plane. However, much effort has been laid in constructing a proper representation of the signal in time and frequency, e.g., adaptive TFRs, optimized STFT, signal decomposition in terms of fixed set of time-frequency atoms, etc., because of their easy interpretation as well as computation. The successful application of time-frequency analysis methods has stimulated recent interest in considering representations that tile the time-frequency plane in a nonrectangular fashion in which case the existing methods are inappropriate. The shear in frequency and shift in time subspace considered in the earlier chapter is one such analysis methodology. As one should essentially operate on a non-finite vocabulary, estimating the parameters is a difficult task but it gives a better representation. The solution is to choose a dictionary of finite vocabulary and then project the signal onto the space spanned by the dictionary. However, unless we assume some apriori information about the characteristics of the signal under analysis, the residue will be of more energy. Atomic decomposition, chirp hunting are such approaches (Bultan, 1999 and O'Neil *et al*, 1998). It is the purpose of the present work to find a robust mechanism that adapts the tilings to suit the signal's characteristics and eliminate the

difficulties associated with finite size dictionaries. The outline of the algorithm is as follows:

We try to decompose/synthesize a signal as a linear combination of Gaussian chirplets. The computed / specified spectrogram of the signal to be analyzed/synthesized is modeled as a mixture of normal densities. This modeling of spectrogram as a mixture of normal densities is accomplished using the incremental variant of the Expectize-Maximize (EM) algorithm. K-means clustering algorithm is used to pass initial estimates to EM algorithm and the realizations corresponding to the normalized spectrogram are generated using band-rejection algorithm. After the t-f plane is well modeled, we derive a set of mapping rules that synthesize the signal corresponding to the component.

5.2. CHIRPLETS

It is known that the Fourier transform represents a signal as a linear combination of the weighed complex exponentials (waves). Similarly, wavelet transform expands a signal in terms of the scaled and shifted versions of the mother wavelet. In simple terms, a wavelet is an amplitude modulated version of the wave with a rapidly decaying envelope and when it satisfies certain criteria (like the admissibility condition, etc.) we call it a mother wavelet. The waves localize the events in frequency and wavelets offer varying time-frequency resolutions as discussed in Chapter 2. For signals of fractal in nature, these representations perform better than Fourier transform-based representations. However, the tilings are not adaptive and hence they also perform prominently only for certain classes of signals. In an attempt to motivate ourselves to tile the time-frequency plane in a nonrectangular fashion and generalize all existing classes, we have considered chirps

which act as shear operator in frequency (convolving with a chirp in time domain causes shearing in time direction) in the earlier chapter. As wavelets are to waves, chirplets are to chirps (shown in Fig. 5.1). Different tilings obtained by choosing different atoms are depicted in Fig. 5.2.

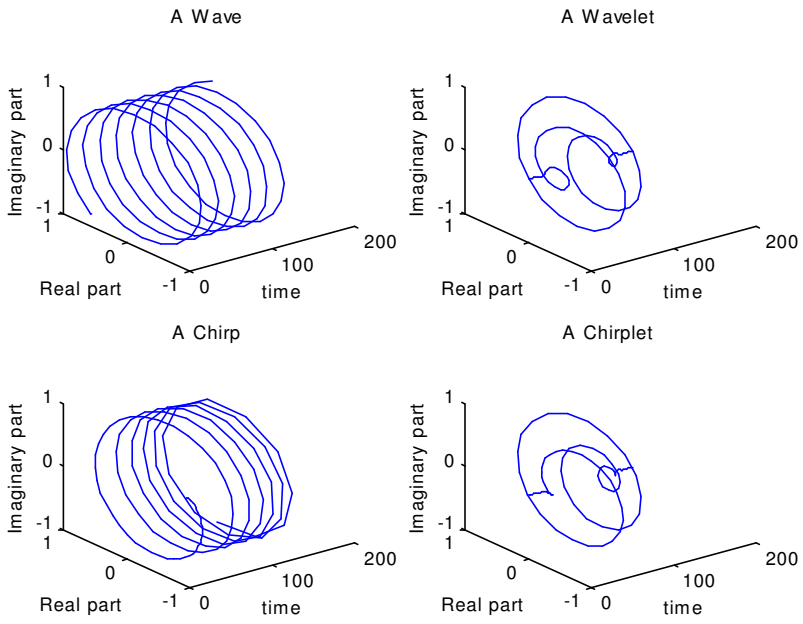

Fig. 5.1 Different atoms considered for signal analysis

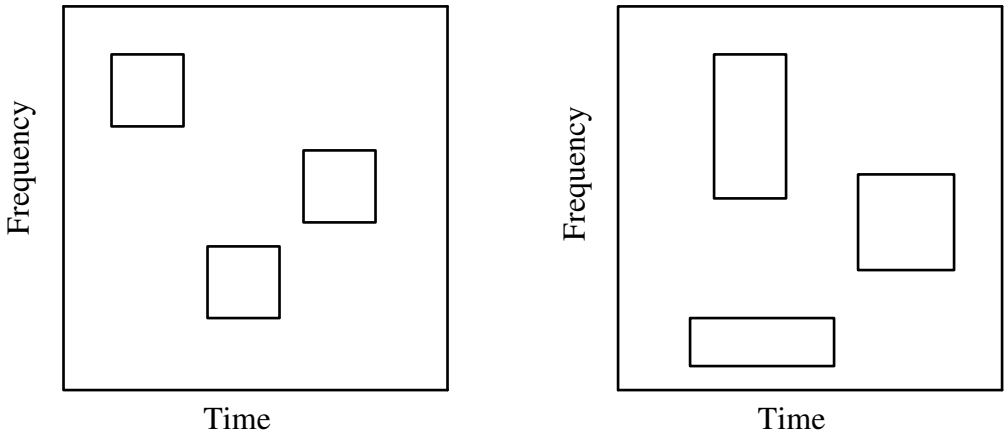

(a) **(b)**

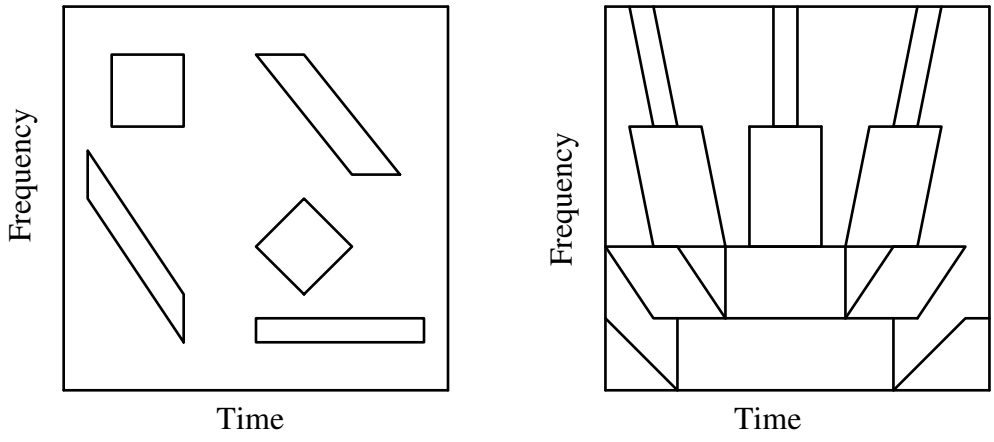

(c) **(d)**

Fig. 5.2. Time-frequency tilings obtained by (a) STFT, (b) Wavelet analysis, (c) Chirptlet decomposition and (d) Shear-time representation

It can be observed from Fig. 5.2(a) that employing constant windows in the STFT analysis tile the time-frequency plane in a fixed manner, i.e., rectangular throughout. However, the wavelets being proportional bandwidth representations go on scaling the analysis grid and yet maintain the same area (any arbitrary tiling obtained as a result of modification in representing the scheme has to satisfy the uncertainty principle) shown in Fig. 5.2(b). Employing chirplets to decompose a signal unifies the above tilings as shown in Fig. 5.2(c), i.e., rotation, shearing, scaling and shifting. The tilings obtained by convolving with a chirp are exemplified in Fig. 5.2(d). Hence, we proceed with the following assumption that any signal can be represented as a weighed sum of Gaussian chirplets given by:

$$s(t) = \sum_{i} c_i \, g_i(t; t_c, f_c, \beta, \alpha) \quad , \tag{5.1}$$

where

$$g_{t_c,f_c,\beta,\alpha}(t) = \left(\frac{\alpha}{\pi}\right)^{\frac{1}{4}} e^{\frac{\alpha(t-t_c)^2}{2}} e^{j\beta(t-t_c)^2/2 + j\omega_c(t-t_c)}. \quad (5.2)$$

The parameters t_c, f_c, β and α represent, respectively, the location in time, the location in frequency, the chirp rate and the amplitude modulation parameter; and *g* is defined such that

$$\left\| g_{t_c f_c,\beta,\alpha} \right\|^2 = \int |g(t; t_c, f_c, \beta, \alpha)|^2 dt = 1. \quad (5.3)$$

There exists different methodology to construct nice wavelets and so as with chirplets eventhough the latter was not extensively investigated. We have considered the Gaussains for simplicity sake and tractability in evaluation. Moreover, they are the ones which meet the equality sign in uncertainty principle which states that if two functions $f(t)$ and $F(\omega)$ form a Fourier integral pair, then they both cannot be short of duration, i.e., $Dd \geq \frac{1}{2}$ where

$$d^2 = \frac{1}{E}\int t^2 |f(t)|^2 dt,\ D^2 = \frac{1}{2\pi E}\int \omega^2 |F(\omega)|^2 d\omega \text{ and } E = \int |f(t)|^2 dt. \quad (5.4)$$

Now our objective is to find the parameters of these chirplets by modeling the t-f space as a mixture of normal pdfs. It requires interpretation of the spectrogram as an arbitrary bivariate pdf which would be modeled as a mixture of normal pdfs.

5.3. MIXTURE MODELING

Any random signal space can be modeled by a mixture of normal densities which is commonly known as mixture modeling. The arbitrary pdfs can be represented as a weighed combination of the normal pdfs as

$$f_X(x) = \sum_{i=1}^{N} \lambda_i \, f_i(x;\theta_i), \tag{5.5}$$

where x is the random vector with histogram specified by the spectrogram, N the number of normal distributions $f_i(x;\theta_i)$, where θ_i is the parameter vector of the i^{th} component consisting of the mean vector μ_i and covariance matrix $\sum_i$ and λ_i are the mixing weights, constrained to be positive and unity sum. In general, there are an infinite number of different *M*–mixture Gaussian densities that can be used to tile up the signal space. Hence, modeling the signal space can be regarded as a many-to-one, non-invertible mapping. The tractability in estimating the component parameters is due to the availability of the tools like the EM algorithm. Recently, t-f plane was modeled using the finite mixture modeling given in (Coates *et al*, 1998) to facilitate separation of multicomponent signals. To model the t-f space by means of mixture modeling, we first have to generate realizations that will drive the EM algorithm in such a way that their histogram resembles the spectrogram to be modeled. At first it may appear strange that we are tying to view the t-f space as a mixture of normal pdfs by applying a random process modeling technique to a deterministic problem. However, we are using it just as a means to accomplish the task of decomposing the signal into chirplets. We will consider the random vector (RV) generation in the following subsection.

5.3.1. Random Vector Generation

Generation of random vectors (RVs) for the specified bivariate pdf requires interpretation of the spectrogram as an arbitrary bivaraite pdf. Hence, we need to normalize the time dependent spectrum in such a way that it obeys the fundamental relation that a pdf should satisfy, i.e., integrating a pdf should give rise to one. The normalization can be done as follows:

Let $SP(t,\omega)$ be the spectrogram of the signal under analysis, $S_t(t)$ the time marginal and $S_\omega(\omega)$ the frequency marginal. Then, the normalization of the spectrogram should be done in such a way that:

$$\int S_t(t)\,dt = 1, \int S_\omega(\omega)\,d\omega = 1, \int SP(t,\omega)\,dt = S_\omega(\omega) \text{ and } \int SP(t,\omega)\,d\omega = S_t(t). \tag{5.6}$$

Then, the marginals of the scaled spectrogram are given by:

$$S_t^{modified}(t) = \frac{S_t(t)}{\iint SP(t,\omega)\,dt\,d\omega} \text{ and } S_\omega^{modified}(\omega) = \frac{S_t(t)S_\omega(\omega)}{\int S_\omega(\omega)\,d\omega} \;\forall\, S_t(t) \neq 0. \tag{5.7}$$

Now our task is to generate realizations corresponding to this scaled spectrogram. There exist different algorithms to generate RVs, namely, conditional pdf method, rejection algorithm, inverse transformation, etc (Devroye, 1986). The conditional pdf method is quite useful when we do not have closed form expressions for the conditional pdf and the disadvantage is that we cannot exploit any apriori information or speed up the procedure in generating the samples (or realizations). Whereas the band-rejection algorithm works on acceptance-rejection criteria that is one way sampling a target pdf to obtain the desired pdf, where target pdf is a pdf close to the desired pdf. The Band-rejection

algorithm is described in Table 5.1. It is essentially a sampling scheme that accepts the samples from the target pdf depending upon an acceptance criterion and associates them to the desired pdf. The rejection ratio defined in the algorithm determines the speed at which we can generate the desired realizations. A lesser rejection ratio means the target pdf is close to the pdf we wish and the ideal rejection ratio is one. In the present context of mixture modeling it serves two-fold purposes: Firstly, the lesser rejection ratio speeds up the process of RV generation and secondly it is a measure of our initial estimate in the modeling phase. Hence, the difficult task is in choosing a good target pdf that results in a lesser rejection ratio. Since we are dealing with mixture of bivarite normal densities, we should have an efficient way of generating samples for a normal bivarite pdf and then shuffle the samples of individual realizations according to the mixture probabilities. This algorithm can be found in generating realizations for a given Hidden Marokov Model (HMM), called Toy-Markov model generator (Rabiner *et al*, 1993). It is very logical to borrow the concept from Toy-Markov generator to compute realizations for the mixture density because we can consider the mixture density to be a one state HMM. Once the realizations for all the components in the mixture are generated, we can mix the realizations in a specified manner to obtain the realizations for the mixture density. The algorithm is described in Table 5.2. We review the EM algorithm in the following subsection.

5.3.2. EM Algorithm

It has long since been recognized that computing the maximum-likelihood (ML) parameter estimates can be a highly complicated task in many relevant estimation problems. The EM algorithm presented by Dempster et al (Dempster *et al*, 1977) is a

Table. 5.1: Band-rejection algorithm for generating random vectors of a specified pdf

---

Step-1. Initialization:

- Target pdf: $g(\mathbf{y})$
- Desired pdf (spectrogram to be modeled): $f(\mathbf{y})$
- A uniform distribution in the interval *[0,1] : U [0,1]*
- Rejection ratio: $R = max \frac{g(\mathbf{y})}{f(\mathbf{y})} \ \forall \ f(\mathbf{y}) \neq 0$
- Number of samples required: N
- set $i=0$ and $j=0$;

Step-2. Accept-Reject:

- Select a sample from uniform distribution : $r \sim U[0,1]$
- Select a sample from target pdf : $[\ \mathbf{y}_i\ ] \sim g(\mathbf{y})$
- *if* $r < R\frac{g(\mathbf{y}_i)}{f(\mathbf{y}_i)}$ *then* $j=j+1$;

  Associate the sample $[\ \mathbf{y}_i\ ]$ *with* $f(\mathbf{y})$,

  if $j < N$ go to step-3

  else stop.

else go to step-3;

Step-3. Loop:

- Repeat until N samples from $g(\mathbf{y})$ are associated to $f(\mathbf{y})$: $i=i+1;$ go to step-2.

Table. 5.2: Generation of RVs for a specified mixture of normal pdfs

Step-1. Initialization:

- For i=1:M, generate N_i realizations for the i^{th} component of the target pdf: where $N_i \geq \lambda_i N$.
- Partition the uniform random variable *U [0,1]* into *M*-segments according to the probability given by λ

Step-2. Mixing:

- Select a sample from uniform distribution : $r \sim U[0,1]$
- If the sample falls in the i^{th} segment, select a sample from i^{th} component of the mixture $g(\mathbf{y})$

Step-3. Loop:

- Repeat *step-2* until *N* samples for $g(\boldsymbol{y})$ are generated

general iterative method to compute ML estimates if the observed data can be regarded as "incomplete", like the formulation of $\boldsymbol{y} = h(\boldsymbol{x})$, where *h* is a noninvertible transformation and $\boldsymbol{x}$ is the complete data. As finding the ML estimates of θ by maximizing $ln\, f(\boldsymbol{y};\theta)$ is too difficult, we maximize $ln\, f(\boldsymbol{x};\theta)$. Since we do not have access to the complete data, at best we can maximize the conditional expectation of the complete data log-likelihood, given the incomplete data $\boldsymbol{y}$. This is given by

$$E\,[ln\, f_{X;\Theta}(\boldsymbol{x},\theta)/\,\boldsymbol{y}\,] = \int_X f_{X/Y;\Theta}(\boldsymbol{x}/\boldsymbol{y};\theta)\, ln\, f_{X;\Theta}(\boldsymbol{x};\theta)\, dx\,. \tag{5.8}$$

In the above equation, computation of the term $f_{X/Y;\Theta}(\boldsymbol{x}/\boldsymbol{y};\theta)$ requires an estimate of the unknown parameter vector θ. For this reason, the expectation of the likelihood function is maximized iteratively starting with an initial estimate of θ, and updating the estimate as described in Table 5.3. It has been demonstrated in (Vaseghi, 1996) that each iteration of the EM algorithm improves the convergence of the likelihood function and is monotonically non-decreasing. Before we apply EM algorithm to mixture modeling problem, we need to define the complete data and the incomplete data.

Table 5.3: EM Algorithm

Step-1. Initialization:

- Select an initial parameter estimate $\hat{\theta}_0$, and
- For i = 0, 1, … until convergence

Step-2. Expectation:

- Compute $U(\theta,\hat{\theta}_i) = E[\ln f_{X;\Theta}(\boldsymbol{x};\theta)/\boldsymbol{y};\hat{\theta}_i]$

Step-3.Maximization:

- Select $\hat{\theta}_{i+1} = \arg\max_{\theta} U(\theta,\hat{\theta}_i)$

Step-4.Convergence:

- If not converged then go to *step-2*.

As usual the observation vectors form the incomplete data and the complete data may be viewed as the observation vectors with a label attached to each vector $\boldsymbol{y}(k)$ to indicate the component of the mixture that generated it. They are defined as:

Incomplete data (observed data): $\mathbf{y}(n)$ $n=0,1,\ldots N-1$.

Complete data (unobserved data) : $[\mathbf{x}(n)=\mathbf{y}(n)_k]$ $n=0,1,\ldots N-1$, $k \in (1,\ldots,M)$.

Now the probability of the complete data, given the observed data, is the probability that the observation vector has the label k. Hence the E-step in Table 5.3 can be written as:

$$\begin{aligned} U(\theta,\hat{\theta}_i) &= E[\ln f_{X;\Theta}(\mathbf{x}(n);\theta)/\mathbf{y}(n);\hat{\theta}_i] \\ &= E[\ln f_{X;\Theta}(\mathbf{y}(n),k;\theta)/\mathbf{y}(n);\hat{\theta}_i] \\ &= \sum_{n=0}^{N-1}\sum_{k=1}^{M}\frac{f_{Y,K;\Theta}(\mathbf{y}(n),k/\hat{\Theta}_i)}{f_{Y/\Theta}(\mathbf{y}(n)/\hat{\Theta}_i}\ln f_{Y,k;\Theta}(\mathbf{y}(n),k;\Theta), \end{aligned} \tag{5.9}$$

where $\Theta = \{\theta_k = [\lambda_k, \mu_k, \Sigma_k]\ k = 1,2,...,M\}$ are the parameters of the mixture density. The joint probability density function of $\mathbf{y}(n)$ and the k^{th} component of the mixture density is given by:

$$f_{Y,K;\Theta}(\mathbf{y}(n),k/\hat{\Theta}_i) = \lambda_{k_i}\ f_k(\mathbf{y}(n)/\hat{\theta}_{k_i}), \tag{5.10}$$

where $f_k(\mathbf{y}(n)/\theta_k)$ is a Gaussian density of mean vector μ_k and the covariance matrix Σ_k is given as:

$$f_k(\mathbf{y}(n)/\hat{\theta}_{k_i}) = \frac{1}{\sqrt{2\pi|\Sigma_k|}}\exp\left(-\frac{1}{2}(\mathbf{y}(n)-\mu_k)^T\Sigma_k^{-1}(\mathbf{y}(n)-\mu_k)\right). \tag{5.11}$$

The pdf of $\mathbf{y}(n)$ and the mixture of N Gaussian densities is given by:

$$f_{\mathbf{Y}/\Theta}(y(n)/\hat{\Theta}_i) = \sum_{k=1}^{M}\lambda_{k_i} f_k(y(n);\hat{\theta}_{k_i}). \tag{5.12}$$

Substitution of the Gaussian densities of Eqn. (5.10) and Eqn. (5.11) into Eqn. (5.9) yields

$$U(\theta,\hat{\theta}_i) = \sum_{n=0}^{N-1}\sum_{k=1}^{M}\frac{\hat{\lambda}_{k_i} f_k(\mathbf{y}(n)/\theta_{k_i})}{f_{\mathbf{Y}/\Theta}(\mathbf{y}(n)/\hat{\Theta}_i)} \ln[\lambda_k f_k(\mathbf{y}(n);\theta_k)]$$

$$= \sum_{n=0}^{N-1}\sum_{k=1}^{M}\left(\frac{\hat{\lambda}_{k_i} f_k(\mathbf{y}(n)/\theta_{k_i})}{f_{\mathbf{Y}/\Theta}(\mathbf{y}(n)/\hat{\Theta}_i)} \ln\lambda_k + \frac{\hat{\lambda}_{k_i} f_k(\mathbf{y}(n)/\theta_{k_i})}{f_{\mathbf{Y}/\Theta}(\mathbf{y}(n)/\hat{\Theta}_i)} \ln[f_k(\mathbf{y}(n);\theta_k)]\right) \tag{5.13}$$

To maximize the above equation, we should set the derivative of the likelihood function with respect to λ_k, μ_k *and* Σ_k to zero. The weight of the k^{th} component is given by:

$$\hat{\lambda}_{k_{i+1}} = \arg\max_{\lambda_k} U[\theta,\hat{\theta}_{i+1}]. \tag{5.14}$$

However, we should set the derivative to zero subject to the constraint that $\sum_{m=1}^{M}\lambda_k = 1$. As our constraint is an equality condition, we use the Lagrangean method of optimization (Rau, 1970) which can be formulated as described below:

Let the objective function be $f(x_1, x_2 ..., x_M)$ and constraint function be $g(x_1, x_2 ..., x_M)$. Define $L = f(x) - \zeta g(x)$, where ζ is the Lagrangean multiplier, which need be determined. To optimize *L,* set its partial derivative to zero, i.e., $\frac{\partial}{\partial x_i}(L) = 0$. Solving the expressions obtained by setting the partial derivatives of *L* to zero gives the optimal solution. This algorithm can be extended to cases involving multiple constraints. In the present context, our objective function is $U(\theta,\hat{\theta}_i;\lambda_k)$ and the constraint function is $\sum_{k=1}^{M}\lambda_k - 1 = 0$. Hence,

$$L = \sum_{n=0}^{N-1}\sum_{k=1}^{M}\left(\frac{\hat{\lambda}_{k_i} f_k(\mathbf{y}(n)/\theta_{k_i})}{f_{\mathbf{Y}/\Theta}(\mathbf{y}(n)/\hat{\Theta}_i)} \ln\lambda_k + \frac{\hat{\lambda}_{k_i} f_k(\mathbf{y}(n)/\theta_{k_i})}{f_{\mathbf{Y}/\Theta}(\mathbf{y}(n)/\hat{\Theta}_i)} \ln[f_k(\mathbf{y}(n);\theta_k)]\right) - \zeta\left(\sum_{k=1}^{M}\lambda_k - 1\right). \tag{5.15}$$

Setting the partial derivative with respect to λ_k to zero, we get

$$\frac{\partial L}{\partial \lambda_k} = \sum_{n=0}^{N-1} \left(\frac{\hat{\lambda}_{k_i} f_k(\mathbf{y}(n)/\theta_{k_i})}{f_{\mathbf{Y}/\Theta}(\mathbf{y}(n)/\hat{\Theta}_i)} \frac{1}{\lambda_k}) \right) - \zeta = 0. \tag{5.16}$$

The solution of the above equation is given by

$$\zeta = \sum_{n=0}^{N-1} \left(\frac{\hat{\lambda}_{k_i} f_k(\mathbf{y}(n)/\theta_{k_i})}{f_{\mathbf{Y}/\Theta}(\mathbf{y}(n)/\hat{\Theta}_i)} \frac{1}{\lambda_k}) \right) \quad for\ k = 1,2,....,M. \tag{5.17}$$

By equating the above expression for $k = a$ and $k = b$, we can represent λ_a in terms of λ_b as:

$$\lambda_b = \lambda_a \frac{\sum_{n=0}^{N-1} \left(\frac{\hat{\lambda}_{b_i} f_b(\mathbf{y}(n)/\theta_{b_i})}{f_{\mathbf{Y}/\Theta}(\mathbf{y}(n)/\hat{\Theta}_i)} \right)}{\sum_{n=0}^{N-1} \left(\frac{\hat{\lambda}_{a_i} f_a(\mathbf{y}(n)/\theta_{a_i})}{f_{\mathbf{Y}/\Theta}(\mathbf{y}(n)/\hat{\Theta}_i)} \right)} . \tag{5.18}$$

By using the above result, we can rewrite the constraint function as:

$$\lambda_a + \sum_{k=1\ k\neq a}^{M} \lambda_k \frac{\sum_{n=0}^{N-1} \left(\frac{\hat{\lambda}_{k_i} f_k(\mathbf{y}(n)/\theta_{k_i})}{f_{k/\Theta}(\mathbf{y}(n)/\hat{\Theta}_i)} \right)}{\sum_{n=0}^{N-1} \left(\frac{\hat{\lambda}_{a_i} f_a(\mathbf{y}(n)/\theta_{a_i})}{f_{\mathbf{Y}/\Theta}(\mathbf{y}(n)/\hat{\Theta}_i)} \right)} = 1 . \tag{5.19}$$

Simplifying the above equation by noting the fact that $\sum_{k=1}^{M} \sum_{n=0}^{N-1} \left(\frac{\hat{\lambda}_{k_i} f_k(\mathbf{y}(n)/\theta_{k_i})}{f_{k/\Theta}(\mathbf{y}(n)/\hat{\Theta}_i)} \right) = N$,

the parameter λ_k is given by

$$\hat{\lambda}_{k_{i+1}} = \frac{1}{N} \sum_{n=0}^{N-1} \frac{\hat{\lambda}_{k_i} f_k(\mathbf{y}(n)/\theta_{k_i})}{f_{\mathbf{Y}/\Theta}(\mathbf{y}(n)/\hat{\Theta}_i)} . \tag{5.20}$$

To obtain the remaining parameters, we may require the following matrix identities (Mix, 1995):

$$\frac{d}{dX}(X^T AX) = X(A + A^T),\ \frac{d}{dX}|X| = |X| X^{-1} \text{ and } \frac{d}{dX}(A^T X^{-1} A) = -X^{-1} AA^T X^{-1}.$$

(5.21)

Similarly, the mean vector μ_k can be obtained by maximizing Eqn. (5.15) with respect to μ_k and we get :

$$\frac{\partial}{\partial \mu_k} U(\theta, \hat{\theta}_i) = \sum_{n=0}^{N-1} \frac{\hat{\lambda}_{k_i} f_k(\mathbf{y}(n)/\theta_{k_i})}{f_{Y/\Theta}(\mathbf{y}(n)/\hat{\Theta}_i)} \left(0 + \frac{\partial}{\partial \mu_k} \ln[f_k(\mathbf{y}(n); \theta_k)]\right) = 0. \quad (5.22)$$

Using the product rule of the logarithm and Eqns. (5.10) and (5.11), we can express Eqn. (5.22) as:

$$\sum_{n=0}^{N-1} \frac{\hat{\lambda}_{k_i} f_k(\mathbf{y}(n)/\theta_{k_i})}{f_{\mathbf{Y}/\Theta}(\mathbf{y}(n)/\hat{\Theta}_i)} \frac{\partial}{\partial \mu_k} \left(ln\left(\frac{1}{\sqrt{2\pi|\Sigma_k|}}\right) + ln\left[exp\left[-\frac{1}{2}(\mathbf{y}(n) - \mu_k)^T \Sigma_k^{-1} (\mathbf{y}(n) - \mu_k)\right] \right) = 0. \quad (5.23)$$

Using the matrix identies given in Eqn. (5.21), we get

$$\sum_{n=0}^{N-1} \frac{\hat{\lambda}_{k_i} f_k(\mathbf{y}(n)/\theta_{k_i})}{f_{\mathbf{Y}/\Theta}(\mathbf{y}(n)/\hat{\Theta}_i)} \left(-\frac{1}{2}(\mathbf{y}(n) - \mu_k) 2(\Sigma_k^{-1} + \Sigma_k^{-1^T}) \right) = 0, \quad (5.24)$$

which gives

$$\hat{\mu}_{k_{i+1}} = \frac{\sum_{n=0}^{N-1} \frac{\hat{\lambda}_{k_i} f_k(\mathbf{y}(n)/\theta_{k_i})}{f_{Y/\Theta}(\mathbf{y}(n)/\hat{\Theta}_i)} \mathbf{y}(n)}{\sum_{n=0}^{N-1} \frac{\hat{\lambda}_{k_i} f_k(\mathbf{y}(n)/\theta_{k_i})}{f_{Y/\Theta}(\mathbf{y}(n)/\hat{\Theta}_i)}}. \quad (5.25)$$

Similarly $\hat{\Sigma}_{k_{i+1}}$ can be obtained by maximizing $U[\theta, \hat{\theta}_{i+1}]$ with respect to Σ_k as:

$$\frac{\partial}{\partial \Sigma_k} U(\theta, \hat{\theta}_i) = \sum_{n=0}^{N-1} \frac{\hat{\lambda}_{k_i} f_k(\mathbf{y}(n)/\theta_{k_i})}{f_{Y/\Theta}(\mathbf{y}(n)/\hat{\Theta}_i)} \left(0 + \frac{\partial}{\partial \Sigma_k} \ln[f_k(\mathbf{y}(n); \theta_k)]\right) = 0.$$

(5.26)

Expanding Eqn. (5.26) using the relation in Eqn. (5.12), we obtain

$$\sum_{n=0}^{N-1} \frac{\hat{\lambda}_{k_i} f_k(\mathbf{y}(n)/\theta_{k_i})}{f_{\mathbf{Y}/\Theta}(\mathbf{y}(n)/\hat{\Theta}_i)} \frac{\partial}{\partial \Sigma_k} \left(ln\left(\frac{1}{\sqrt{2\pi|\Sigma_k|}} \right) + ln\left[exp\left[-\frac{1}{2}(\mathbf{y}(n)-\mu_k)^T \Sigma_k^{-1}(\mathbf{y}(n)-\mu_k) \right] \right] \right) = 0. \tag{5.27}$$

Using the matrix identities given in Eqn. (5.21), the partial derivative of the term inside the bracket of the left hand side of the above equation gives us:

$$\sum_{n=0}^{N-1} \frac{\hat{\lambda}_{k_i} f_k(\mathbf{y}(n)/\theta_{k_i})}{f_{\mathbf{Y}/\Theta}(\mathbf{y}(n)/\hat{\Theta}_i)} \left(-\frac{1}{2} \frac{|\Sigma_k| \, \Sigma_k^{-1}}{|\Sigma_k|} + \frac{1}{2}(\Sigma_k^{-1}\mathbf{y}(n)-\mu_k)(\mathbf{y}(n)-\mu_k)^T \Sigma_k^{-1}) \right) = 0. \tag{5.28}$$

Then, it is straightforward to get Σ_k as:

$$\hat{\Sigma}_{k_{i+1}} = \frac{\sum_{n=0}^{N-1} \frac{\hat{\lambda}_{k_i} f_k(\mathbf{y}(n)/\theta_{k_i})}{f_{\mathbf{Y}/\Theta}(\mathbf{y}(n)/\hat{\Theta}_i)} (\mathbf{y}(n)-\hat{\mu}_{k_i})(\mathbf{y}(n)-\hat{\mu}_{k_i})^T}{\sum_{n=0}^{N-1} \frac{\hat{\lambda}_{k_i} f_k(\mathbf{y}(n)/\theta_{k_i})}{f_{\mathbf{Y}/\Theta}(\mathbf{y}(n)/\hat{\Theta}_i)}}, \tag{5.29}$$

which completes the parameter estimation process. Eventhough EM algorithm results in an accurate model depending on the initial estimate, it is computationally intensive. Recently, variants of EM algorithm which improve the convergence rate significantly have been proposed (Fessler *et al*, 1994 and Neal *et al*, 1993). We try to re derive Eqn. (5.9) using the incremental view point of (Neal *et al*, 1993) in the following section.

5.3.3. Incremental-Based EM Algorithm

There exist many variants of the EM algorithm, some of them differ from the standard algorithm in the way the E-step and M-steps are implemented. The M-step of the

algorithm may be partially implemented, with the new estimate for the parameters improving the likelihood given the distribution found in E-step, but necessarily maximizing it. Such a partial M-step also results in the true likelihood improvement, referred to as *Generalized EM* (GEM) algorithms (Neal *et al*, 1993). The basic idea behind the *Incremental-based EM algorithm* is the partial implementation of the E-step. In many cases, partial implementation of the E-step is also natural. As the unobserved variables are commonly independent, they influence the likelihood of the parameters only through simple sufficient statistics. If the statistics for the E-step are incrementally collected and the parameters are frequently estimated, it should speed up the convergence, since the information from the new data contributes to the parameter estimation more quickly than the standard algorithm. The incremental EM algorithm is described in Table 5.4. This view point can be applied when the observed data $\boldsymbol{y} = (\boldsymbol{y}^1, \boldsymbol{y}^2, ..., \boldsymbol{y}^L)$ are L independent sets and the complete data can be decomposed as $\boldsymbol{x} = (\boldsymbol{x}^1, \boldsymbol{x}^2, ..., \boldsymbol{x}^L)$. The general approach is to collect subset of the data that essentially meets the above requirement and then update the parameters based on the subset until the convergence of the parameters. In the context of mixture modeling, the spectrogram of the signal under analysis/synthesis, we can generate the L independent sets of observed data by performing the RV generation algorithm that many times. Then, the joint probability for Y and X can be factored as:

$$f_{X,Y/\Theta}(\boldsymbol{x}, \boldsymbol{y} / \theta) = \prod_{l=1}^{L} f_{X^l,Y^l/\Theta^l}(\boldsymbol{x}^l, \boldsymbol{y}^l / \theta^l), \tag{5.30}$$

where θ^l represents the parameter estimates of the l^{th} segment.

Table 5.4: Incremental-based EM algorithm

Step-1.Initialization:

- Select an initial parameter estimate for each of the L segments
- $\hat{\theta}_0^l \quad l = 1, 2, ..., L$, and for the whole data $\hat{\theta}_0^{tot}$
- For i = 0, 1, … until convergence

Step-2: Expectation:

- Choose the data segment, l, to be updated
- Set $U(\theta^m, \hat{\theta}_i^m) = U(\theta^m, \hat{\theta}_{i-1}^m)$ for $m \neq l$
- Compute $U(\theta^l, \hat{\theta}_i^l) = E[\ln f_{X^m;\Theta^m}(\boldsymbol{x}^m; \theta^m) / \boldsymbol{y}; \hat{\theta}_{i-1}^m]$

Step-3: Maximization:

- Select

$$\hat{\theta}_i^{tot} = \arg\max_{\theta} [\, U(\theta, \hat{\theta}_{i-1}^{tot}) - U(\theta, \hat{\theta}_{i-1}^l) + U(\theta, \hat{\theta}_i^l) \,]$$

Step-4: Convergence:

- If not converged then go to step-2.

Now, we can expand the E-step in Table 5.4 as:

$$\begin{aligned} U(\theta, \hat{\theta}_i^{tot}) &= E[\ln f_{X;\Theta}(\mathbf{x}(n); \theta) / \mathbf{y}(n); \hat{\theta}_i] \\ &= E[\ln f_{X;\Theta}(\mathbf{y}(n), k; \theta) / \mathbf{y}(n); \hat{\theta}_i]. \end{aligned} \tag{5.31}$$

By imposing the constraint on the data segments that they are independent, Eqn. (5.31) can be rewritten as:

$$U(\theta,\widehat{\theta}_{\mathrm{i}}^{\mathrm{tot}}) = E[ln\prod_{l=1}^{L}\left(f_{X^l;\Theta^l}(\mathbf{y}^l(n),k;\theta^l)/\mathbf{y}^l(n);\widehat{\theta}_i^l\right)]. \tag{5.32}$$

Taking the logarithmic operation of the product of the conditional pdfs, we get

$$U(\theta,\widehat{\theta}_{\mathrm{i}}^{\mathrm{tot}}) = E[\sum_{l=1}^{L} ln[\, f_{X^l;\Theta^l}(\mathbf{y}^l(n),k;\theta^l)/\mathbf{y}^l(n);\widehat{\theta}_i^l\,]. \tag{5.33}$$

As expectation operator is linear, we can rewrite the above equation as:

$$U(\theta,\widehat{\theta}_{\mathrm{i}}^{\mathrm{tot}}) = \sum_{l=1}^{L} E[\, ln\left(f_{X^l;\Theta^l}(\mathbf{y}^l(n),k;\theta^l)/\mathbf{y}^l(n);\widehat{\theta}_i^l\right)]. \tag{5.34}$$

Now, we implement the partial E-step on the data segment *m* and then Eqn. (5.34) can be split as

$$\begin{aligned} U(\theta,\widehat{\theta}_i^{tot}) &= E[ln\left(f_{X^m;\Theta^m}(\mathbf{y}^m(n),k;\theta^m)/\mathbf{y}^m(n);\widehat{\theta}_i^m\right)] \\ &\quad + \sum_{l=1\ l\neq m}^{L} E\,[\ ln\left(f_{X^l;\Theta^l}(\mathbf{y}^l(n),k;\theta^l)/\mathbf{y}^l(n);\widehat{\theta}_i^l\right)]. \end{aligned} \tag{5.35}$$

Since we are updating the parameters for the m^{th} segment, the expected log-likelihood of the other data segments remain unchanged. Hence,

$$U(\theta,\widehat{\theta}_{\mathrm{i}}^{\mathrm{tot}}) = E[ln\left(f_{X^m;\Theta^m}(\mathbf{y}^m(n),k;\theta^m)/\mathbf{y}^m(n);\widehat{\theta}_{i-1}^m\right)] + \sum_{l=1\ l\neq m}^{L} U(\theta,\widehat{\theta}_{i-1}^l). \tag{5.36}$$

Adding and subtracting the term $U(\theta,\widehat{\theta}_{i\text{-}1}^m)$ to the right hand side of the above equation gives us:

$$\begin{aligned} U(\theta,\widehat{\theta}_i^{tot}) &= E[ln\left(f_{X^m;\Theta^m}(\mathbf{y}^m(n),k;\theta^m)/\mathbf{y}^m(n);\widehat{\theta}_{i-1}^m\right)] + \sum_{l=1\ l\neq m}^{L} U(\theta,\widehat{\theta}_{i-1}^l) \\ &\quad + U(\theta,\widehat{\theta}_{i\text{-}1}^m) - U(\theta,\widehat{\theta}_{i\text{-}1}^m) \\ &= E[ln\left(f_{X^m;\Theta^m}(\mathbf{y}^m(n),k;\theta^m)/\mathbf{y}^m(n);\widehat{\theta}_{i-1}^m\right)] + \sum_{l=1}^{L} U(\theta,\widehat{\theta}_{i-1}^l) - U(\theta,\widehat{\theta}_{i\text{-}1}^m). \end{aligned} \tag{5.37}$$

By denoting $E[ln\left(f_{X^m;\Theta^m}(\boldsymbol{y}^m(n),k;\theta^m)/\boldsymbol{y}^m(n);\hat{\theta}_{i-1}^m\right)]$ as $U(\theta,\hat{\theta}_i^m)$, we obtain

$$U(\theta,\hat{\theta}_i^{tot}) = U(\theta,\hat{\theta}_{i-1}^{tot}) + U(\theta,\hat{\theta}_i^m) - U(\theta,\hat{\theta}_{i-1}^m). \tag{5.38}$$

It appears that eventhough we perform partial E-step on a selected segment, we have to maximize the likelihood function on the whole data. However, usage of sufficient statistics leads to an efficient way of implementing the M-Step (Neal *et al*, 1993). Sufficient statistics for a Gaussian process are the mean and the covariance matrix (Kay, 1993). For a mixture of densities, the parameters that characterize the whole process are the weight vector, the mean vector and the covariance matrix. As we do not have the idea of sufficient statistics for the mixture density, we resort to the conventional method of maximizing Eqn. (5.38) to obtain the parameters. The expected log-likelihood has to be maximized with respect to λ_k, μ_k *and* Σ_k to obtain the parameters $\hat{\lambda}_{k_{i+1}}, \hat{\mu}_{k_{i+1}}$ *and* $\hat{\Sigma}_{k_{i+1}}$ as:

$$\begin{aligned}
\lambda_{k_i} &= \lambda_{k_{i-1}} + \frac{1}{N_m}\left(\lambda_{k_i}^m - \lambda_{k_{i-1}}^m\right), \\
\mu_{k_i} &= \frac{N\lambda_{k_{i-1}}\mu_{k_{i-1}} + N_m\lambda_{k_i}^m\mu_{k_i}^m - N_m\lambda_{k_{i-1}}^m\mu_{k_{i-1}}^m}{N\lambda_{k_i}} \quad \textit{and} \\
\Sigma_{k_i} &= \frac{N\lambda_{k_{i-1}}\Sigma_{k_{i-1}} + N_m\lambda_{k_i}^m\Sigma_{k_i}^m - N_m\lambda_{k_{i-1}}^m\Sigma_{k_{i-1}}^m}{N\lambda_{k_i}}.
\end{aligned} \tag{5.39}$$

where N is the total number of realizations of $\boldsymbol{y}$, N_m number of realizations of the segment $\boldsymbol{y}^m$; and $\lambda_{k_i}^m, \mu_{k_i}^m$ and $\Sigma_{k_i}^m$ are the parameters of the m^{th} segment. Using Eqns. (5.20), (5.25) and (5.29) to compute the parameters $\lambda_{k_i}^m, \mu_{k_i}^m$ and $\Sigma_{k_i}^m$, respectively, on the subset of the data labeled $\boldsymbol{y}_m$ reduces the complexity to a direct maximization of the likelihood function, since we are computing only $\lambda_{k_i}^m, \mu_{k_i}^m$ and $\Sigma_{k_i}^m$ at each iteration and are using the earlier estimates adequately to obtain λ_k, μ_k *and* Σ_k. The proof of Eqn.

(5.39) can be given on similar lines as was done for the EM algorithm. A comparison of the Incremental EM and the standard EM algorithm is shown in Fig. 5.3. for the parameters given in Table 5.5.

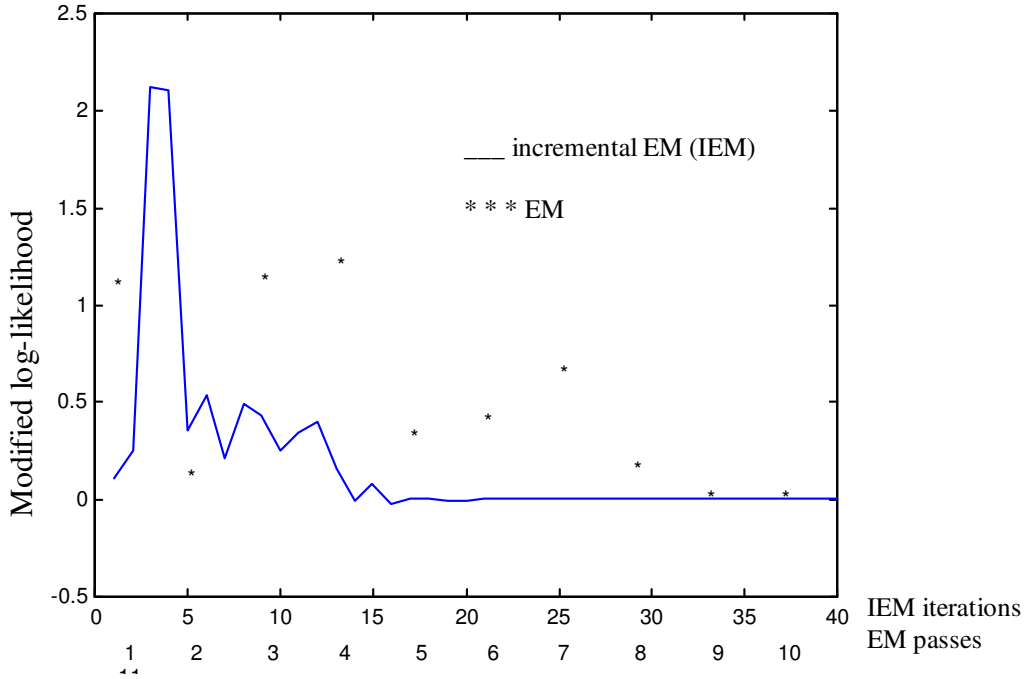

Fig. 5.3. Comparison of incremental-based and standard EM algorithms

Table 5.5: A comparison of the estimated components from the EM and the Incremental EM algorithms

		Mixture model parameters	Initial estimates	Estimated parameters after 10 passes of EM algorithm	Estimated parameters after 5 passes of incremental EM algorithm
Component 1	μ	$\begin{bmatrix}40\\64\end{bmatrix}$	$\begin{bmatrix}20\\40\end{bmatrix}$	$\begin{bmatrix}40.892\\63.923\end{bmatrix}$	$\begin{bmatrix}40.086\\64.135\end{bmatrix}$
	Σ	$\begin{bmatrix}30 & 0\\0 & 20\end{bmatrix}$	$\begin{bmatrix}80 & 20\\20 & 40\end{bmatrix}$	$\begin{bmatrix}22.82 & 1.287\\1.287 & 13.120\end{bmatrix}$	$\begin{bmatrix}22.82 & 1.244\\1.244 & 13.161\end{bmatrix}$
	λ	0.3	0.5	0.345	0.342
Component 2	μ	$\begin{bmatrix}70\\64\end{bmatrix}$	$\begin{bmatrix}20\\40\end{bmatrix}$	$\begin{bmatrix}69.601\\64.932\end{bmatrix}$	$\begin{bmatrix}69.619\\64.135\end{bmatrix}$
	Σ	$\begin{bmatrix}30 & 0\\0 & 20\end{bmatrix}$	$\begin{bmatrix}40 & -8\\-8 & 30\end{bmatrix}$	$\begin{bmatrix}29.861 & 0.756\\0.756 & 21.030\end{bmatrix}$	$\begin{bmatrix}29.852 & 0.742\\0.741 & 20.891\end{bmatrix}$
	λ	0.7	0.5	0.654	0.657

Total number of samples *(N)* = 128
Number of segments *(I)* = 4
Number of samples in each segment (N_l) = 32
Number of components = 2

It can be observed from the figure that the IEM converges within the 6th pass of the EM algorithm, i.e., at 20th iteration of the IEM algorithm (one pass of the EM algorithm is

equivalent to L iterations of the IEM, where L is the number of segments of the data), whereas EM algorithm converges only after the 10^{th} pass. On the y-axis is shown the modified likelihood defined as:

$$U_{ml} = U(\theta,\hat{\theta}_i) - U(\theta,\hat{\theta}_{i-1}) \quad . \tag{5.40}$$

Since each estimate of the parameter should result in an improved likelihood, expressed in terms of the log-likelihood as:

$$U(\theta,\hat{\theta}_i) \geq U(\theta,\hat{\theta}_{i-1}) \,, \tag{5.41}$$

the modified likelihood function, U_{ml}, is non-negative and becomes zero when the parameters converge. The complexity of computing the parameters can be reduced by noting the fact that convergence rate depends on the initial estimates passed in the *Initialization* step of Table 5.4. A good initial estimate always results in quick convergence. K-means clustering can be used to classify the segments into the desired number of components and estimate the mean vectors (McLachlan, 1987). The obvious question that arises is: K-means clustering and mixture modeling themselves are two random signal space modeling techniques. Then, why cannot we use K-means instead of Mixture modeling? The reason is that K-means clustering cannot associate a classified sample to another, i.e., the clusters are disjoint, whereas in mixture modeling, a sample can have joint observation in adjacent clusters since Guassian densities can be overlapping, with the result that in an area of overlap a data point can be associated with various probabilities to different components of the Gaussian mixture (Vaseghi, 1996). However, this procedure helps us in automating the selection of number of components in the mixture after the realizations are generated using band-rejection algorithm. We will now review K-means clustering algorithm.

5.3.4. K-Means Clustering

The K-means clustering algorithm, also known as generalized Lloyds algorithm, is an iterative method for classifying the realizations (Vaseghi, 1996). The random vector process $\boldsymbol{y}$ is partitioned into M clusters or regions $\mathbf{y}_1, \mathbf{y}_2, ..., \mathbf{y}_M$, and each cluster $\boldsymbol{y}_i$, is represented by centroid $\boldsymbol{c}_i$. The centroid computation and classification of samples are performed iteratively. Each iteration consists of two steps: (a) Partitioning the realizations of the random process into M regions or clusters and (b) Computing the centroid of each of the clusters. The centroids obtained can be considered as initial mean vector estimates given by:

$$\bar{\mu}_{i_0} = c_i = \frac{1}{N_i} \sum_{n=1}^{N_i} y_i(n) \qquad \text{for } i = 1,2,...,M \ . \tag{5.42}$$

Instead of using an arbitrary covariance matrix as initial estimate, we may compute the initial covariance matrix of the i^{th} component from the samples in that cluster as:

$$\bar{\Sigma}_{i_0} = \frac{1}{N_i} \sum_{n=0}^{N_i} (y_i(n) - \bar{\mu}_{i_0})(y_i(n) - \bar{\mu}_{i_0})^T, \quad \text{for } i = 1,2,...,M \ . \tag{5.43}$$

For the comparison purpose we initialize the parameters for each segment $\boldsymbol{y}_i$, using a stance of the EM algorithm. From then onwards, Eqn. (5.39) can be implemented recursively. Once the spectrogram is modeled appropriately by mixture modeling, our objective is to synthesize signals corresponding to the components given by the mixture model. In the next section, we present a novel algorithm to directly synthesize a signal from a component given by the mixture model.

Deleted: ¶

5.4 MAPPING OF COMPONENTS

The estimated components have to be utilized in synthesizing the signal. Coates *et al* (Coates *et al*, 1998) have used these components to separate multicompoennt signals and the isolated components are mapped into a time domain signal by using time-frequency projection filters (Hlawatsch, 1994). It is equivalent to saying that the pass region required by the filters is specified in terms of the mixture model with a choice to select the pass region in an orderly manner. Hence, the whole effort has been just confined to select the pass region. In the present work, we try to use the information provided by the mixture model alone to synthesize the signal rather than using the time-frequency projection filters, which require eigen value decomposition. With the belief that a bivariate pdf and a joint distribution of time and frequency have strong correlation, we make the analogy between a bivariate pdf and time-frequency distribution, since the general concepts of average, standard deviation, moments, etc. apply to any distributions irrespective of the physical quantities they represent (Cohen, 1995). Now at our disposal we have a bivariate pdf and TFD, and we need to make transition from the former to the latter. Since our pdf is a normal pdf, it can be sufficiently represented by standard deviation, mean and covariance. Henceforth, we must have a TFD that can also be represented by these quantities. For a pdf, the mean vector specifies where the distribution is located (or centered around) and the standard deviation specifies the spread. When we talk about TFD, the mean vector has to represent the time-frequency centering of the distribution and the standard deviation vector has to represent the spread in time and spread in frequency. Modulating a signal with a window to obtain different spreads and modulating with a complex exponential to obtain the desired frequency shift,

Deleted: ¶

together with a shift in time parameter, essentially capture all the information given by the pdf parameters. However, the additional parameter involved in pdf is the covariance. This can be considered as a shearing operator and multiplying the signal with a chirp signal can take care of this parameter. Now we resort to comparing the normal pdf and spectrogram of the signal having the above parameters.

Let *s(t)* be a signal of the form given by

$$s(t) = \left(\frac{\alpha}{\pi}\right)^{\frac{1}{4}} e^{-\frac{\alpha(t-t_c)^2}{2}} e^{j\beta(t-t_c)^2/2 + j\omega_c(t-t_c)}, \tag{5.44}$$

with the parameters as explained in Eqn. (5.2).

Spectrogram of $s(t)$ is given by

$$SP(t,\omega) = \frac{P(t-t_c)}{\sqrt{2\pi\sigma^2_{\omega/t}}} exp\left[-\frac{(\omega - \omega_c - \langle\omega\rangle_t)^2}{2\sigma^2_{\omega/t}}\right] \quad \text{where} \tag{5.45}$$

$$P(t) = \sqrt{\frac{a\alpha}{\pi(\alpha+a)}}\ exp\left[-\frac{a\alpha}{\alpha+a}\ t^2\right],$$

$$\sigma^2_{\omega/t} = \frac{1}{2}(\alpha+a) + \frac{1}{2}\frac{\beta^2}{(\alpha+a)} \quad \text{and}$$

$$\langle\omega\rangle_t = \frac{a}{(\alpha+a)}\beta(t - t_c)\ .$$

A bivariate Gaussian pdf is given by

$$f(y) = \frac{1}{2\pi\sigma_1\sigma_2\sqrt{(1-\rho^2)}} exp\left(-\frac{(y_1-\mu_1)^2\sigma_2^2 + (y_2-\mu_2)^2\sigma_1^2 - 2\sigma_1\sigma_2(y_1-\mu_1)(y_2-\mu_2)}{2\sigma_1^2\sigma_2^2(1-\rho^2)}\right), \tag{5.46}$$

Deleted: ¶

where $[\mu_1, \mu_2]^T$ form the mean vector μ as $\begin{bmatrix} \mu_1 \\ \mu_2 \end{bmatrix}$, and σ_1, σ_2, ρ form the elements of the covariance matrix Σ as $\begin{bmatrix} \sigma_1^2 & \rho\sigma_1\sigma_2 \\ \rho\sigma_1\sigma_2 & \sigma_2^2 \end{bmatrix}$.

After rewriting Eqn. (5.46) and by comparing the like terms of Eqns. (5.45) and (5.46), we obtain the following relationships:

$$\frac{a}{(a+\alpha)}\beta = \rho\frac{\sigma_2}{\sigma_1},$$

$$\begin{bmatrix} \mu_1 \\ \mu_2 \end{bmatrix} = \begin{bmatrix} t_c \\ \omega_c \end{bmatrix},$$

$$\frac{a}{(a+\alpha)}\alpha = \frac{1}{2\sigma_1^2} \quad \text{and}$$

$$\sigma_2^2(1-\rho^2) = \frac{1}{2}(\alpha+a) + \frac{1}{2}\frac{\beta^2}{(\alpha+a)}. \tag{5.47}$$

The following mapping rules satisfy the above equation simultaneously. They are:

$$\alpha = \frac{a\left(\frac{\sigma_2}{\sigma_1}\right)^2(1-\rho^2)}{a^2 + \left(\frac{\rho\sigma_2}{\sigma_1}\right)^2} \quad \text{and}$$

$$\beta = \frac{\rho(a+\alpha)}{a}\left(\frac{\sigma_2}{\sigma_1}\right). \tag{5.48}$$

And the weight of the mixture can be used to measure the weight of the chirplet, i.e., $\lambda_i = c_i$. Hence, λ, μ *and* Σ can totally estimate the parameters c, t_c, ω_c, α *and* β which are used to decompose/reconstruct a signal in terms of the chiprlets as given in Eqn. (5.1).

Deleted: ¶

5.5. ANALYSIS OF THE MAPPING RULES

The argument we made earlier that the Gaussain mixture model parameters sufficiently characterize the chirplets will be reinforced with the following analysis. However, we are least interested in the mean vector information, as it only determines the location of the chirplets. We take up the following cases:

Case 1: $\frac{\sigma_2}{\sigma_1} = 1$

The specific case of interest is at $\rho = 0$, where the pdf will be totally unskewed and has equal spreads in either direction. The equivalent representation in the t-f plane is that it forms the oblique cell, i.e., it is the only point where the Fourier transform and the signal will have equal duration. It is to be observed that the mapping rule depends only on the ratio $\frac{\sigma_2}{\sigma_1}$ but not individually on σ_1 and σ_2; and it is a many-to-one transformation. For example, the histogram of the pdf $\frac{\sigma_2}{\sigma_1} = 1$ with larger individual variances has larger spread than the one with lower individual variances, whereas in the time-frequency plane it cannot be as exemplified as in Figs. 5.4 and 5.5. The covariance matrices and the mean vectors are also shown in figures. Any σ_1 and σ_2 that satisfy $\frac{\sigma_2}{\sigma_1} = 1$ are mapped to the same signal. The variation of ρ in the positive direction causes skewing of the pdf and hence the effect of ρ now is a steady increase in β and duration of the window as shown in Fig. 5.6. Finally, when $\rho = 1$, the signal is a chirp of infinite duration with $\beta = 1$ which can be inferred from the mapping rules.

Deleted: ¶

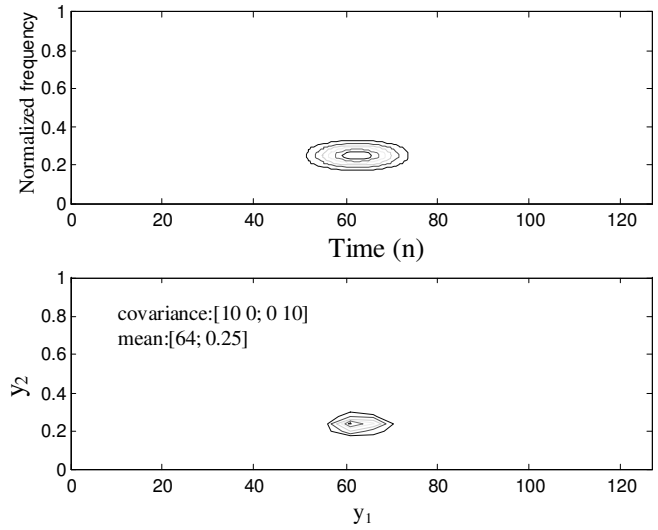

Fig. 5.4. Spectrogram of the synthesized signal using mapping rules and the histogram of the mixture density

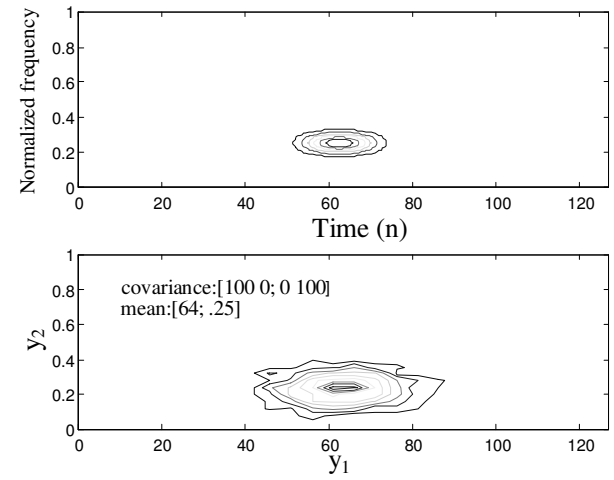

Fig. 5.5. Spectrogram of the synthesized signal using mapping rules and the histogram of the mixture density with lager variance

Deleted: ¶

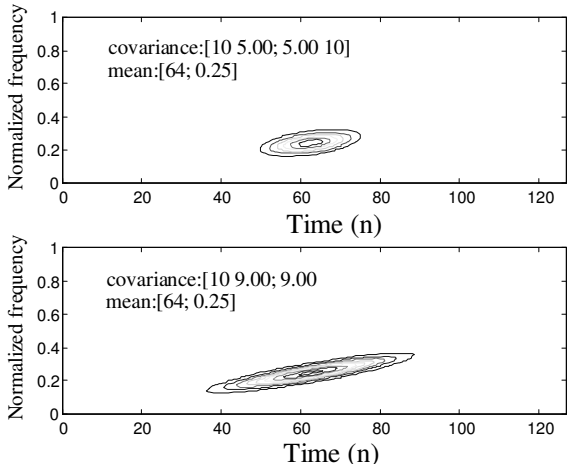

Fig. 5.6. The effect of ρ on the window duration of the chirplets synthesized from mapping rules with different ρ in each case

Case 2: $\rho = 0$

Now from Eqn. (5.48), we obtain $\alpha = \dfrac{2\left(\dfrac{\sigma_2}{\sigma_1}\right)^2}{a}$ and $\beta = 0$. It can be observed that any increase in $\dfrac{\sigma_2}{\sigma_1}$ causes an increase in α and hence shortens the window. An impulse can be modeled theoretically at $\dfrac{\sigma_2}{\sigma_1} \approx \infty$. Impulses at different time instants synthesized from the mapping rules are shown in Fig. 5.7. An impulse located at different time can be modeled by the same covariance matrix but with a different mean vector. When $\dfrac{\sigma_2}{\sigma_1}$ decreases, it has an effect of increasing the window duration and can be considered scaling of the window as depicted in Fig. 5.8.

Deleted: ¶

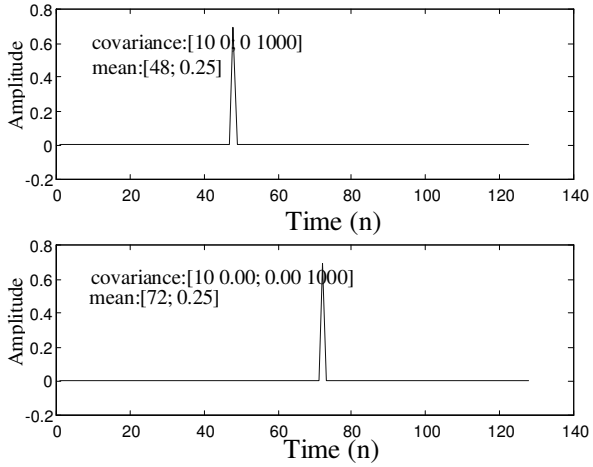

Fig. 5.7. Impulses located at different time instants obtained from the mixture model having different mean vectors

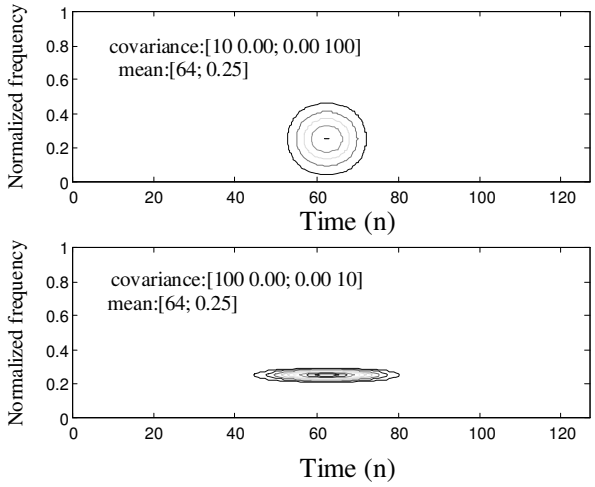

Fig. 5.8. Comparison of the spectrograms of two signals at different scales synthesized from mixture model

Deleted: ¶

And finally, analytic part of sinusoid of arbitrary frequency can be modeled at $\frac{\sigma_2}{\sigma_1} \approx 0$ with μ_2 determining the frequency of the sinusoid. Two truncated sinusoids of different frequencies derived from the mapping rules are shown in Fig. 5.9.

Case 3: $\rho = 1$

In this particular case, the pdf will be having the maximum skewness and from the mapping rules we obtain an infinite duration window. With increase in $\frac{\sigma_2}{\sigma_1}$, we observe an increase in β by which chirps of infinite duration can be modeled.

Case 4: $\frac{\sigma_2}{\sigma_1} \neq 1 \; and \; 0 < \rho < 1$

As we have been mentioning, we can rotate the t-f plane or tile the t-f plane in an arbitrary fashion using chirplets and this can be obtained by coordinated shearing and scaling (Baraniuk, 1996b). Together with $\frac{\sigma_2}{\sigma_1}$, ρ causes the effect of rotation as demonstrated in Fig 5.10. Hence, we can analyze the signal in the space shift in time, shift in frequency, scale, shear in time, shear in frequency and rotation. To test the algorithm in a multicomponent scenario, we have considered a sinusoidal frequency modulated signal, WVD of which is shown in Fig. 5.11. Five components were used in the mixture density with four segments in the incremental EM algorithm. After ten iterations of incremental EM, mapping rules are used to synthesize from the mixture density parameters. The WVD of the synthesized signal is shown in Fig. 5.12. The synthesized signals corresponding to individual components in the mixture can be added according to the weights given by λ. It is the mixture modeling that resolves the

Deleted: ¶

nonlinearity inherently associated with the spectrogram which necessitates over-estimating the number of components in the mixture.

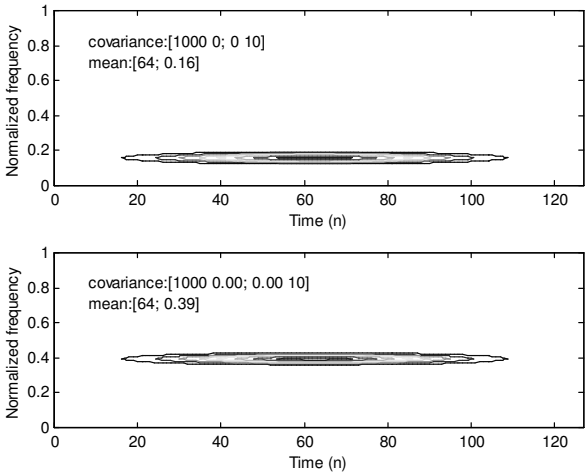

Fig. 5.9 Modeling of sinusoids at different frequencies obtained from the mixture model with different mean vectors

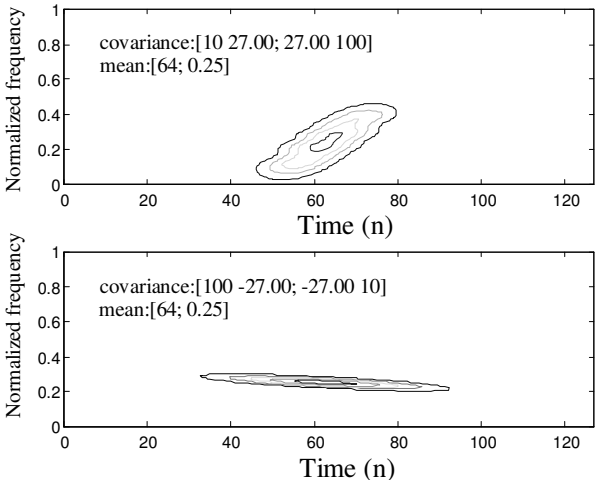

Fig. 5.10. The effect of rotation obtained by a simultaneous shearing and scaling

Deleted: ¶

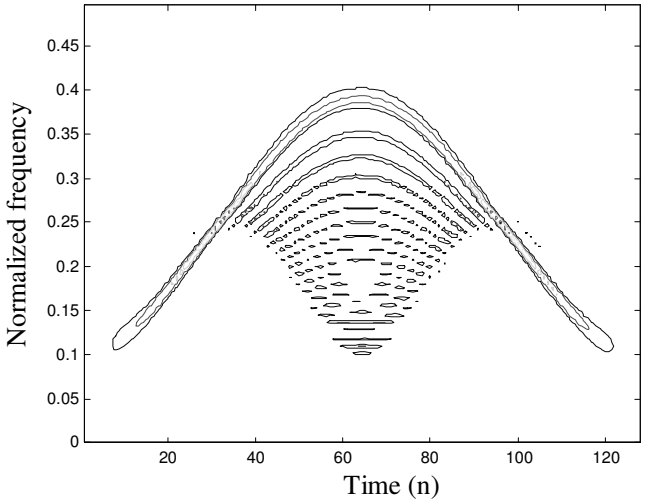

Fig. 5.11. Spectrogram of a sinusoidal frequency modulated signal

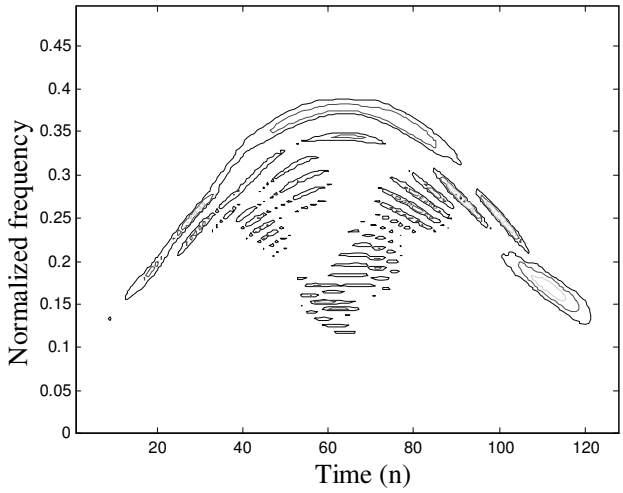

Fig. 5.12. Spectrogram of the signal used in Fig.5.11 synthesized after ten passes of the EM algorithm

Deleted: ¶

However, if the chirplets are time-frequency disjoint, then the number of components in the mixture is equal to the number of components in the signal, otherwise over estimation is required. The real part of the synthesized signal after thirty iterations of incremental EM algorithm, together with the real part of the signal, subjected to analysis is shown in Fig. 5.13.

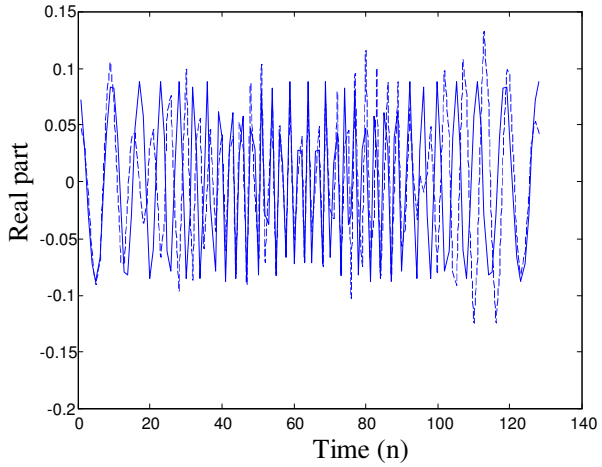

Fig. 5.13. Real part of the signal (solid) and the synthesized signal (dashed) after thirty iterations of incremental EM algorithm

In general, we choose '*a*', the analysis window parameter used in computing the spectrogram, in such a way that the length of analysis window will be one fourth of the signal length. Because of this window effect, we cannot obtain the exact envelope in many situations. To demonstrate this point, we have considered a rectangular windowed sinusoid. We first used a single component and estimated the signal using the above algorithm. The estimated and the true envelope of the signal are shown in Fig. 5.14(a). It is theoretically possible to obtain any abrupt edges by assuming it as a weighed

Deleted: ¶

combination of impulses. Because of the smearing of the signal by the window, the envelope is not preserved, since spectrogram does not satisfy the marginals property. We have considered five components in the mixture to model the spectrogram. It can be observed from Fig. 5.14(b) that even the five component model tries to follow the time marginal. True estimation of the desired signal is not always possible. We cannot consider any other distribution for modeling the t-f plane that satisfies the marginals because they inherently violate the positivity condition required for viewing it as a pdf.

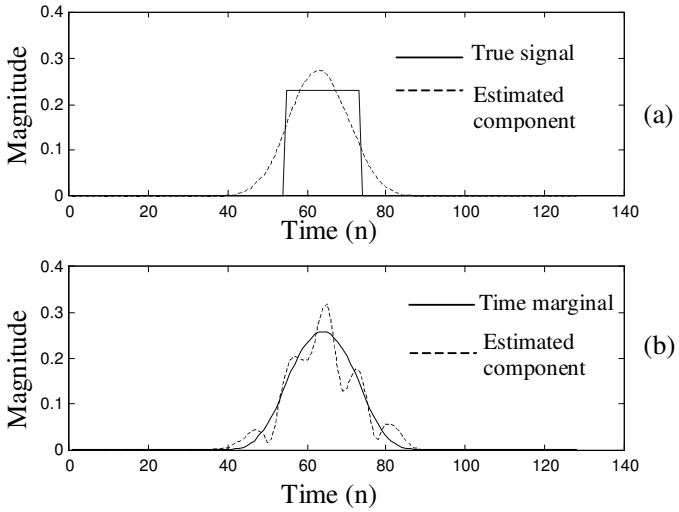

Fig. 5.14. (a) Magnitude of the rectangular windowed signal and the envelope of the estimated using a single component mixture density and (b) Time marginal obtained from spectrogram and the signal estimated from a five component mixture density

Deleted: ¶

5.6. CONCLUSIONS

We have developed an algorithm to decompose the signal specified as a spectrogram in terms of chirplets. The modeling of the spectrogram is accomplished by mixture modeling. The parameters of the mixture density are estimated using incremental EM algorithm that speeds up the convergence rate to standard EM algorithm. K-Means clustering has been used prior to mixture modeling to speed up the convergence by passing good initial estimates. We have devised a set of mapping rules that synthesize a signal from the mixture-modeled spectrogram of the signal under analysis. We analyzed the rules with an insight into the *chirplet decomposition*, wherein we observed that the orientation of the chirplet is solely determined by the covariance matrix and the location of the chirplet is determined by the mean vector. The mapping rules does not require any projection filters as they use the information provided by mixture modeling, thus considering it not only as a tool to resolve multicomponent signals but also to synthesize them.

Deleted: ¶

CHAPTER 6

PARALLEL ARCHITECTURES FOR GTFDs

6.1. INTRODUCTION

The advent of Fourier transform has revolutionized the implementation of many signal processing algorithms in real-time; The implementation of generalized time-frequency representations is no exception. The interpretation of GTFDs as the Fourier transform of the generalized autocorrelation function has motivated many researchers to consider applying the FFT techniques, e.g., the butterfly structure ,to compute the GTFDs without paying any attention to the computation of the GACF (Qian *et al*, 1990). In this Chapter, we shall deviate from this viewpoint and propose a method that directly operates on the signal and requires no knowledge of the kernel in the Fourier domain. We use time-recursive approach to compute the GTFDs and show that this approach is very suitable for computing running-windowed GTFDS. Time-recursive approach to compute discrete Sine/ Cosine/ Hartley transform has gained much attention because its hardware for serial data has less complexity, as many applications involve the computation on sequential data (Liu *et al*, 1994). The butterfly structures have less latency compared to time-recursive approaches but they are more complex in terms of hardware and need global interconnections. Some of the reasons to use time-recursive approach instead of the butterfly structure are because it:

- Has local communications.
- Is highly parallel, modular and regular.

- Is less complex in terms of hardware.

The time-recursive approach is similar to the multiply and accumulate (MAC) operation as in many digital signal processors. It does not decimate the sequence in either time or frequency but directly operates on the sequence and acts as a mere summation involving multiplications. We first review the time-recursive approach to compute the discrete Fourier transform and then deal with STFT and GTFDs.

6.2. DISCRETE FOURIER TRANSFORM

The discrete time Fourier transform of a discrete time sequence *x(n)* can be related to continuous time Fourier transform, given by

$$X(\omega) = \sum_{n=-\infty}^{\infty} x(n) e^{-j\omega n}, \tag{6.1}$$

where ω is a continuous variable denoting the frequency. In general, we operate on finite size sequences and hence we compute the discrete time Fourier transform of an N-point sequence as:

$$X(\omega) = \sum_{n=0}^{N-1} x(n) e^{-j\omega n}. \tag{6.2}$$

The discrete Fourier transform is obtained by sampling the frequency spectrum as:

$$X(k) = \sum_{n=0}^{N-1} x(n) e^{-j\frac{2\pi nk}{N}}, \; k = 0,1...,N-1. \tag{6.3}$$

To compute the above equation in a time recursive fashion, we start with the induction

step as:

- Induction: $X(-1,k) = 0$.
- Compute: $X(t,k) = \left[X(t-1,k) + x(t)\right] e^{j\frac{2\pi k}{N}}$.
- Stop at $t = N-1$, assign $X(k) = X(N,k)$.

We get the DFT of the sequence after *N* such iterations. The architecture for the above equation is shown in Fig. 6.1. Using only real multiplications, the above equation can be rewritten as:

Let $X(t,k) = X_r(t,k) + jX_i(t,k)$ and similarly $x(n) = x_r(n) + jx_i(n)$, then

$X_r(t+1,k) = X_r(t,k)\cos(\omega_k) - X_i(t,k)\sin(\omega_k)$, where $\omega_k = 2\pi k / N$ and

$$X_i(t+1,k) = X_i(t,k)\cos(\omega_k) + X_r(t,k)\sin(\omega_k), \tag{6.4}$$

which can be implemented as shown in Fig. 6.2. The total number of complex multipliers required are *(N-1)* and the number of complex adders needed are *(N+1)*. A radix-2 FFT algorithm requires $\frac{N}{2}\log_2(N)$ complex multipliers. However, the number of complex multplications that ripple through the stages from input to the output are $\log_2(N)$ in the case of radix-2 FFT whereas they are *N* in time-recursive approach. Throughout our discussion we use this measure to compare the throughput rates of different schemes in terms of complex multiplications defined as:

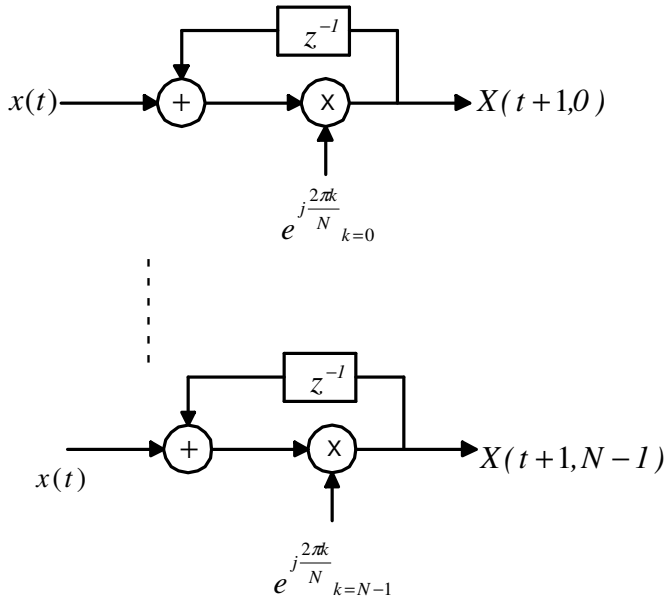

Fig.6.1. Architecture for DFT

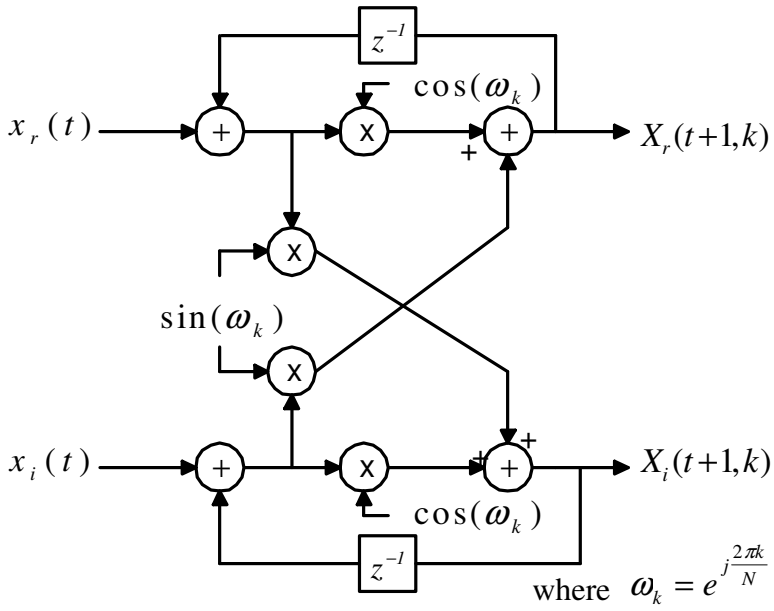

Fig. 6.2. Implementation of Eqn. (6.4) using real multiplications

OPs = Number of complex multiplications whose output ripples through the succeeding stages. (6.5)

While defining the *OPs,* we have not considered the complex multiplications that take place across parallel stages as long as they do not effect the remaining parallel stages. We are considering the computational complexity in terms of complex multiplications only and not complex additions since multiplications are more cumbersome than additions. However, as a special, our comparison of various algorithms in terms of *OPs* may not be valid when the complexity of additions exceeds the complexity of multiplications. We observe that the data flow the architecture assumes is sequential and serial. When we mean sequential, the data is quite regular, i.e., $x(0), x(1), x(2) ..., x(N-1)$ and if the same order is not followed e.g., $x(2), x(N-1), x(0) ..., x(1)$, we call it as nonsequential data. In many cases the data can be nonsequential and we need to wait until all samples arrive and then start pumping them serially in to the architecture in which case we need this extra buffering time when compared to the radix-2 algorithms that operate on parallel data. To circumvent the problem, we have proposed a pre-processor that avoids this buffering time. The pre-processor design is just trivial but of theoretical importance when the throughput rate is important. We consider this issue in the following Section.

6.3. COMPUTATION OF DFT FOR NONSEQUENTIAL DATA

Most of the algorithms that compute DFT consider either sequential serial or parallel data. The DFT/ inverse DFT implemented using time-recursive approach where the data is of nonsequential nature, necessitates buffering of data to make it sequential. We

propose a pre-processor, which takes care of the nonsequential nature of the data. The pre-processor has to introduce a pre-multiplication factor of $e^{j\frac{2\pi k\tau}{N}}$, where τ is determined by the occurrence of the bit position, e.g., a bit delayed by L samples has to undergo a phase offset of $e^{j\frac{2\pi k(N-L)}{N}}$ and for L bit positions in advance it is $e^{j\frac{2\pi kL}{N}}$. Selection of proper value of the pre-multiplication factor is determined jointly by *modulo-N* counters which increment their content by one every time and a two-dimensional kernel that holds the multiplication factor, the address of which is determined by the content in the counter. The architecture is shown in Fig. 6.3.

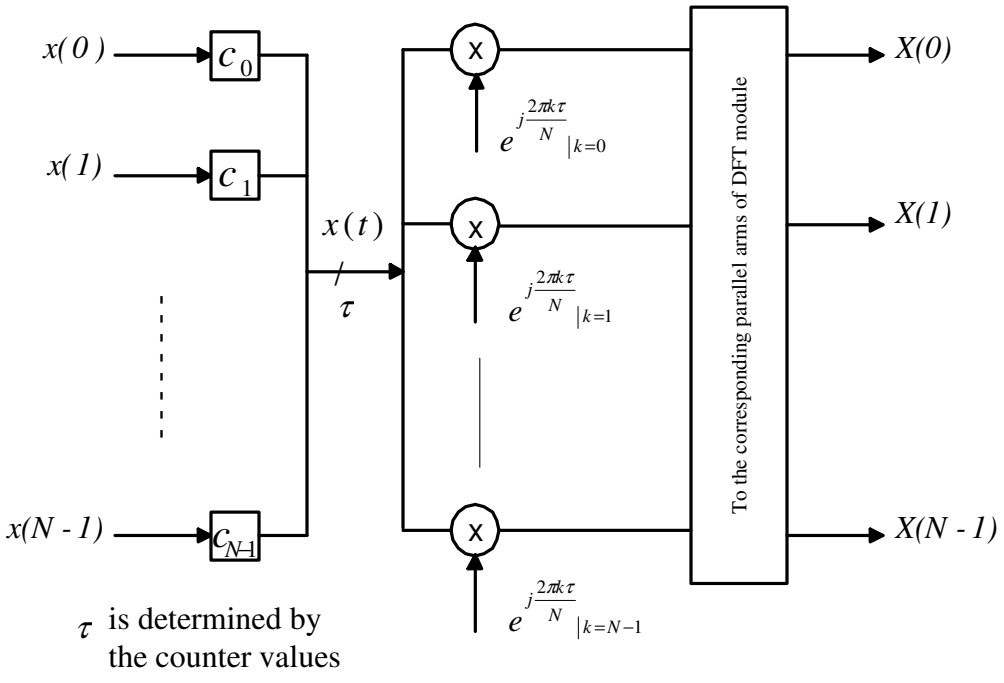

Fig. 6.3. Architecture of the pre-processor for computing DFT of nonsequential data

The algorithm is described below:

- Initialize each counter C_i as $C_i = (N - i - 1)$ for $i = 0,1,...,N - 1$.
- Increment the counters unless and until that particular bit position has occurred.
- Determine which column of the two dimensional kernel, defined as $\phi(\mathrm{k}, \tau) = \mathrm{e}^{\mathrm{j}\frac{2\pi \mathrm{k}\tau}{\mathrm{N}}}$, has to be selected using the final count in the *modulo-N* counter corresponding to bit-position whose data is available.
- Feed the pre-multiplied data to the corresponding parallel arms of the DFT module.

The remaining operations are similar to that of DFT described in Section 6.3. Various stages of the algorithm are exemplified in the Table 6.1 shown below, for a five point sequence given in the order $x(4), x(2), x(3), x(0), x(1)$.

Table 6.1: Illustration of the algorithm for the test sequence *x*

Natural order	Non sequential	c_i	t=0	t=1	t=2	t=3	t=4	t=5
x(0)	x(4)	c_0	4	0	1	2	**3**	X
x(1)	x(2)	c_1	3	4	0	1	2	**3**
x(2)	x(3)	c_2	2	3	**4**	X	X	X
x(3)	x(0)	c_3	1	2	3	**4**	X	X
x(4)	x(1)	c_4	0	**1**	X	X	X	X

The 'bold faced' entries show the counter values in use to select that particular column of the kernel $\phi(k,\tau) = e^{j\frac{2\pi k\tau}{N}}$, and X are 'don't care' entries.

After pre-multiplication, the modified data would be $x(4)e^{j\frac{2\pi k}{5}}, x(2)e^{j\frac{2\pi 4k}{5}}, x(3)e^{j\frac{2\pi 4k}{5}}, x(0)e^{j\frac{2\pi 3k}{5}}$ *and* $x(1)e^{j\frac{2\pi 3k}{5}}$. By substituting the above modified data in Eqn. (6.4), it easily follows that DFT of the sequence in natural order can be obtained. Comparisons of our approach to different methods for serial data are tabulated in Table 6.2

Table 6.2: Comparison of various approaches for computing DFT of serial data

	Butterfly structure (Radix-2)	Time-recursive approach	Proposed method
complex multipliers	$\frac{N}{2}log_2(N)$	$(N-1)$	$2(N-1)$
complex multiplications	$\frac{N}{2}log_2(N)$	$(N-1)$	$(N-1)(D+1)$
Throughput	$B+log_2(N)$	$(N+B)$	$(N+1)$

B: Number of *OPs* that can be performed during the buffering time

D: Number of bit positions that differ from natural order

The proposed architecture requires (N-1) complex multipliers besides (N-1) needed for computing DFT. The throughput of the structure is *(N+1),* since the modules can be operated in a two stage pipelined fashion, as compared to *(N+B)* for time-recursive approach and $B+log_2(N)$ for butterfly structure, where B is the number of *OPs* that can be performed in the buffering time. It can be observed that the order of computations is directly dependent on the number of bit-positions that differ by. For D differences in bit-

positions, the total complex multiplications required are $N(N-1)+D(N-1)$, which indicates that, for data in natural order the computational complexity is the same for the proposed architecture and time-recursive approach without pre-processor. The algorithm can be easily extended to compute DCT/ DST/ DHT on similar lines with the same pre-processing. Eventhough we have proposed this algorithm for the DFT, we have not considered GTFD implementation of nonsequential data.

6.4. SHORT-TIME FOURIER TRANSFORM

The discrete time STFT can be related to DFT given in Eqn. (6.2). The STFT of *x(n)* is a set of such DFTs corresponding to different time sections of *x(n)*. The time section for time *i* is obtained by multiplying *x(n)* with a time shifted sequence *w(i-n)*,where *w(n)* represents a window function, and for simplicity we assume the window to be a rectangular one.

$$X(i,\omega) = \sum_{n=i}^{i+N-1} x(n) e^{-j\omega(n-i)} \quad . \tag{6.6}$$

The relation between $X(i+1,\omega)$ and $X(i,\omega)$ can be shown to be (Liu *et al*, 1994):

$$X(i+1,\omega) = e^{j\omega}[X(i,\omega) - x(i) + x(i+N)e^{-j\omega N}] \, . \tag{6.7}$$

Discrete STFT can be obtained from the discrete time STFT through the following relation:

$$X(i+1,k) = X(i+1,\omega)\Big|_{\omega=\frac{2\pi k}{N}\ k=0,1,..,N-1}$$

$$= e^{j\frac{2\pi k}{N}} [\, X(i,k) + x(i+N) - x(i)]_{k=0,1,\ldots N-1}. \qquad (6.8)$$

The architecture for implementing the above equation is the same as the one for the DFT except that instead of x(n) used for DFT computation, $x(i+N) - x(i)$ has to be used. Using only real multiplications, the above equation can be rewritten as

$$X_r(i+1,k) = [X_r(i,k) + x_r(i+N) - x_r(i)]\cos(\omega_k) - [X_j(i,k) + x_j(i+N) - x_j(i)]\sin(\omega_k),$$

where $\omega_k = 2\pi k / N$ and

$$X_r(i+1,k) = [X_r(i,k) + x_r(i+N) - x_r(i)]\sin(\omega_k) + [X_j(i,k) + x_j(i+N) - x_j(i)]\cos(\omega_k), \qquad (6.9)$$

which can be implemented using the same architecture used for computing DFT as shown in Fig. 6.2. The total number of complex multipliers required are *(N-1)* and the number of complex adders needed are *(N+1)*. The throughput rate is the one *OP* to obtain $X(n_0 + 1, \omega)$ from $X(n_0, \omega)$ and the throughput rate of obtaining nonoverlapped STFT is *N OPs* as given in (Liu, 1993).

6.5. WIGNER-VILLE DISTRIBUTION

We consider the WVD, which is a special case of GTFDs, in this Section. The WVD can be represented in GTFD form by setting the kernel to one (i.e., $\phi(\theta, \tau) = 1$), which is given by

$$C(t, \omega) = \int x(t + \frac{\tau}{2})\, x^*(t - \frac{\tau}{2})\, e^{-j\omega\tau} d\tau \,. \qquad (6.10)$$

As discussed in Section 3.5, after sampling using the half-outer product sampling scheme, the discrete WVD can be given by

$$C(n,k) = 2 \sum_{\tau=-\frac{(N-1)}{2}}^{\frac{(N-1)}{2}} x(n+\tau)\, x^*(n-\tau)\, e^{-j\frac{2\pi k\tau}{N}} . \qquad (6.11)$$

Throughout the discussion, we make the following assumptions:

- The signal length (window length) is always odd.
- L, which represents the total number of samples of $\phi_\tau(\theta)$ is also odd.

A direct interpretation of Eqn. (6.11) as Fourier transform results in excessive computations. A closer look at the data flow reveals that there zero-valued samples exist in an orderly fashion (Barry, 1992). To compute Eqn. (6.11), simple DFT module can be used with proper data shuffling, which is illustrated Fig. 6.4.

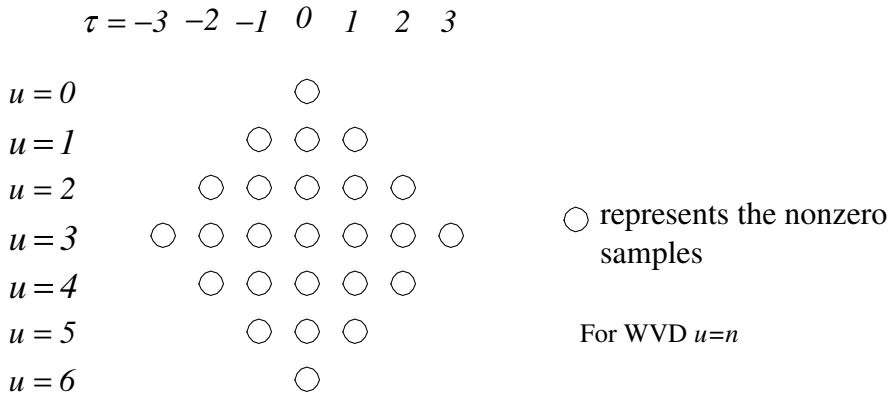

Fig. 6.4. Data flow for *N=7* in WVD and GTFDs

It can be observed from the above figure that direct the brute force implementation not only computes the summation over zero-valued samples but also does not exploit the real-valuedness of the WVD. When we mean zero-valued samples, the data explicitly becomes zero at those points, where the indices referring them point to samples outside the range. We modify the data flow that has to be fed to the time-recursive architecture in a serial manner by noting the fact that Eqn. (6.11) can be rewritten as:

$$C(n_0,k) = 2\sum_{\tau=-(N-1)/2}^{-1} x(n_0+\tau)\,x^*(n_0-\tau)\,e^{-j\frac{2\pi k\tau}{N}} + 2\sum_{\tau=1}^{(N-1)/2} x(n_0+\tau)\,x^*(n_0-\tau)\,e^{-j\frac{2\pi k\tau}{N}} + 2\,|\,x(n_0)\,|^2, \tag{6.12}$$

which reduces to

$$C(n_0,k) = 4\sum_{\tau=1}^{(N-1)/2}\left[\,x_r(n_0+\tau)x_r(n_0-\tau)+x_i(n_0+\tau)x_i(n_0-\tau)\,\right]\cos\left(\frac{2\pi k\tau}{N}\right) + 4\sum_{\tau=1}^{(N-1)/2}\left[\,x_r(n_0+\tau)x_i(n_0-\tau)-x_i(n_0+\tau)x_r(n_0-\tau)\,\right]\sin\left(\frac{2\pi k\tau}{N}\right) + 2\,|\,x(n_0)\,|^2. \tag{6.13}$$

To implement the above equation, the data to be fed to the architecture is in the positive direction of τ and pruning cannot be done if the data flow is in this order, since time-recursive approach is an accumulate operation and utilizes the periodicity of the Fourier transform kernel. To circumvent this difficulty, we propose a different data flow which prunes the input data to avoid unnecessary computations. We start with the first nonzero value as shown in Fig. 6.4 and feed it to the time-recursive architecture for implementing the WVD as well as GTFDs shown in Fig. 6.5 in the direction of τ till $\tau = 0$.

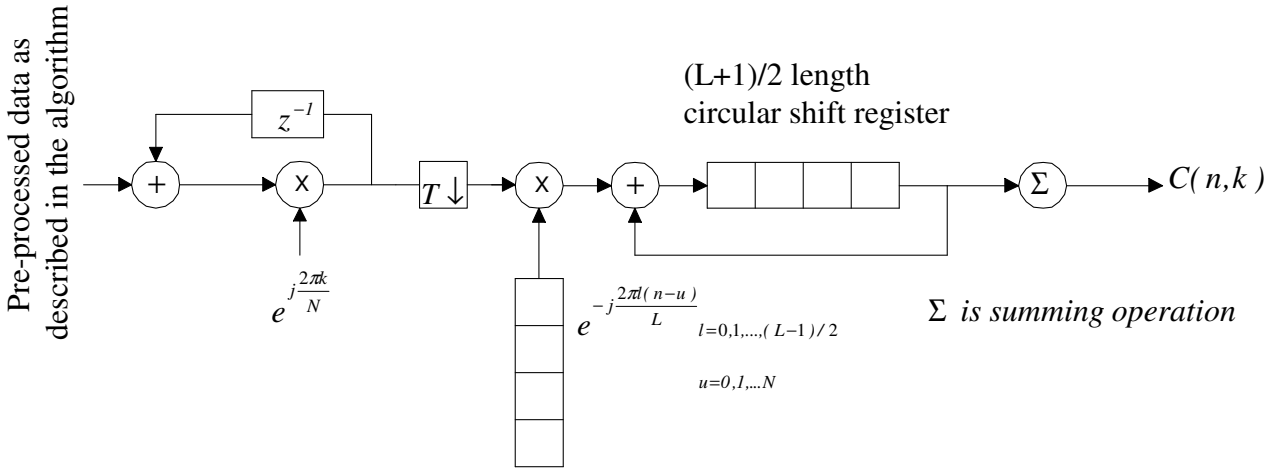

Fig. 6.5. Architecture for WVD and GTFDs

The final value is multiplied by an additional term of $e^{-j\frac{2\pi k}{N}}$. This additional multiplication is done using the same DFT module as explained later. The downsampler in the architecture is set according to the time instant we wish to compute as:

$$T = n+2, \quad 0 \le n \le (N+1)/2$$

$$= N-n+1, \quad (N+3)/2 \le n \le N-1.$$

The DFT module and the downsampler of the architecture are used for computing the WVD, while the remaining blocks are used in computing GTFDs, that will be dealt with in the next Section. Now we consider the WVD algorithm with an example:

Let the discrete time sequence *x(n)* is nonzero in the interval *[0, 4]* and we require Eqn. (6.11) to be evaluated at *n=1*. Then the data at this instant, for $\tau = -2, -1, 0, 1 \text{ and } 2$,

are $0, x(0)x^*(1), |x(2)|^2, x(1)x^*(0)$ and 0, respectively. Since the data is symmetric over τ, we can run the summation either in the positive direction or negative direction of τ and finally consider the real part of the resulting sum. In this case, at the data indexed by $\tau = 2$, we need not compute the summation since it is a zero-valued sample. However, if we were to compute it in a time-recursive manner, we cannot stop the summation since the phase term that every term in the summation has to undergo differs. This problem is very serious if there were more zero-valued samples. Now we start with the first nonzero samples in the negative direction of τ, i.e., $\tau = -1$ and run the summation till $\tau = 0$. After doing the summation, we have to multiply the resultant with a term $e^{-j\frac{2\pi k}{N}}$, i.e., Eqn. (6.13) becomes

$$C(2,k) = 2\,Re[\,(\,2x(0)x^*(1)\,e^{j\frac{2\pi k\,2}{5}} + |\,x(2)|^2\,)\,e^{-j\frac{2\pi k}{N}}\,] \quad . \tag{6.14}$$

We have mentioned earlier that the multiplication of the resulting term by $e^{-j\frac{2\pi k}{N}}$ using the same DFT module can be done by resetting the data at the input side to zero and performing the accumulate operation one more time. This is stemmed from the fact that Eqn. (6.14) can equivalently be obtained from $2\,Re[\,(\,2x(0)x^*(1)\,e^{j\frac{2\pi k\,2}{5}} + |\,x(2)|^2\,)\,e^{j\frac{2\pi k}{N}}\,]$. It can be verified that the same result can be obtained by using Eqn. (6.12) directly without pre-processing and pruning. The WVD of a linear FM signal computed using the above algorithm is shown in Fig. 6.6. It is required that the data has to be multiplied by a factor of two for all τ, except at $\tau = 0$. This modification to the data flow is expressed mathematically as:

$$C(n_0,k) = 2\,Re\Big[\Big(\sum_{\tau=-n_0}^{-1} 2\,x(n_0+\tau)\,x^*(n_0-\tau)\,e^{j\frac{2\pi k(|\tau|+1)}{N}} + |x(n_0)|^2\,e^{j\frac{2\pi k(\tau+1)}{N}}\Big)e^{-j\frac{2\pi k}{N}}\Big],$$

$$0 \le n_0 \le \frac{(N-1)}{2} \qquad (6.15a)$$

and

$$C(n_0,k) = 2\,Re\Big[\Big(\sum_{\tau=N1-n_0}^{-1} 2x(n_0+\tau)\,x^*(n_0-\tau)\,e^{j\frac{2\pi k(|\tau|+1)}{N}} + |x(n_0)|^2\,e^{j\frac{2\pi k(\tau+1)}{N}}\Big)e^{-j\frac{2\pi k}{N}}\Big],$$

$$\frac{(N+1)}{2} \le n_0 \le N-1 \qquad (6.15b)$$

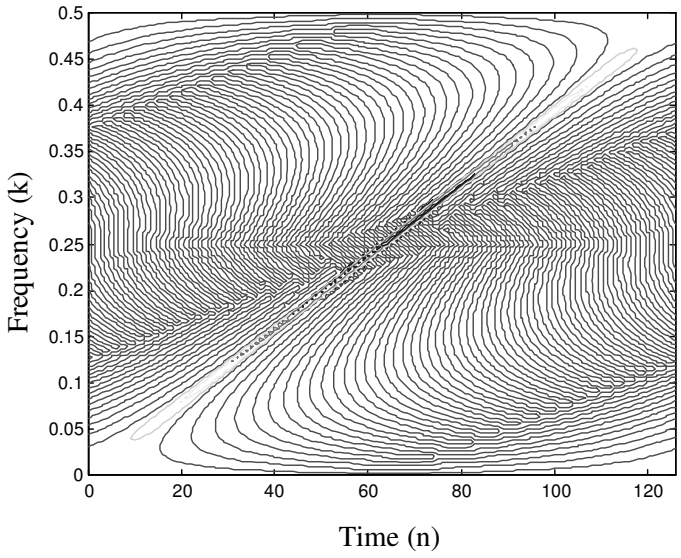

Fig. 6.6. WVD of a linear FM signal computed using the time-recursive approach

When this approach is followed, the complex multiplications required to compute the WVD at each instant increase linearly till *n=(N-1)/2* and then start decreasing linearly till *n=(N-2)* besides another complex multiplication required to obtain the phase offset at all

time instants. We now make conservative estimate of the *OPs* required to obtain the WVD at different time instants.

$$\begin{aligned} OPs &= \sum_{i=1}^{(N+1)/2} i \;+\; \sum_{i=(N-1)/2}^{1} i \;+\; N \\ &= 2\sum_{i=1}^{(N-1)/2} i \;+\; \frac{(N+1)}{2} \;+\; N \\ &= (N^2+6N+1)/4\ . \end{aligned} \tag{6.16}$$

The *OPs* obtained using the FFT approach are $\frac{N}{2}log_2(N)$, with direct brute force are N^2 and by exploiting symmetry conditions, the *OPs* are $N(N+1)/2$. Hence, we have obtained a balance between the FFT and time-recursive approach, i.e., it is less complex in terms of hardware when compared FFT and is computationally more efficient than a direct time-recursive approach. As the FFT based computation is a parallel-in and parallel-out operation, the throughput to obtain WVD at each time is constant and WVD at all time instants is known after $log_2(N)OPs$. In the brute force time-recursive approach that exploits symmetry conditions, the throughput is $\frac{(N+1)}{2}OPs$. In the method proposed, as we are not computing the summation over all possible combinations, the OPs required for each time instant are dependent on the pruning we can do. A comparison of the computational complexity in terms of OPs for the butterfly structure, time-recursive approach with symmetry conditions and our approach has been made in Table. 6.3

Table 6.3: Comparison of various approaches for computing WVD

	Butterfly structure (Radix-2)	Time-recursive approach with symmetry conditions	Proposed method
Complex multipliers	$\frac{N}{2}log_2(N)$	$(N-1)$	$(N-1)$
OPs required to obtain WVD at all time instants	$\frac{N}{2}log_2(N)$	$N(N+1)/2$	$(N^2+6N+1)/4$
Throughput (in *OPs*)	$log_2(N)$	$(N+1)/2$	$n+1,\ 0 \le n \le (N-1)/2$ $N-n,\ (N+1)/2 \le n \le N-1$

6.6. GENERALIZED TFDs

Any distribution that belongs to the Cohen's class can be represented by

$$C(t,\ \omega) = \iiint x(u+\frac{\tau}{2})\, x^*(u-\frac{\tau}{2})\, \phi(\theta,\tau)\, e^{-j\omega\tau}\, e^{j\theta u}\, e^{-j\theta t}\, d\theta\, d\tau\, du, \qquad (6.17)$$

where $\phi(\theta,\tau)$ is the kernel that determines the properties of the distribution. When $\phi(\theta,\tau)$=1, Eqn. (6.17) reduces to the WVD expression, as discussed in the previous Section. In general, most of the distributions are real-valued, for example, Choi-Williams, Born-Jordan, Page, Generalized Exponential Distributions, etc. This property of real-valuedness gets reflected as a constraint on the kernel as conjugate symmetry of the kernel. We are interested in the TFDs of this type, eventhough the same can be extended to any kernel, which obviously reduces the throughput. When put in a mathematical form,

REFERENCES

1. **Abeysekara, S. S. (1990**) Computation of Wigner-Ville Distribution for Complex Data. *Electronics Letters,* **26**, 1315-1317.

2. **Allen, J. B. and Rabiner, L. R. (1977)** A Unified Approach to Short-Time Fourier Analysis and Synthesis. *Proc. of IEEE*, **65**, 1558-1564.

3. **Baraniuk, R. G. (1996a)** Joint Distributions of Arbitrary Variables Made Easy. *Proceedings of the IEEE DSP Workshop,* Leon, Norway, 394-397.

4. **Baraniuk, R. G. and Jones, D. L. (1996b)** Wigner Based Formulation of the Chirplet Transform. *IEEE Trans. on Signal Processing,* **44**, 3129-3535.

5. **Barry, D. T. (1992)** Fast Calculation of the Choi-Williams Time-Frequency Distribution. *IEEE Trans. on. Signal Processing,* **44**, 450-455.

6. **Bergmann, N. (1991)** New Formulation of Discrete Wigner-Ville Distribution. *Electronics Letters,* **26**, 111-112.

7. **Bikdash, U. M. and Yu, K. B. (1993)** Analysis and Filtering using Optimally Smoothed Wigner Distribution. *IEEE Trans. on Signal Processing,* **41**, 1603-1617.

8. **Boashash, B. and Black, P. J. (1987)** An Efficient Real-Time Implementation of the Wigner-Vile Distribution. *IEEE Trans. on Acoust., Speech and Signal Processing,* **ASSP-35**, 16117-1619.

9. **Boudreaux-Bartles, G. F. and Parks, T. W. (1986)** Time-Varying Filtering and Signal Estimation using Wigner Distribution Synthesis Techniques. *IEEE Trans. on Acoust., Speech and Signal Processing,* **ASSP-34**, 442-451.

10. **Bracewell, R. N. and Mihovilovic, D. (1991)** Adaptive Chirplet Representation of Signals on Time-Frequency Plane. *Electronics Letters,* **27**, 1159-1161.

11. **Bultan, A. (1999)** A Four-Parameter Atomic Decomposition of Chirplets. *IEEE Trans. on Signal Processing*, **41**, 731-745.

12. **Bultan, A. and Akansu, A. N. (1998)** A Novel Time-Frequency Exciser in Spread Spectrum Communications for Chirp-Like Interference. *Proc. of ICASP*, Seatle, U.S.A., 3265-3268.

13. **Choi, H. I. and Williams, W. J. (1989)** Improved Time-Frequency Representation of Multicomponent Signals using Exponential Kernels. *IEEE Trans. on Acoust., Speech and Signal Processing,* **ASSP-37**, 861-871.

14. **Claasen, T. A. C. M. and Mecklenbrauker, W. F. G. (1980a)** The Wigner Distribution- A Tool for Time-Frequency Signal Analysis, Part II: Discrete Time Signals. *Philips J. Res.,* **35**, 276-300.

15. **Claasen, T. A. C. M. and Mecklenbrauker, W. F. G. (1980b)** The Aliasing Problem in Discrete-Time Wigner Distribution. *IEEE Trans. on Acoust., Speech and Signal Processing,* **ASSP-31**, 1067-1072.

16. **Coates, M, J., Fitzgerald, W. J. and Molina, C. (1998)** Regionally Optimised Kernels for Time-Frequency Distributions. *Proc. of ICASSP*, Seatle, U.S.A., 1553-1556.

17. **Cohen, L. (1989)** Time-Frequency Distributions: A Review. *Proc. of IEEE,* **77**, 941-981.

18. **Cohen, L.** *Time-Frequency Analysis*. Printice-Hall, Englewood cliffs, New Jersey (1995).

19. **Crochiere, R. E**. **(1980)** A Weighed Overlap-Add Method of Short-Time Fourier Analysis/Synthesis. *IEEE Trans. on Acoust., Speech and Signal Processing,* **ASSP-28**, 99-102.

20. **Cunningham, G. S. and Williams, W. J. (1994a)** Kernel Decomposition of Time-Frequency Distributions. *IEEE Trans. on. Signal Processing,* **42**, 1425-1442.

21. **Cunningham, G. S. and Williams, W. J. (1994b)** Fast Implementation of Generalized Discrete Time-Frequency Distributions. *IEEE Trans. on Signal Processing,* **42**, 1496-1508.

22. **Dembo, A. and Malah, D. (1988)** Signal Synthesis from Modified Discrete Short-Time Transform. *IEEE Trans. on Acoust., Speech and Signal Processing,* **ASSP-36**, 168-181.

23. **Dempster, A . P., Laird, N. M. and Rubun. D. B. (1977)** Maximum Likelihood from Incomplete Data via the EM Algorithm. *J. R. Stat. Soc. B.,* **39**, 1-37.

24. **Devroye, L.** *Non-Uniform Random Variate Generation*. Springer-Verlag 1986.

25. **Fessler, A. and Hero, A. O. (1994)** Space Alternating Generalized Expectation Maximization Algorithm. *IEEE Trans. on Signal Processing*, **42**, 2664-2667.

26. **Flandrin, P. and Martin, W. (1985)** Wigner-Ville Spectral Analysis of Nonstationary Process. *IEEE Trans. on Acoust., Speech and Signal Processing,* **ASSP-33**, 1461-1470.

27. **Giridhar, J. (1998)** Time-Frequency Distributions and Their Applications in Radar Signal Processing. *M. S. Thesis*. Indian Institute of Technology, Madras, May 1998.

28. **Hlawatsch, F. and Boudreaux-Bartles, G. F. (1992a)** Linear and Quadratic Time-Frequency Signal Representations. *IEEE Signal Processing Magazine,* 21-67

29. **Hlawatsch, F. and Kozek, W. (1993)** The Wigner Distribution of a Linear Signal Space. *IEEE Trans. on Signal Processing,* **41**, 1248-1258.

30. **Hlawatsch, F. and Kozek, W. (1994)** Time-Frequency Projection Filters and Time-Frequency Signal Expansions. *IEEE Trans. on Signal Processing,* **42**, 3321-3334.

31. **Hlawatsch, F. and Krattenthaler, W. (1992b)** Bilinear Signal Synthesis. *IEEE Trans. on Signal Processing,* **40**, 351-3363.

32. **Jeong, J. and Williams, W. J. (1992a)** Kernel Design for Reduced Interference Distributions. *IEEE Trans. on Signal Processing,* **40**, 402-412.

33. **Jeong, J. and Williams, W. J. (1992b)** Alias-Free Generalized Discrete-Time Time-Fequency Distributions. *IEEE Trans. on Signal Processing,* **40**, 2757-2765.

34. **Johnson, M. E.** *Multivariate Statistical Simulation*. John-Wiley & sons, Inc 1987.

35. **Jones, D. L. and Baraniuk, R. G. (1993a)** Shear Madness: New Orthonormal Bases and Frames using Chirp Functions. *IEEE Trans. on Signal Processing, Special Issue on Wavelets in Signal Processing,* **41**, 12, 3543-3548.

36. **Jones, D. L. and Baraniuk, R. G. (1993b)** A Signal-Dependent Time-Frequency Representation: Optimal Kernel Design. *IEEE Trans. on Signal Processing*, **41**, 4, 1589-1602.

37. **Jones, D. L. and Baraniuk, R. G. (1993c)** Signal-Dependent Time-Frequency Analysis Using a Radially Gaussian Kernel, *IEEE Trans. on Signal Processing*. **32**, 263-284.

38. **Jones, D. L. and Baraniuk, R. G. (1994a)** A Simple Scheme for Adapting Time-Frequency Representations. *IEEE Trans. on Signal Processing,* **42**, 3530-3535.

39. **Jones, D. L. and Baraniuk, R. G. (1994b)** A Signal-Dependent Time-Frequency Representation: Fast Algorithm for Optimal Kernel Design. *IEEE Trans. on Signal Processing*, **42**, 1, 134-146.

40. **Jones, D. L. and Parks, T. W. (1992a)** A Resolution Comparision of Several Time-Frequency Representations. *IEEE Trans. on Signal Processing,* **40**, 413-420.

41. **Jones, D. L. and Parks, T. W. (1992b)** A High Resolution Data-Adaptive Time-Frequency Representation. *IEEE Trans. on Acoust., Speech and Signal Processing,* **ASSP-38**, 2127-2135.

42. **Kay, S. M.** *Fundamentals of Stastical Signal Processing, Estimation Theory.* Printice-Hall, New Jersey, 1993.

43. **Krattenthaler, W. and Hlawatsch, F. (1991)** Improved Signal Synthesis from Pseudo-Wigner Distribution. *IEEE Trans. on Signal Processing,* **39**, 506-509.

44. **Lawrance, M.** *Transformations in Optics*. John-Wiley & Sons, 1965.

45. **Leon, S.** *Linear Algebra with Applications.* McMillan, 1994.

46. **Liu, K. J. R. (1993)** Novel Paralel Arcitrecures for Short-Time Fourier Transform. *IEEE Trans. on Circuits and Systems,* **40**, 786-789.

47. **Liu, K. J. R., Chui, C. T., Kolagata, R. K. and Jaja, J. F. (1994)** Optimal Unified Arcitrecures for Real-time Computation of Time-Recursive Discrete Sinusoidal Transforms. *IEEE Trans. on Circuits and Systems for Video Technology,* **4**, 168-180.

48. **Mallat, S. G. and Zhang, Z. (1993)** Matching Pursuits with Time-Frequency Dictionaries. *IEEE Trans. on Signal Processing,* **41**, 3397-3415.

49. **Mann, S. and Haykin, S. (1995**) The Chirplet Transform: Physical Considerations. *IEEE Trans. on Signal Processing,* **44**, 2745-2761.

50. **McLachlan, G. J. and Basford, K. E.** *Mixture Models.* Marcel Dekker, 1987.

51. **Mix, D. F.** *Random Signal Processing.* Printice-Hall, Englewood cliffs, New Jersey, 1995.

52. **Morris, J. M. and Wu, D. (1996)** On Alias-Free Formulations of Discrete-Time Cohen's Class of Distributions. *IEEE Trans. on. Signal Processing,* **44**, 1335-1364.

53. **Nawab, S. H. and Quatieri, T. F.** *Short-time Fourier Transform, In* **Lim, J. S. and Opeenhiem, A. V**. (eds.) *Advanced Topics in Signal Processing*, Printice-Hall, Englewood cliffs, New Jersey, 1988.

54. **Nawab, S. H., Quatieri, T. F. and Lim, J. S. (1983)** Signal Reconstruction from Short-Time Fourier Transform Magnitude. *IEEE Trans. on Acoust.,, Speech and Signal Processing,* **ASSP-31**, 986-998.

55. **Neal, R. M. and Hinton, G. E. (1993)** A New View of the EM Algorithm that Justifies the Incremental and Other Variants, *submitted to Biometrica 1993*, (Available on-line at ftp:\\ftp.cs.utoronto.ca/pub/radford/em.ps.z)

56. **O'Neill, J. C. (1997)** Shift Covariant Time-Frequency Distributions of Discrete Signals. *Ph. D. Thesis*. Univeristy of Michigan, May 1997.

57. **O'Neill, J. C. and Flandrin, P. (1998)** Chirp Hunting. *Proc. of the IEEE-SP International Symposium on Time-Frequency and Time-ScaleAanalysis*. 425-428.

58. **O'Neill, J. C. and Williams, W.J. (1999)** A Function of Time, Frequency, Lag, and Doppler. *IEEE Trans. on Signal Processing*, **47,** 789-799.

59. **Papandreou, A., Hlawatsch, F. and Boudreaux-Bartles, G. F. (1993)** The Hyperbolic Class of QTFRs- Part I: Constant-Q Warping, Hyperbolic Paradigm, Properties, and Members. *IEEE Trans. on Signal Processing*, **41,** 3425-3444.

60. **Papoulis. A.** *Signal Analysis*. McGraw-Hill, 1984.

61. **Pei, S. C. and Yang, I. I (1992)** Computing Pseudo-Wigner Distribution by the Fast Hartley Transform. *IEEE Trans. on Signal Processing,* **40**, 2346-2349.

62. **Prabhu, K. M. M. and Sundaram, R. S. (1996)** Fast Algorithm for Pseudodiscrete Wigner-Ville Distribution using Moving Discrete Hartley Transform. *IEE Proc.-Vis. Image, Signal Proessing,* **143**, 383-386.

63. **Qian, S. E. and Morris, J. M (1990)** Fast Algorithm for Real Joint Time-Frequency Transformations of Time-Varying Signals. *Electronics Letters,* **26**, 537-539.

64. **Rabiner, L. R. and Jaung, B. H.** *Fundamentals of Speech Recognition*. Printice-Hall, New Jersey, 1993.

65. **Rao, R. M. and Bopardikar, A. S.** *Wavelet Transforms, Introduction to Theory and Apllications*. Addison Wisley longman, Inc, 1998.

66. **Rau, J. G.** *Optimization and Probability in Systems Engineering*. Van Nostrand Reinhold Company, 1970.

67. **Rihaczek, A. (1968)** Signal Energy Distribution in Time and Frequencies. *IEEE Trans. on Information Theory,* **42**, 3241-3244.

68. **Reily, A. and Boashash, B. (1994)** Anlytical Signal Generation-Tips and Taps. *IEEE Trans. on Signal Processing,* **42**, 3241-3244.

69. **Shalvi, O. and RWeinstein, E. (1996)** System Identification using Nonstationary Signals. *IEEE Trans. on Signal Processing,* **44**, 2055-2063.

70. **Smith, M. J and Barnwell, T. P (1987)** A New Filter bank Theory for Time-Frequency Representation. *IEEE Trans. on Acoust., Speech and Signal Processing,* **ASSP-35**, 314-327.

71. **Stankovic, L. (1994b)** A Multitime Definition of the Wigner Higher Order Distribution: L-Wigner Distribution.. *IEEE Letters in Signal Processing,* **1**, 106-109.

72. **Vaseghi, S. V.** *Advanced Topics in Signal Processing and Digital Noise Reduction.* Wiley-Teubner, 1996.

73. **Xia, X. G. (1997)** System Identification using Chirp Signals and Time-Variant Filters in the Joint Time-Frequency Domain. *IEEE Trans. on Signal Processing,* **45**, 2072-2085.

74. **Yu, K. B. and Cheng, S. (1987)** Signal Synthesis from Pseudo-Wigner Distribution ans Its Applicstions. *IEEE Trans. on Acoust., Speech and Signal Processing,* **ASSP-35**, 1289-1302.